Lecture notes for Scottish Universities' Summer School,
Middleton Hall, Gorebridge, Midlothian, Scotland,
July 30-August 18, 1973

LBL-2079

c.1

For Reference
Not to be taken from this room

INTRODUCTION TO HADRONIC INTERACTIONS AT HIGH ENERGIES

J. D. Jackson

September 1973

LAWRENCE BERKELEY LABORATORY
UNIVERSITY OF CALIFORNIA
BERKELEY

Prepared for the U.S. Atomic Energy Commission
under Contract W-7405-ENG-48

DISCLAIMER

This document was prepared as an account of work sponsored by the United States Government. While this document is believed to contain correct information, neither the United States Government nor any agency thereof, nor the Regents of the University of California, nor any of their employees, makes any warranty, express or implied, or assumes any legal responsibility for the accuracy, completeness, or usefulness of any information, apparatus, product, or process disclosed, or represents that its use would not infringe privately owned rights. Reference herein to any specific commercial product, process, or service by its trade name, trademark, manufacturer, or otherwise, does not necessarily constitute or imply its endorsement, recommendation, or favoring by the United States Government or any agency thereof, or the Regents of the University of California. The views and opinions of authors expressed herein do not necessarily state or reflect those of the United States Government or any agency thereof or the Regents of the University of California.

Table of Contents

I. Introduction 2

II. Total Cross Sections, Elastic Scattering and Two-body Processes 6

1. Basic facts and samples of data 6

2. Crossing symmetry, signature, power law behavior and phase, Pomeranchuk theorems 20

3. Froissart bound 30

4. Ratio of real to imaginary part of the forward scattering amplitude 39

5. Partial wave distribution for proton-proton scattering, MacDowell-Martin bound on B(s) 51

6. Asymptotics and J-plane structure 65

III. Inclusive Processes 70

1. Preamble 70

2. Basic facts and samples of data 72

3. Theoretical framework assuming a finite correlation length: Feynman-Wilson "gas" 91

4. Relation of the Feynman-Wilson gas to a Regge description, the approach to scaling 98

5. Brief remarks on a two-component description 104

Appendix A: S-matrix formulas, cross sections, two-body kinematics

Appendix B: Partial waves, helicity amplitudes, impact parameter representation

Appendix C: Eikonal approximation

Appendix D: Kinematics of inclusive processes

Appendix E: Distributions, correlations, moments, sum rules in inclusive processes

Bibliography

INTRODUCTION TO HADRONIC INTERACTIONS AT HIGH ENERGIES

J. D. Jackson

Department of Physics and Lawrence Berkeley Laboratory
University of California
Berkeley, California 94720

Notes prepared for a series of lectures at the 1973 Scottish Universities' Summer School, Middleton Hall, Gorebridge, Midlothian, Scotland, July 30-August 18, 1973.

I. INTRODUCTION

The subject of the phenomenology of hadronic interactions at high energies is extremely broad. In these lectures it is necessary to limit the discussion to only a few topics and merely to scratch the surface of most of these. Since my charge is to provide an introduction on which concurrent and subsequent lecturers can build I stick to basics. Furthermore, my approach is down-to-earth in the extreme. Elegance and rigor take a back seat to "Anschaulichkeit" and intuitive understanding. The lectures are thus aimed at plain and simple folk. Theorists and other sophisticates may, while wincing, also benefit, but they are not the intended audience.

In strong interactions at high energies for the past year and a half the scene has been dominated by the great extension of the energy range for controlled experimentation made available by the Intersecting Storage Rings (ISR) at CERN, Geneva, Switzerland, and the proton synchrotron at the National Accelerator Laboratory, Batavia, Illinois (NAL). Prior to the start-up of these facilities the highest available energy was at Serpukhov in the U.S.S.R. where a 70 GeV proton beam provided a c.m.s. energy $W \simeq 11.5$ GeV in collisions with a stationary nucleon. Now we have available c m.s. energies of $W = 20\text{-}60$ GeV at the ISR in proton-proton collisions and $W \sim 20\text{-}27$ GeV at NAL from 200-400 GeV protons or mesons on a stationary nucleon target. For the first time we have been able to look in detail at truly high energy phenomena. At these energies the symbol, $\gg$, in the statement $W \gg m_N$ almost takes on its rigorous mathematical meaning, not merely the physicist's interpretation of somewhat larger than or at least slightly greater than! Of course, many of the phenomena observed at the ISR and NAL have been known, in outline at

least, for many years from experiments with cosmic rays, as the experts in that field hasten to point out (e.g., Feinberg, 1972). Nevertheless, the wealth of detail possible with controlled experimental conditions and intense beams of particles has meant that gross features seen in cosmic rays are now firmly established and finer details, energy dependences, or rare processes are being explored for the first time.

Since the time of Rutherford elastic scattering has occupied an honorable position among phenomena designed to elucidate the forces between particles and their structures. Inelastic scattering, too, has played its role in the study of structures and excitations since the days of Franck and Hertz. In particle physics both elastic and inelastic scattering have been pursued continuously over the years, but with the availability of meson and baryon beams with energies of several GeV and the attendant production of particles emphasis shifted to the detailed study of the complete final state of three, four, or more particles. Quasi-two-body processes with one or two resonances in the final state were studied, decay correlations and energy dependences observed. A tremendous amount of information was and still is being accumulated on these so-called exclusive processes and a semi-quantitative understanding and theoretical framework was gained. Some aspects of this are summarized in Chapter II. As higher energies became available the most probable occurrence in a hadronic collision was the production of many particles. Two-body or quasi-two-body channels were relatively improbable. Attempts were made to study resonance formation among the final state particles and to interpret the various invariant mass plots within some theoretical framework (e.g., n-point Veneziano amplitudes or Van Hove phase space plots). At energies like Serpukhov or higher, however, the average

number of produced particles is so large that little can be learned from exclusive experiments--the number of degrees of freedom is just too great. It is necessary to fall back on simpler things--total cross section measurements, topological cross sections, single particle production spectra (with elastic and inelastic scattering of the incident particle as special cases), two-particle correlations and perhaps slightly more complicated situations. We speak then of inclusive experiments or processes. The total cross section σ_{ab} is the zero-particle inclusive process--$a + b \rightarrow$ anything. The reaction $a + b \rightarrow c +$ anything, where the type of particle (c), its momentum and perhaps spin, is all that is observed, is called a single-particle inclusive process, and so on. Over the past three or four years inclusive processes have become an industry at least as large as the quasi-two-body industry once was. Counter experimenters have found their beam surveys upgraded in theoretical respectability and bubble chamber physicists have been able to get publishable results from the tremendous number of previously useless unfitted events. At first glance it might seem surprising that much of interest could come out of single-particle spectra, but we will see in Chapter III that simplicity allows application of ideas closely related to two-body phenomenology.

The most important single feature of hadronic interactions to be discovered with the extension of the available energy range is the rising total cross section for proton-proton collisions [again, this was anticipated somewhat from cosmic ray evidence (Yodh, Pal, and Trefil, 1972)]. This raises the question of bounds on total and differential cross sections and other aspects. These topics are

discussed in Chap. II after a review of the basic experimental facts and the general theoretical framework. The Froissart bound on total cross sections, a different treatment of the ratio of real to imaginary part of the forward scattering amplitude, discussion of the partial wave (impact parameter) distribution for p-p scattering, the MacDowell-Martin bound and the connection between the energy dependence of amplitudes and their J-plane structure completes this chapter. An introduction to inclusive processes is given in Chap. III. Again the basic facts are presented, followed by a discussion of the main theoretical ideas via the Feynman-Wilson fluid analogy. The relation between the fluid analogy and the Mueller-Regge description is outlined briefly, as is the "two-component" model of prong cross sections. A series of appendices summarize notation and some details that would burden and disturb the flow of argument in the text proper. A major omission is the discussion of processes involving large transverse momenta. Reliable data are just beginning to emerge and there are some fascinating theoretical speculations, but could take a whole lecture series in itself.

References are cited in the text by authors and year of publication and are given in full in the bibliography, alphabetically by first author. Papers from conference or "summer" school proceedings are cited in the text in the same manner, but are listed in the bibliography by the conference location. The full citations for the conferences are given at the beginning of the bibliography. In such a rapidly developing field as high-energy physics the best sources of background information and leads to more detail are the conference proceedings, summer school notes, and the review literature (Physics Reports, Reviews of Modern Physics). Two recent books are noteworthy--

D. Horn and F. Zachariasen, Hadron Physics at Very High Energies, W. A. Benjamin, Reading, Mass. (1973) and R. P. Feynman, Photon-Hadron Interactions, W. A. Benjamin, Reading, Mass. (1972).

II. TOTAL CROSS SECTIONS, ELASTIC SCATTERING, AND TWO-BODY PROCESSES

1. Basic facts and Samples of data

The most recent reviews of total cross sections and elastic scattering are those of Diddens (1972), Giacomelli (1972), and Amaldi (1973), and on two-body and quasi-two-body inelastic processes those by Chiu (1972), Michael (1972), Phillips and Ringland (1972), Barloutaud (1973), and Fox and Quigg (1973). I shall lean heavily on these and other reviews both in the topics I discuss and for excuse on the topics I omit.

While the emphasis in this chapter is more on total cross sections and elastic scattering at high energies than on processes with nontrivial quantum number exchanges, it is expedient to summarize the gross empirical facts and main theoretical concepts for all two-body processes:

"(i) There exist SU(3) singlets and octets of mesons, and singlets, octets, and decimets of baryons, of a variety of different spins and parities. Some of these mesons and baryons are stable, apart from electromagnetic or weak decays. Others appear as resonant states in scattering or production experiments.

(ii) The quantum numbers of the observed meson and baryon multiplets can be generated by the mnemonic of the quark model, with $(\bar{q}q)$ for the mesons and (qqq) for the baryons. (This particular empirical fact will need modification as soon as any "exotic" resonance is firmly established.)

(iii) Two-body and quasi-two-body processes are peripheral, showing peaking at forward directions (small t) and/or backward directions (small u).

(iv) Integrated cross sections, or differential cross sections at fixed momentum transfer, show approximate power-law behavior in the energy. In particular, total cross sections seem to become constant asymptotically and obey Pomeranchuk's theorem.

(v) Virtually all occurrences or nonoccurrences of peripherality in a given process (iii) can be understood in terms of the exchanges of the internal quantum numbers of the known SU(3) multiplets of mesons and baryons (i).

(vi) A modest amount of analyticity in the kinematic invariants, plus crossing symmetry, relates the phase of an amplitude at high energies to its power-law behavior (iv). This connection is the same as, but more general than, that given by Regge pole theory.

(vii) The known mesonic and baryonic states (i) can plausibly be placed on Regge trajectories, and the trajectories are approximately linear in the square of the masses. This gives great impetus to the use of Regge exchanges to unify items (iv), (v), and (vi) into an aesthetically pleasing whole."

The above seven points were written down four years ago (Jackson, 1970) and are subject to some slight modification. On item (ii) there is increasing evidence, though not yet overwhelming, of the existence of exotic baryonic resonances (See Lovelace, 1972). In point (iv) the statement that "total cross sections seem to become constant asymptotically" should be omitted. Total cross sections may become constant asymptotically or they may not. As we shall discuss subsequently in detail, at the highest available energies total cross sections show energy dependence. If they become constant ultimately, it occurs at very much higher energies.

(a) Total cross sections

The high-energy behaviors of total cross sections of $\bar{p}$, p, π^-, π^+, K^-, and K^+ on protons are shown in Fig. 1(a), taken from Denisov et al. (1971). With the exception of the K^+p total cross section, which shows a very slight rise, all the cross sections fall smoothly from 5 to 60 GeV/c incident momentum. The total cross section differences, $\Delta\sigma = \sigma_t(\bar{x}p) - \sigma_t(xp)$ with $x = p, \pi^+, K^+$, are displayed in Fig. 1(b) on a log-log plot. The differences can be fitted by a power-law form $\Delta\sigma_i = A_i/P_{Lab}^{n_i}$, with $n = 0.64 \pm 0.02$, 0.54 ± 0.02, and 0.32 ± 0.02 for $(\bar{p},p)$, (K^-,K^+), and (π^-,π^+) differences, respectively (Table 4 of Giacomelli, 1972). This power-law behavior supports the first part of statement (iv) above, and Fig. 1a the now discredited second part.

The constancy of total cross sections at high energies, so nicely indicated in Fig. 1a, received a jolt with the commencement of operation of the ISR at energies equivalent to 300 to 2000 GeV incident in the laboratory. Right from the beginning there were rumors of large cross sections (45 to 50 mb). Furthermore, an analysis of cosmic ray data on the very high energy proton flux at an atmospheric depth of 550 gm/cm^2 on Mt. Chacaltya in Bolivia, compared with the flux at the top of the atmosphere, gave evidence that the nucleon-nucleon total cross section increased with energy significantly at laboratory energies above 500 GeV (Yodh, Pal, and Trefil, 1972). Data from the ISR were published early in 1973 (Amaldi et al., 1973a,b; Amendolia et al., 1973; Braccini, 1973). These and other results on the proton-proton total cross section are displayed in Fig. 2. The dashed curve is a lower bound deduced from analysis of the cosmic ray data. The data show that the asymptotic constancy inferred from the

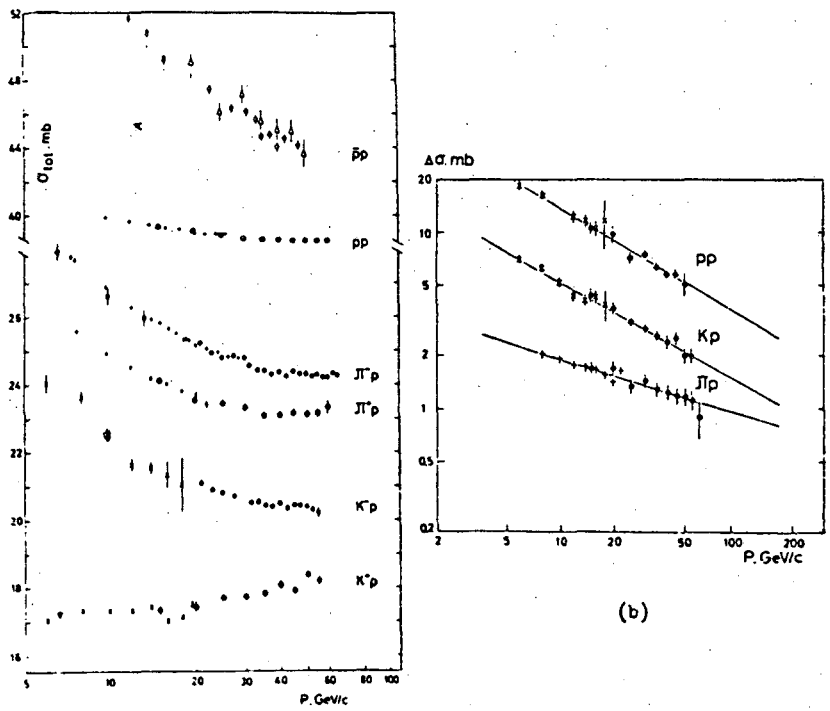

(a)

(b)

Fig. 1. (a) Total cross sections in millibarns for $\bar{p}$, p, π^-, π^+, K^-, K^+ on protons versus incident laboratory momentum in GeV/c (from Denisov et al., 1971).

(b) Cross section differences in millibarns versus incident laboratory momentum in GeV/c on a log-log plot (from Denisov et al., 1971).

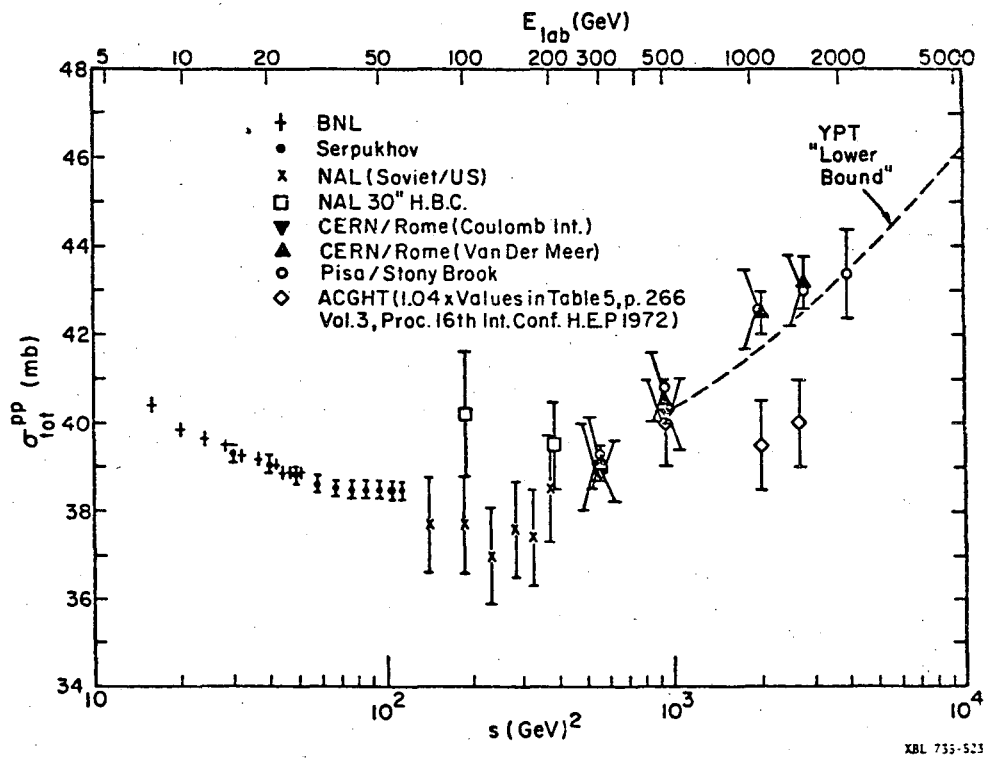

Fig. 2. Total cross section in millibarns for pp collisions versus $s = W^2$ in GeV^2 (bottom scale) and incident laboratory energy in GeV (top scale). The dashed curve is a lower bound estimated from cosmic ray data (Yodh, Pal, and Trefil, 1972).

left-hand side of Fig. 2 (and all of Fig 1a) is only a local minimum at $E \sim 100$ GeV and that the cross section rises from this minimum of 38.5 mb to 43^+ mb at the highest ISR energy of $W \simeq 60$ GeV.

For incident particles other than protons, data at energies higher than 70 GeV are almost nonexistent. While the next year will bring many results from NAL, at present the only very high-energy datum is $\sigma_t = 24.0 \pm 0.5$ mb at 205 GeV incident energy for π^- on protons in the NAL 30" hydrogen bubble chamber (Huson, 1973). From Fig. 1a it can be seen that this result throws no light on the question of constancy versus rise of the π^-p cross section.

(b) Differential cross sections for elastic scattering

The well-known peripheral nature of elastic scattering at high energies is illustrated for π^-p, K^-p, and $\bar{p}p$ scattering in Fig. 3. For small momentum transfers the cross sections are fitted roughly by $\exp(Bt)$ where $t = -q^2$ is the invariant momentum transfer variable (see Appendix A) and $B \simeq 7.8$, 8.7, and 11.5 $(\mathrm{GeV/c})^{-2}$ for K^-p, π^-p, and $\bar{p}p$, respectively. In naive geometrical terms these "slope" parameters correspond to an extended scattering region with root mean square impact parameter $\langle b^2\rangle^{\frac{1}{2}} = (2B)^{\frac{1}{2}} = \sqrt{0.0389[2B(\mathrm{GeV/c})^{-2}]}\,\mathrm{fm}$ $\simeq 0.78$-0.95 fm.

That there is some structure within the forward peak and also backward peaks of various sizes is indicated by the data shown in Fig. 4. The K^-p differential cross section snakes back and forth around the smooth and featureless K^+p cross section. In the very forward direction ($|t| < 0.2(\mathrm{GeV/c})^2$, not shown in Fig. 4a) the K^-p cross section is larger and falls off more rapidly than the K^+p cross section. For $0.2 < |t| < 1.0$ $(\mathrm{GeV/c})^2$ the K^-p cross section is smaller than the K^+p, but at $|t| \sim 1.0$ it crosses over and lies

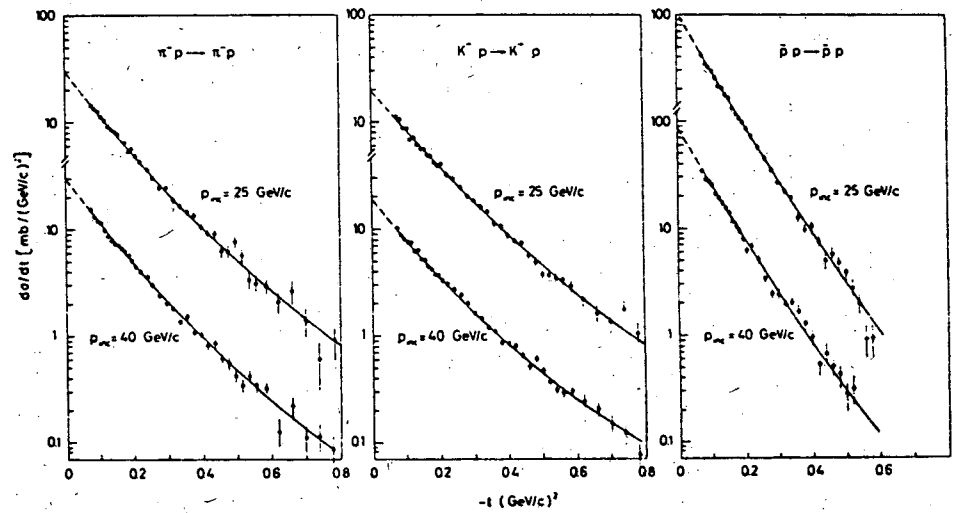

Fig. 3. Differential cross sections $d\sigma/dt$ for elastic scattering of π^-p, K^-p, and $\bar{p}p$ at 25 and 40 GeV/c incident momentum and $0 < |t| < 0.8$ $(\mathrm{GeV/c})^2$ (Serpukhov data, Fig. 17 of Giacomelli, 1972).

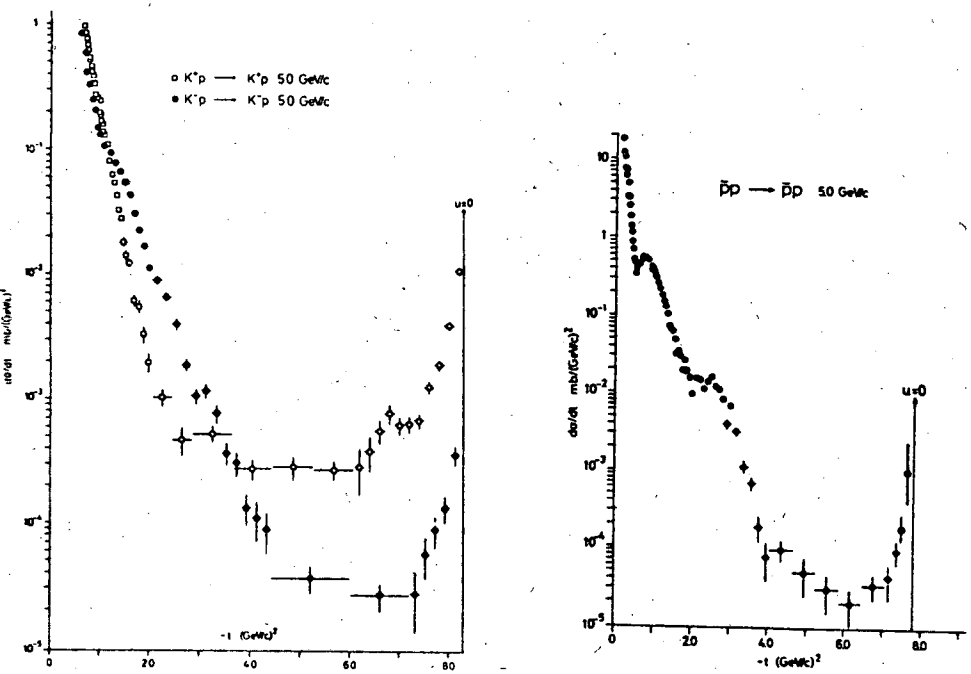

(a) (b)

Fig. 4. (a) K^+p and K^-p elastic differential cross sections over the entire momentum transfer range at 5 GeV/c (from Chabaud et al., 1972).

(b) $\bar{p}p$ elastic differential cross section over the entire momentum transfer range at 5 GeV/c (from Chabaud et al., 1972).

above the K^+p. Only beyond $|t| \sim 3.5$ does it fall below and stay much below the K^+p cross section, each having a backward peak. The hints of diffraction maxima and minima in the K^-p cross section are more than hints in the $\bar{p}p$ cross section shown in Fig. 4b. By contrast, the pp differential cross section at the same momentum is extremely smooth, as can be seen in the compilation of Fig. 5. The evidence of Figs. 1, 4, and 5 indicates that in geometrical terms $\bar{p}p$ and K^-p interactions correspond to larger absorbing regions, with more sharply defined edges, than pp and K^+p interactions.

The differential cross section for proton-proton elastic scattering at various energies is summarized in Fig. 5. The energy dependence is quite striking. The smooth behavior at "low" energies gradually evolves into structure at $|t| \sim 1\text{-}2\ (\mathrm{GeV/c})^2$ at ISR energies as the cross section "shrinks" (becomes compressed to smaller and smaller $|t|$ values). The shrinkage of the very small $|t|$ region is best described by the energy dependence of the "slope parameter" B, defined by

$$B(s,t) = \frac{d}{dt} \ln\left[\frac{d\sigma}{dt}(s,t)\right] . \qquad (1)$$

To the extent that B changes slowly with t this is equivalent to writing the differential cross section as

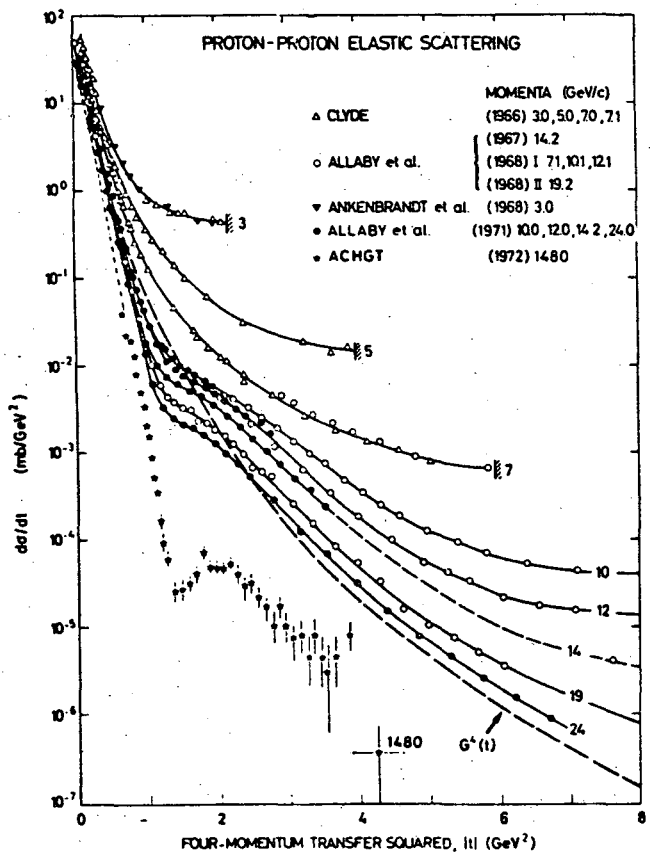

Fig. 5. Compilation of differential cross sections for p-p elastic scattering at various energies. The incident laboratory momentum is indicated at the right-hand end of each curve (Fig. 15 of Giacomelli, 1972).

$$\frac{d\sigma}{dt}(s,t) = \frac{d\sigma}{dt}(s,0)\exp[B(s,t)t] \ . \qquad (2)$$

Furthermore, when we speak of <u>the</u> slope parameter $B(s)$ we mean $B(s,0)$, or more commonly, some sort of an average value obtained by fitting $d\sigma/dt$ with an exponential in $|t|$ at small $|t|$. For p-p scattering the slope parameters $B(s,t)$ for two different small $|t|$ ranges are shown as functions of energy in Fig. 6. From 5 GeV/c to 2000 GeV/c laboratory momentum B increases by about 50 percent. At high energies simple Regge theory would predict $B(s,t) = A_1(t)\,\ln s + A_2(t)$, corresponding to a straight line on Fig. 6. For $P_{Lab} > 10$ GeV c the data are consistent with such a variation, but at ISR energies it is possible that the shrinkage has stopped at least momentarily. More will be said on this question in Section 5 below. At larger $|t|$ values, too, data from the ISR (the $W = 53$ GeV results are shown in Fig. 5) are consistent with little energy dependence from $W = 30$ to 53 GeV (Strolin, 1973).

(c) <u>Power law behavior</u>

Part of the lore of high-energy phenomenology is that differential cross sections at fixed t, or cross sections integrated over the forward (or backward) peaks, show power law behavior in energy and that the power depends on the reaction mechanism (Morrison, 1970). Simple Regge theory predicts, for the exchange of a single Regge pole in the t-channel,

$$\frac{d\sigma}{dt}(s,t) \simeq \beta(t)\, s^{2\alpha(t)-2} \qquad (3)$$

where $\alpha(t)$ is the trajectory function of the pole.

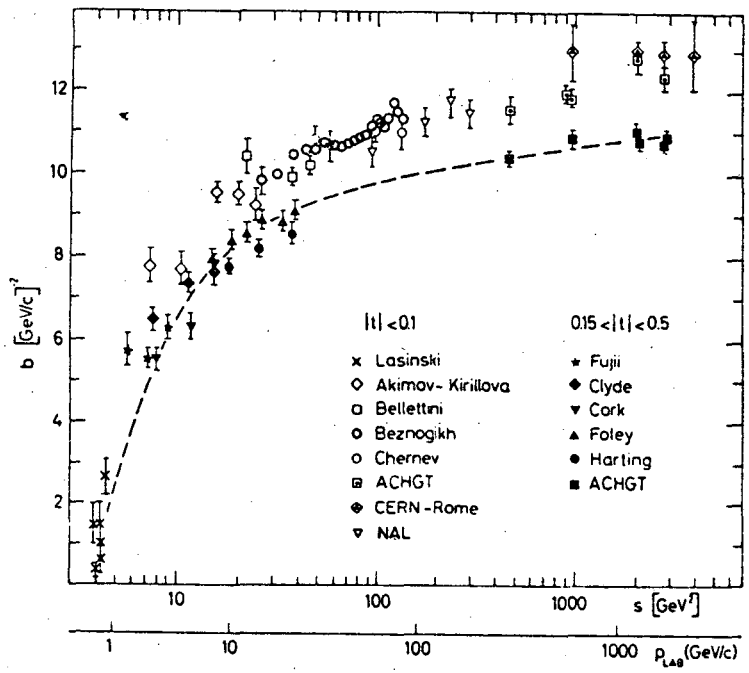

Fig. 6. The slope parameter $B(s,t)$ in $(\mathrm{GeV}/c)^{-2}$ for p-p elastic scattering versus s in $(\mathrm{GeV})^2$ for $0 < |t| < 0.1$ (open points) and $0.15 < |t| < 0.5$ $(\mathrm{GeV}/c)^2$ (solid points) (Fig. 14 of Giacomelli, 1972).

Figure 7 shows six examples of integrated cross sections for inelastic processes with nontrivial quantum number exchange in the t-channel (graphs from HERA reports, Bracci et al., 1972a,b). All these processes show a narrow forward peak in t; the integrated cross sections should, according to (3), show a power law behavior with an exponent corresponding to a value of $\alpha(t)$ at some small negative value of t. The compilers have in each case fitted a power law in $P_{lab}(\propto s)$ to the higher energy data. The six reactions, the anticipated t-channel exchanges, and the effective values of α deduced from the exponents, are

Reaction	Exchanges	Effective α
$\pi^- p \to \pi^0 n$	ρ	0.41 ± 0.07
$\pi^+ p \to \pi^0 \Delta^{++}$	ρ	0.48 ± 0.09
$\pi^- p \to \eta^0 n$	A_2	0.24 ± 0.09
$K^- p \to \bar{K}^0 n$	ρ, A_2	0.28 ± 0.12
$\pi^- p \to \rho^0 n$	π, A_2	0.06 ± 0.05
$\pi^- p \to \rho^+ p$	π, ω, A_2	0.04 ± 0.09 .

The first two reactions are classic ρ-exchange processes. The value $\alpha \simeq 0.4$-0.5 is in excellent agreement with a linear Regge trajectory $\alpha \simeq \frac{1}{2} + t$ that passes through the ρ $(J = 1^-,\ m_\rho^2 = 0.58 \pm 0.10\ \mathrm{GeV}^2)$ and the g $(J = 3^-,\ m_g^2 = 2.82 \pm 0.27\ \mathrm{GeV}^2)$. The third and fourth processes involve A_2 or A_2 and ρ exchange and seem to have a smaller effective α. Part of this may be a result of broader differential cross sections which sample more negative t values and so smaller $\alpha(t)$, but there is probably a residue that is evidence for the breaking of exact exchange degeneracy (EXD) of the even and

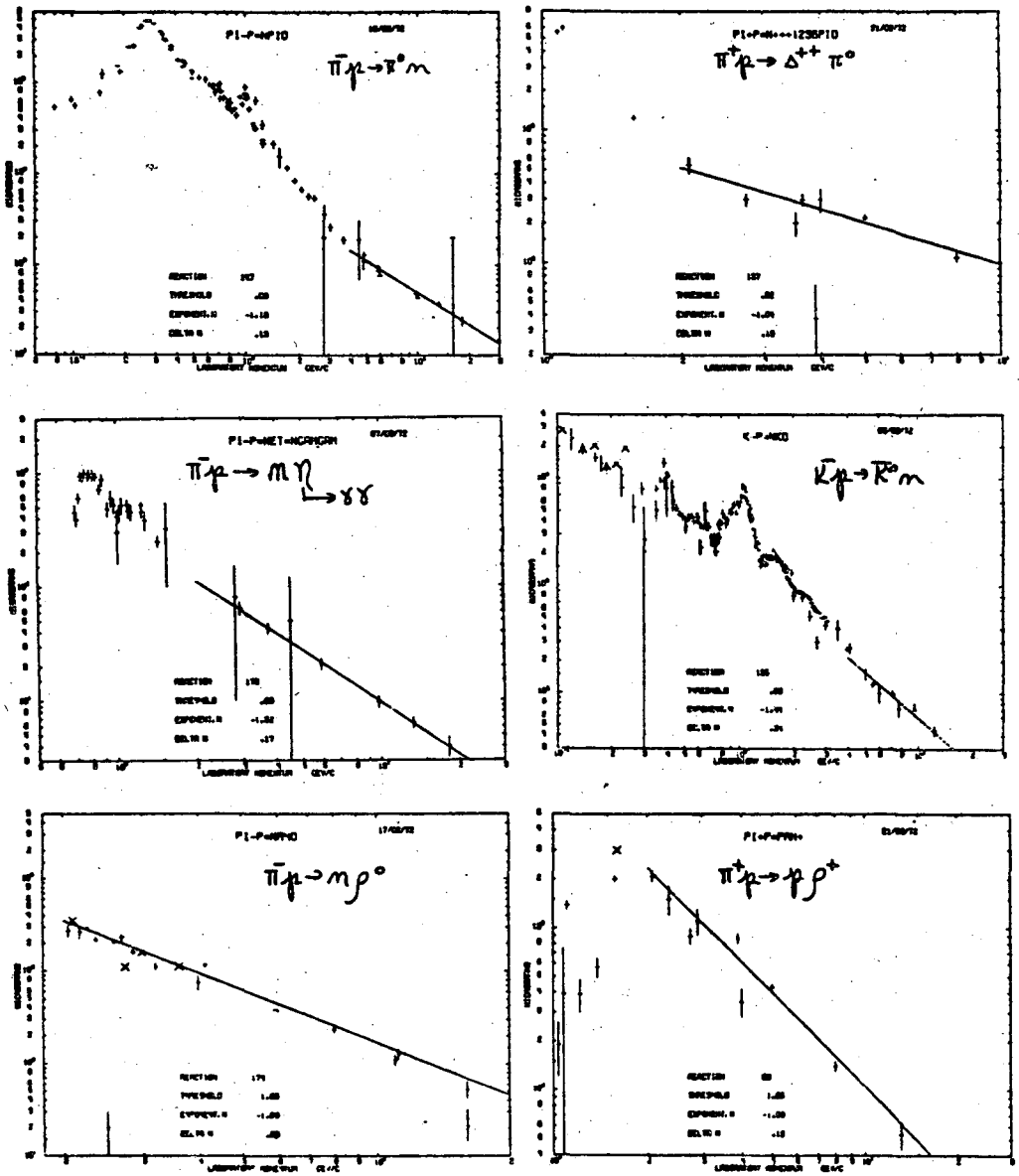

Fig. 7. Examples of the energy dependences of cross sections for inelastic processes with the exchange of mesonic quantum numbers in the t-channel. The data above a few GeV/c incident momentum are fitted with a power law, P^n_{Lab}. The exponents are given on each graph (Bracci et al., 1972a,b).

odd signatured Regge trajectories See Chapter III. The final pair of reactions, ρ-meson production with and without charge transfer in the t-channel, show a much faster falloff with energy $(\alpha \simeq 0^+)$. This behavior is consistent with pion exchange as the dominant mechanism, at least in the forward peak, and is supported by the characteristic population of the zero helicity state of the ρ-meson.

Other examples of power law behavior are less easy to understand, but the general trends are consistent and satisfying from a Regge exchange point of view. Barloutaud (1973) cites several more examples, including hypercharge (K^*, K^{**}) exchange reactions.

A final observation on power law behavior is that it has been traditional to parametrize the total cross sections shown in Fig. 1a with the form,

$$\sigma_i = a_i + b_i P_{Lab}^{-n_i} \tag{4}$$

with $n_i \simeq 1/2$, consistent with the intercept $\alpha(0) \simeq 0.5$ of the high lying Regge trajectories (ρ, ω, P', A_2). The range of exponents associated with the $\Delta\sigma$'s of Fig. 1b and more particularly the rising cross section shown in Fig. 2 show that (4) is at best a rough parametrization over a limited energy interval.

2. Crossing Symmetry, Signature, Power Law Behavior and Phase, Pomeranchuk Theorems

In order to discuss the phenomenology of total and elastic cross sections there are a few basic ideas that must be mentioned. These follow from the substitution law of field theory and from a modest amount of analyticity in the kinematic variables.

(a) Substitution law

Consider the process,

$$A + B \rightarrow C + D \qquad (5)$$

where the 4-momenta of the particles are a_μ, b_μ, c_μ, d_μ, respectively. For simplicity suppose that the particles are spinless. Then there is one invariant amplitude $\mathcal{M}(s,t,u)$ describing the scattering, where according to Appendix A.5 s,t, and u are the standard kinematic variables, $s = (a + b)^2$ being the square of the total energy in the c.m.s., and $t = (a - c)^2$, $u = (b - c)^2$ being momentum transfer variables. From field theory it is known, and it is generally accepted as having wider applicability, that the amplitudes for other related processes can be obtained from $\mathcal{M}(s,t,u)$ by substitution according to the substitution law. For example, if we leave the 4-momenta of B and D unchanged but substitute $a_\mu \rightarrow -\bar{a}_\mu$ and $c_\mu \rightarrow -\bar{c}_\mu$, then $s \rightarrow s' = (\bar{a} - b)^2$, $t \rightarrow t' = (\bar{a} - \bar{c})^2$, $u \rightarrow u' = (\bar{c} + b)^2$, and

$$\mathcal{M}(s,t,u) \rightarrow \mathcal{M}' = \mathcal{M}(s',t',u')$$

with the amplitude $\mathcal{M}'$, which is just the old amplitude $\mathcal{M}$ evaluated at a different point in the (s,t,u) space, describing the process,

$$\bar{C} + B \rightarrow \bar{A} + D \quad , \qquad (6)$$

where $\bar{A}$ and $\bar{C}$ are the antiparticles of A and C, respectively. Process (5) is called the s-channel process, process (6) the u-channel process, because s plays the role of the energy variable in (5)

while u plays that role for (6). The substitution $(a_\mu \rightarrow -\bar{a}_\mu$, $c_\mu \rightarrow -\bar{c}_\mu)$ is called crossing or line reversal, or more specifically s-u crossing because of the interchange of the roles of s and u.

(b) Crossing symmetry, analyticity, and signature

The idea that a single amplitude $\mathcal{M}(s,t,u)$ can, depending on the range of the variables, describe several processes is a very important concept. With s-u crossing in mind, we note that the constraint $s + t + u = m_a^2 + m_b^2 + m_c^2 + m_d^2$ indicates that for fixed t positive s requires generally a negative value of u and vice versa.* Thus positive u can be equally interpreted as negative s and the s-u crossing can be viewed as a transformation from the positive s region to the negative s region. It is useful to introduce a new variable,

$$\nu = \frac{1}{4m_b}(s - u) \qquad (7)$$

which together with t can be used as kinematic variables.

For elastic scattering in the forward direction $(t = 0)$ ν has the simple interpretation of the total laboratory energy of A (or the negative of the lab energy of $\bar{C}$).

The invariant amplitude $\mathcal{M}(\nu,t)$ satisfies a dispersion relation in ν at fixed t. The dispersion relation follows from the

---

* This can be seen most easily at high energies where masses can be neglected. Then the constraint is $s + t + u \simeq 0$ and (A.16) and (A.18) show that for large positive s, the range of t is $-s \leq t \leq 0$.

analyticity of $\mathcal{M}(\nu,t)$ in the cut ν plane, as shown schematically in Fig. 8. The cut structure along the positive and negative real axes stems from unitarity in a familiar way, the s-channel thresholds opening up on the right and the u-channel on the left. The physical amplitude for the s-channel process $A + B \to C + D$ is obtained by letting ν approach the positive real axis from above, indicated by $\nu + i\epsilon$. For the u-channel process $\bar{C} + B \to \bar{A} + D$ the physical region is just below the cut for ν negative.

The physical amplitudes for the s- and u-channel processes can be written

$$\mathcal{M}_s(\nu,t) = \mathcal{M}(\nu + i\epsilon,t)$$
$$\mathcal{M}_u(\nu,t) = \mathcal{M}(-\nu - i\epsilon,t) \quad . \tag{8}$$

It is useful to consider instead of $\mathcal{M}_s$ and $\mathcal{M}_u$ amplitudes that are even and odd in ν. We thus define for complex as well as real ν the even and odd amplitudes:

$$\mathcal{M}^{(\pm)}(\nu,t) = \tfrac{1}{2}[\mathcal{M}_s(\nu,t) \pm \mathcal{M}_u(\nu,t)] \quad . \tag{9}$$

(Sometimes these are called crossing-even or crossing-odd amplitudes.) These amplitudes satisfy dispersion relations of the form,

$$\mathcal{M}^{(\pm)}(\nu,t) = \frac{1}{\pi}\int_0^\infty d\nu' \, \mathrm{Im}\, \mathcal{M}^{(\pm)}(\nu',t)\left[\frac{1}{\nu' - \nu} \pm \frac{1}{\nu' + \nu}\right] . \tag{10}$$

In (10) the pole terms are implicit in the integral and the necessity of subtractions has been ignored.

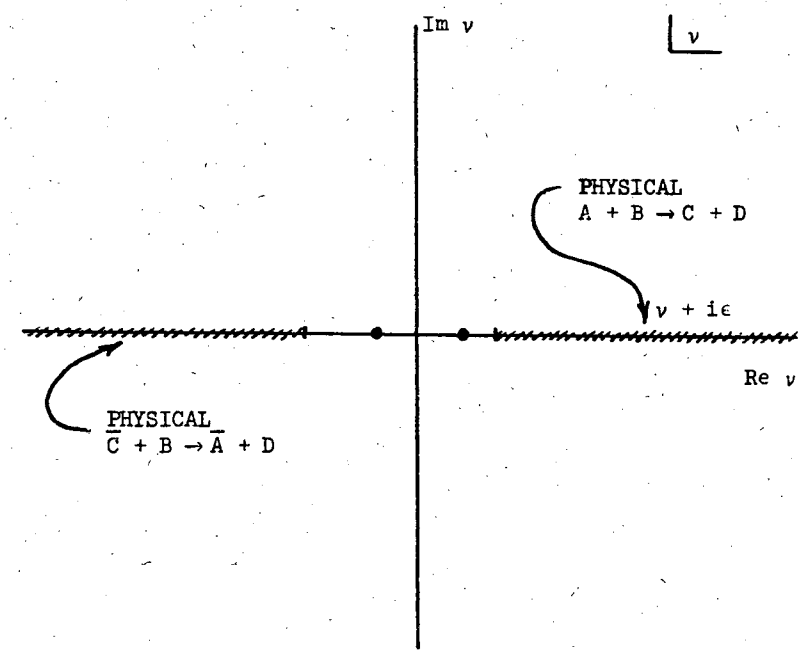

Fig. 8. The complex ν plane showing schematically the branch cut and pole structure of the scattering amplitude. For $A + B \to C + D$ the physical region is just above the right-hand cut, for $\bar{C} + B \to \bar{A} + D$ it is just below the left-hand cut.

The distinction between crossing-even and crossing-odd amplitudes has physical meaning when the amplitudes are considered in the t-channel ($A\bar{C} \to \bar{B}D$). Here t is the energy variable and s and u are momentum transfer variables related to the scattering angle θ_t. From Eq. (A.20) we see that for elastic scattering at least (actually $m_a = m_c$ or $m_b = m_d$ is sufficient)

$$\nu = \frac{p_t\, p_t'}{m_b} \cos \theta_t \,. \tag{11}$$

Since p_t and p_t' are just functions of t, ν is equivalent in the t-channel to $\cos \theta_t$. Now in discussing the dynamics of Regge exchanges in the t-channel one first considers a partial wave expansion. Then because of the possibility of Majorana exchange forces (see Blatt and Weisskopf, 1952, p. 136, for this ancient terminology) one considers separately the forces occurring in the even partial waves and the odd partial waves. The Regge poles that arise from these two sets of forces are different in general.

The poles coming from the even (odd) partial waves and having physical particles with even (odd) J values are called even (odd) signature Regge poles.

Because of the connection (11) between ν and $\cos \theta_t$ it is evident that for t-channel exchanges even-signature Regge poles contribute only to crossing-even amplitudes and odd-signature to crossing-odd amplitudes. Examples of even-signature Regge trajectories are the $P' \equiv f$ with the f^0 meson ($I = 0$, $J^P = 2^+$, $m^2 = 1.60\ \mathrm{GeV}^2$) as an observed physical state, the A_2 with the A_2 meson ($I = 1$, $J^P = 2^+$, $m^2 = 1.72$) and the K^{**} with the K^{**}-meson ($I = \frac{1}{2}$,

$J^P = 2^+$, $m^2 = 2.02$). Some odd-signature Regge trajectories are the ρ with the ρ-meson ($I = 1$, $J^P = 1^-$, $m^2 = 0.58$) and the g-meson ($I = 1$, $J^P = 3^-$, $m^2 = 2.82$) as physical states, the ω with the ω-meson ($I = 0$, $J^P = 1^-$, $m^2 = 0.61$), and the K^* with the K^*-meson ($I = \frac{1}{2}$, $J^P = 1^-$, $m^2 = 0.79$) as particles.

(c) Power law behavior and associated phase, Pomeranchuk theorems

The evidence presented in Fig. 7 shows that high-energy reaction amplitudes exhibit power law behavior in the energy, at least approximately. Such behavior has important consequences for the phase of the amplitudes. The operative theorem of complex variables [for we do need to assume analyticity of the type displayed in Fig. 8 or Eq. (10)] is the Phragmén-Lindelöf theorem (Titchmarsh, 1950, p. 183; Eden, 1967, p. 194). The application of the theorem is straightforward. We only state the results relevant for our purposes.

Let us assume the following properties for $\mathcal{M}(\nu,t)$ at fixed t:

(i) $\mathcal{M}(\nu,t)$ is analytic in the upper half ν plane,

(ii) $\mathcal{M}(\nu,t)$ does not increase exponentially for $|\nu| \to \infty$,

(iii) $\mathcal{M}(\nu,t) \to c(t)\, \nu^{\alpha(t)} (\ln \nu)^{\beta(t)}$ as $\nu \to \infty$ along the positive real axis, where $\alpha(t)$ and $\beta(t)$ are real functions of t,

(iv) $\mathcal{M}(\nu,t) \to \bar{c}(t)(-\nu)^{\alpha(t)} \left(\ln(-\nu)\right)^{\beta(t)}$ as $\nu \to -\infty$ along the negative real axis.

Note that $\alpha(t)$ and $\beta(t)$ are the same in both limits, but $c(t)$ and $\bar{c}(t)$ are in principle different complex functions of t.

Application of the Phragmén-Lindelöf theorem establishes that

$$c(t) = \bar{c}(t)^* e^{-i\pi\alpha(t)} . \tag{12}$$

Suppose that $\mathcal{M}(\nu,t)$ is crossing-even. Then $\bar{c}(t) = c(t) = c^{(+)}(t)$ and (12) yields

$$c^{(+)}(t) = \pm|c(t)|e^{-i\pi\alpha^{(+)}(t)/2} = \gamma^{(+)}(t)\left(i - \cot\frac{\pi\alpha^{(+)}(t)}{2}\right) \tag{13}$$

where $\gamma^{(+)}(t)$ is real. If $\mathcal{M}(\nu,t)$ is odd under crossing, $\bar{c}(t) = -c(t) = -c^{(-)}(t)$ and (12) gives

$$c^{(-)}(t) = \pm i|c(t)|e^{-i\pi\alpha^{(-)}(t)/2} = \gamma^{(-)}(t)\left(i + \tan\frac{\pi\alpha^{(-)}(t)}{2}\right) \tag{14}$$

and $\gamma^{(-)}(t)$ is real. The phases given by (13) and (14) are the same as those that occur for even and odd signature Regge poles. The Regge amplitudes are of the form,

$$R^{(\pm)} \propto \frac{P_{\alpha^{(\pm)}(t)}(-\cos\theta_t) \pm P_{\alpha^{(\pm)}(t)}(\cos\theta_t)}{\sin\pi\alpha^{(\pm)}(t)} .$$

Using (11) and assuming that ν is large we find

$$R^{(\pm)} \propto \frac{(-\nu)^{\alpha^{(\pm)}(t)} \pm (\nu)^{\alpha^{(\pm)}(t)}}{\sin\pi\alpha^{(\pm)}(t)}$$

$$\propto \nu^{\alpha^{(\pm)}(t)} \begin{Bmatrix} i - \cot\pi\alpha^{(+)}(t)/2 \\ \\ i + \tan\pi\alpha^{(-)}(t)/2 \end{Bmatrix} \tag{15}$$

The results (13) and (14) are more general, however, since they follow even if there is a $(\ln\nu)^{\beta(t)}$ variation of the amplitude times the power law behavior.

The result (12) allows some other conclusions:

(i) Equality of elastic differential cross sections for particle and antiparticle scattering:

$$\lim_{\nu\to\infty}\left[\frac{d\sigma}{dt}(\bar{A}B \to \bar{A}B)/\frac{d\sigma}{dt}(AB \to AB)\right] = 1 . \tag{16}$$

(ii) Pomeranchuk theorem of equality of particle and antiparticle total cross sections:

$$\lim_{\nu\to\infty}[\sigma_t(\bar{A}B)/\sigma_t(AB)] = 1 , \tag{17}$$

provided $\alpha(0) = 1$. Pomeranchuk's original proof, based only on dispersion relations like (10), assumed $\sigma_t \to$ constant and required the weak condition, $\mathrm{Re}\,\mathcal{M}(\nu,0)/\mathrm{Im}\,\mathcal{M}(\nu,0)\,\ln\nu \to 0$. The present proof permits logarithmic variation of σ_t, but has the stricter assumption $\mathrm{Re}\,\mathcal{M}(\nu,0)/\mathrm{Im}\,\mathcal{M}(\nu,0) \to$ constant (perhaps zero). Needless to say, with the results of Fig. 2 known, there are more general proofs (e.g., Grunberg and Truong, 1973). Similarly, Eq. (16) has been put on a firm and general footing for 2-body inelastic as well as elastic scattering by Cornille and Martin (1972).

The extent of the testing of (16) and (17) can be judged by inspection of Fig. 1 and 2 for total cross sections and Fig. 9 for the differential cross sections where the slope parameter defined in Eq. (1) is shown for π^+p, π^-p, K^+p, K^-p, pp, and $\bar{p}p$ elastic scattering.

Cetainly the trends of the data in these figures support the asymptotic validity of (16) and (17), but as the data of Fig. 2 show

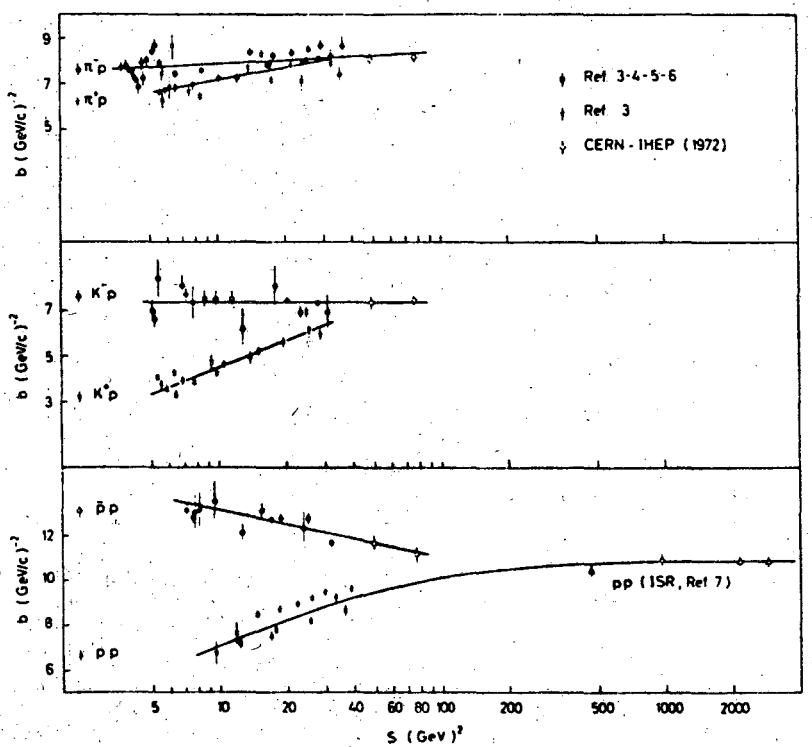

Fig. 9. Slope parameters for $\pi^{\pm}$, $K^{\pm}$, and $p^{\pm}$ elastic scattering cross sections on hydrogen as a function of s, obtained from a fit of $d\sigma/dt$ to an exponential in t over the range $0.1 < |t| < 0.4$ $(GeV/c)^2$ (Figure 18 of Giacomelli, 1972).

asymptopia may be far away. Experiments with meson and antiproton beams at NAL are eagerly awaited.

3. Froissart bound

On the basis of the analyticity in s and t contained in the Mandelstam representation Froissart (1961) proved that the total cross section is bounded from above according to

$$\sigma_t < C(\ell n\ s)^2 \tag{18}$$

as $s \to \infty$. The right-hand side of (18) is called the Froissart bound. Its derivation has been generalized, simplified, made more rigorous, made plausible by many (not the same!) authors (e.g., Martin, 1963, 1966; Eden, 1967; Eden, 1971; Roy, 1972; Horn and Zachariasen, 1973). We will therefore not discuss the careful proofs, but confine our attention to the physical intuitive aspects.

Suppose that the interaction between two spinless particles is mediated by the exchange of a particle of spin J and mass μ in the t-channel. Then the lowest order amplitude will be real and at high energies of the form,*

$$F_B(s,t) = g^2 \frac{s^J}{\mu^2 - t} . \tag{19}$$

* In the t-channel the single partial wave $\ell = J$ gives rise to a numerator proportional to barrier penetration factors $(p_t p_t')^J$ times $P_J(\cos\theta_t)$. At high energies in the s-channel, (11) leads to the stated form.

If we use the eikonal approximation (discussed in Appendix C) as an approximation to the full scattering amplitude, we obtain via Eq. (C.14) an eikonal phase,

$$\delta_{\text{eikonal}}(s,b) = g^2 s^{J-1} K_0(\mu b) . \tag{20}$$

The behavior of δ as a function of b is indicated in the top part of Fig. 10. Asymptotically the modified Bessel function falls off as $\exp(-\mu b)/(\mu b)^{\frac{1}{2}}$. Hence the phase shift is small compared to unity provided

$$\mu b \gg \mu b_c = \ln(g^2 s^{J-1}) . \tag{21}$$

The square of the partial wave scattering amplitude is sketched in the bottom part of Fig. 10. It is small compared with unity for $\mu b \gg \mu b_c$, rises to unity for $\mu b \lesssim \mu b_c$ and with the example of a real phase shift (20) oscillates between zero and unity for smaller values of μb. The integral (B.25) defining the elastic cross section (equal to the total here) can be estimated to be

$$\sigma_{e\ell} = \sigma_t \simeq 4\pi \int_0^{b_c} d(b^2) \times \frac{1}{2} = 2\pi b_c^2 . \tag{22}$$

With the critical impact parameter given by (21) we obtain at high energies the estimate,

$$\sigma_t \sim \frac{2\pi}{\mu^2}(J-1)^2(\ln s)^2 . \tag{23}$$

Note that (23) only has meaning for $J > 1$. For $J = 1$ the phase (20) is independent of s. This would lead to a constant cross

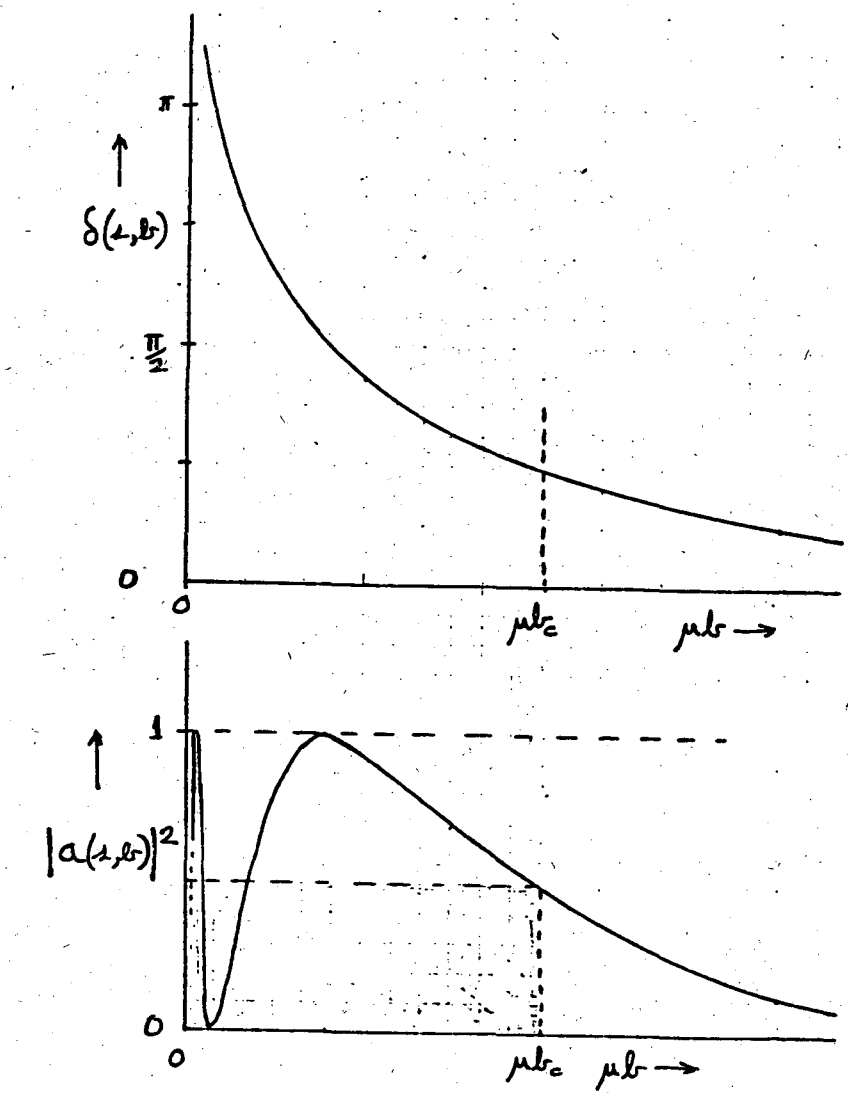

Fig. 10. Phase shift $\delta(s,b)$ as a function of impact parameter (top) and absolute square $|a(s,b)|^2$ of the partial wave amplitude as a function of impact parameter (bottom).

section. For $J < 1$, μb_c decreases with increasing s; the phase is small at all impact paramters and the cross sections fall with s.

While the above example is somewhat unrealistic it does show how unitarization via the eikonal partial wave representation imposes the Froissart bound on the full amplitude even though the lowest order approximation (the t-channel exchange of something) may increase as a high power of s and violate the Froissart bound itself. This is, of course, related very intimately to Froissart's original proof.

A more realistic example would have had the phase shift becoming complex for $b < b_c$. Then the partial wave amplitude (B.26) would rapidly approach $i/2$ for $b < b_c$. Using (B.25) for σ_t and the above method of estimation we would still arrive at (22) for the total cross section, but would find $\sigma_{e\ell} \simeq \sigma_t/2$.

The exchange of a Regge pole as the lowest order amplitude affords an instructive example of a complex phase shift and some subtleties in impact parameter space. For definiteness, consider the exchange of an even-signature Regge pole with amplitude,

$$F_B(s,t) = -\beta\, e^{\gamma t}\, e^{-i\frac{\pi}{2}\alpha(t)}\, s^{\alpha(t)}$$

where β and γ are real, $\beta > 0$, and the exponential residue is chosen for convenience. With a linear Regge trajectory, $\alpha(t) = \alpha(0) + \alpha'(0)t$, this can be written

$$\left.\begin{aligned} F_B(s,t) &= -\beta(-is)^{\alpha(0)}\, e^{B(s)t/2} \\ \text{where} \quad & \\ \tfrac{1}{2}\, B(s) &= \gamma + \alpha'(0)\, \ell n(-is) \end{aligned}\right\} \qquad (24)$$

From (C.16) we deduce that the eikonal phase shift is

$$\delta_{\text{eikonal}}(s,b) = i\beta\, \frac{(-is)^{\alpha(0)-1}}{B(s)} \cdot e^{-b^2/2B(s)} \quad . \qquad (25)$$

At high energies $B(s)$ is predominantly real with a small negative imaginary part. Thus the phase of δ is determined almost entirely by the factor, $i^2 \exp[-i\,\frac{\pi}{2}\,\alpha(0)]$. For $0 < \alpha(0) < 2$, this factor has a positive imaginary part.* For fixed impact parameter the power law increase in the magnitude of δ implies that for $1 < \alpha(0) < 2$ the phase shift will develop a large positive imaginary part and $e^{2i\delta} \to 0$ rapidly as $s \to \infty$. Another way to look at it is that $e^{2i\delta} \simeq 0$ for all values of b less than a critical value b_c that grows with energy. From (B.25) or (B.27) the total cross section will be given roughly by (22). All that remains is to estimate b_c.

To estimate b_c from (25) we rewrite it as

$$\delta_{\text{eikonal}}(s,b) = \frac{i\beta}{B(s)} \exp[\big(\alpha(0) - 1\big)\, \ell n(-is) - b^2/2B(s)]. \qquad (26)$$

Evidently whatever the value of β, the imaginary part of δ will be very large until the second term in the exponent overcomes the first. This defines the critical impact parameter,

$$b_c^{\,2} = 2B(s)[\alpha(0) - 1]\ell n\, s \qquad (27)$$

---

* The intercept $\alpha(0)$ is expected to be smaller than 2 on the basis of a theorem by Jin and Martin (1964) concerning the number of subtractions necessary in fixed-t dispersion relations.

Note that if $B(s)$ were in fact independent of s, as occurs if the Regge trajectory has zero slope, the total cross section would grow only as $\ln s$, not as $(\ln s)^2$. This is just what we would expect with a phase shift that was a Gaussian of fixed shape rather than an exponential in impact paramter as was our elementary particle exchange. Assuming $\alpha'(0) \neq 0$, however, we obtain at high enough energies the estimate,

$$b_c^2 \simeq 4\,\alpha'(0)[\alpha(0) - 1](\ln s)^2 . \tag{28}$$

The Yukawa (exponential) force and the Regge (Gaussian) force thus both give the same s-dependence. The Regge exchange does it in a sneaky way, however, by having the mean square radius of the Gaussian grow as $\ln s$, as well as having its magnitude increase as a power of s.

As already implied by the earlier discussion, if the full amplitude is described at high energies by a single Regge pole then the Froissart bound is violated if $\alpha(0) > 1$. Since total cross sections do not seem to decrease with energy it was natural within a Regge pole framework to assume that the leading Regge pole had $\alpha(0) = 1$. The pole, with the internal quantum numbers of the vacuum ($Q = 0$, $I = 0$, $Y = 0$, $B = 0, \cdots$), is known as the Pomeranchuk pole or pomeron. It occupies a unique position--it is the highest lying Regge trajectory; furthermore, it does not seem to have any particles associated with it and also seems to have an abnormally small slope (cf. the shrinkage of the forward peak in $d\sigma/dt$ for pp scattering, Fig. 6). The last two points have inevitably raised doubts in many minds as to whether diffraction scattering is properly described by a Regge pole. We now tend to speak of a Pomeranchuk singularity,

leaving deliberately vague the type of singularity in the angular momentum plane. At some point, of course, the J-plane description may become so complicated as to be uneconomical and therefore inappropriate.

An alternative description of diffractive scattering is advocated by Cheng and Wu on the basis of a long study of massive quantum electrodynamics at very high energies (see Cheng and Wu, 1970, and the references cited there). They show that the leading behavior as $s \to \infty$ at small t is given by the "one-tower" diagrams shown in Fig. 11. We call the sum of leading contributions of all the one-tower

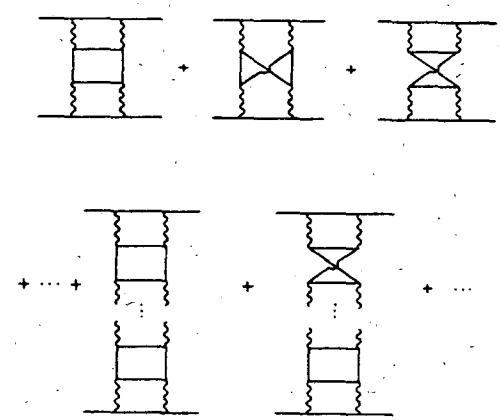

Fig. 11. One-tower diagrams in QED. These diagrams give the leading s dependence at high energies (Cheng and Wu, 1970).

diagrams a single-tower exchange. The general form of this amplitude is

$$F_B(s,t) \sim \frac{i\, s^{1+a}}{(\ln s)^n} f(t) \tag{29}$$

where a is real and positive ($a = 11\pi\,\alpha^2/32$, where α is the fine structure constant) and $n = 2$ in spinor QED. In Regge language this amplitude corresponds to the exchange of a fixed singularity (a cut) in the J-plane with $J > 1$. Cheng and Wu postulate, with plausible theoretical and physical arguments, that this single-tower exchange amplitude is a Born approximation whose two-dimensional Fourier transform gives the eikonal phase. The real function $f(t)$ is such that at large impact parameters $\delta(s,b) \propto e^{-\mu b}$ where $\mu < 2m_V$, m_V being the mass of the "photon" (vector meson). Apart from the logarithmic factors in (29) the Cheng and Wu eikonal phase shift is thus qualitatively similar to the elementary particle exchange (20) with $J = 1 + \epsilon$. In the phenomenological fits (Cheng, Walker, and Wu, 1973a,b) the complicated and not totally explicit phase shift is approximated by

$$\delta_{cww}(s,b) = \frac{i}{2} f_j \frac{(-iE)^c}{[\ell n(-iE)]^n} \cdot \exp\left[-\lambda\sqrt{b^2 + b_{0j}^{\,2}}\right] . \qquad (30)$$

Here E is the lab energy of the incident particle, c and λ are fundamental parameters that are the same for all processes, while f_j and b_{0j} are different constants for πp, Kp, and pp scattering, but the same for particle-proton and antiparticle-proton scattering. Since (30) represents only the diffractive scattering contribution, fits to total cross section data at energies of the order of 2-30 GeV/c require an additional term, taken to be $A_j\, E^{-1/2}$, with A_j different for all six processes. With 14 parameters an adequate fit is obtained to all the total cross section data shown in Figs. 1 and 2, obviously including the rising pp cross section at ISR energies. With $n = 0$ in (30), the parameter $c = 0.083$; with $n = 1$, $c = 0.20$.

The fixed J-plane singularity is only slighly above unity. The estimate analogous to (23) is

$$\sigma_t \sim \frac{2\pi}{\mu^2}\left[\ell n\left(\frac{s^c}{(\ell n\, s)^n}\right)\right]^2 .$$

Ultimately this gives a $(\ell n\, s)^2$ behavior with $\sigma_{e\ell}/\sigma_t = 1/2$, characteristic of a totally absorbing disc with a logarithmically growing radius, but the smallness of c and the presence of the $(\ell n\, s)^n$ factor in the denominator makes asymptopia very far away.

4. Ratio of Real to Imaginary Part of the Forward Scattering Amplitude

Variation in energy of the real part of the forward scattering amplitude has traditionally been associated with structure in the total cross section, the classical optical dispersion of the index of refraction being the most familiar example. Experts in dispersion relations continue to polish the data and the equations in the resonance region and extend them to higher and higher energies. But in the classical age (denoted, I suppose, by B.I.S.R.) when 30 or 70 GeV was considered high energy the interest in real parts was not widespread. Above the resonance region ($P_{lab} > 5$ GeV/c) the ratios of real to imaginary parts, usually denoted in the literature by $\rho(s)$ or $\alpha(s)$, are small and appear to decrease in magnitude smoothly with increasing energy. The ratios tend to be negative (only K^-p is positive; $\bar{p}p$ is nearly zero), with the pp and K^+p values largest in absolute value, of order -0.3 or -0.4 at 5 GeV/c and -0.2 at 30 GeV/c.

The rising total cross section for proton-proton interactions arouses interest in the real parts again. The monotonic decrease in magnitude of the ratio of real to imaginary part is cast in doubt. There is a fancy theorem (Khuri and Kinoshita, 1965) that states that if the total cross section continues to increase with energy then eventually $\rho(s)$ must become positive and stay positive; any approach to zero must be from above. On the experimental side there are recent ISR data (Amaldi et al., 1973a) giving slightly positive or zero values, implying a change of sign of $\rho(s)$ for p-p scattering at ISR energies or below.

We discuss here a simple "do-it-yourself" way of understanding and calculating $\rho(s)$ from data on the total cross section. The method is not efficient (though applicable in principle) when cross sections vary rapidly with energy, but works admirably above the resonance region. Like dispersion relations it is based on analyticity of forward (or fixed t) amplitudes in energy. No integration is necessary, however; only differentiation! First a small amount of elementary complex variable theory. Let $f(z)$ be analytic inside some region of the complex z-plane. For points within that region, $f(z + \lambda)$ can be represented by a Taylor series expansion of $f(z)$:

$$f(z + \lambda) = f(z) + \lambda f'(z) + \frac{\lambda^2}{2!} f''(z) + \cdots .$$

The series converges and represents $f(z + \lambda)$ uniquely provided the point $z + \lambda$ lies inside the circle of convergence defined by the distance from the point z to the nearest singularity of $f(z)$. This Taylor series can be represented compactly by the formal operator statement,

$$f(z + \lambda) = \exp\left(\lambda \frac{d}{dz}\right) f(z) . \tag{31}$$

That is all the complex variable theory we will need.

Now consider the scattering amplitude $F(\nu,t)$ for the s-channel process, $ab \to ab$, where $\nu = (s - u)/4m_b$ and t is the momentum transfer variable. The u-channel process, $\bar{a}b \to \bar{a}b$, is described by the amplitude $\bar{F}(\nu,t)$. The domain of analyticity in ν of $F(\nu,t)$ is shown schematically in the top part of Fig. 12. From the substitution law we know that $\bar{F}(\nu,t) = F(-\nu,t)$, as indicated in Fig. 12 by

the relationship of the points A and C. It is convenient to define symmetric and antisymmetric combinations of amplitudes,

$$F_{\pm}(\nu,t) = \frac{1}{2}[F(\nu,t) \pm F(-\nu,t)] \tag{32}$$

F_+ is said to be even under crossing $(\nu \to -\nu)$, and F_- odd. The s-channel process then has an amplitude,

$$\left.\begin{aligned} F_s(\nu,t) &= F_+(\nu,t) + F_-(\nu,t) \ , \\ &\text{while the u-channel amplitude is} \\ F_u(\nu,t) &= F_+(\nu,t) - F_-(\nu,t) \end{aligned}\right\} \ . \tag{33}$$

We wish to compare amplitudes at the points A and B of Fig. 12. We thus use the Schwarz reflection law for real analytic functions to obtain

$$F_{\pm}(\nu e^{i\pi^-}) = \pm F_{\pm}^*(\nu) \ . \tag{34}$$

In Eq. (34) and subsequent equations I suppress the fixed argument t for brevity.

Suppose now that we choose to use the variable $\xi = \ln \nu$ instead of ν to describe the energy variation of our amplitudes. The analytic structure in the ξ plane is sketched in the bottom part of Fig. 12. We see that now the points A and B are related by a displacement of $i\pi^-$, i.e., $\nu \to \nu e^{i\pi^-}$ is equivalent to $\xi \to \xi + i\pi^-$. We wish to use the Taylor series representation (31) to express the left-hand side of (34), $F_{\pm}$ at the point B, in terms of the function and its derivatives at A. Because of the branch cuts this cannot be done instantly. We must use analytic continuation. First we express

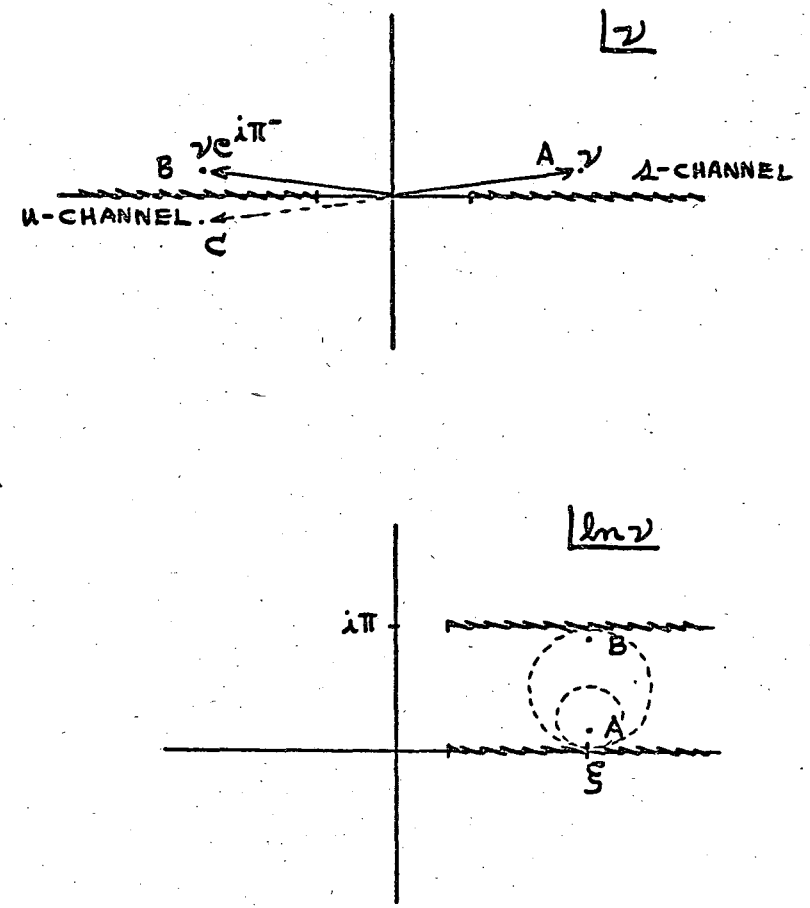

Fig. 12

$F_\pm(\xi + i\pi)$ as a Taylor series expansion around the point $\xi + i\,\frac{\pi}{2}$ (the center of the large circle in Fig. 12):

$$F_\pm(\xi + i\pi) = \exp\left(i\,\frac{\pi}{2}\,\frac{d}{d\xi}\right) F_\pm\left(\xi + i\,\frac{\pi}{2}\right) .$$

Then we express $F_\pm(\xi + i\,\frac{\pi}{2})$ as a Taylor series expansion around the point $\xi + i\,\frac{\pi}{4}$ (the center of the smaller circle in Fig. 12), and so on. The result is

$$F_\pm(\xi + i\pi) = \exp\left[i\,\frac{\pi}{2}\,\frac{d}{d\xi}\left(1 + \frac{1}{2} + \frac{1}{2^2} + \frac{1}{2^3} + \cdots\right)\right] F_\pm(\xi)$$

$$= \exp\left(i\pi\,\frac{d}{d\xi}\right) F_\pm(\xi) .$$

The final expression is just what we would have obtained by blind use of the Taylor series (31) with $\lambda = i\pi$. Our derivation lacks rigor because, among other things, the sequence of successive Taylor series expansions is infinite. Never mind; use the result in (34) to obtain

$$\exp\left(i\pi\,\frac{d}{d\xi}\right) F_\pm(\xi) = \pm F_\pm^*(\xi) . \tag{35}$$

Equation (35) can be put in a more symmetric form by operating on both sides with $\exp\left(-i\,\frac{\pi}{2}\,\frac{d}{d\xi}\right)$:

$$e^{i\frac{\pi}{2}\frac{d}{d\xi}} F_\pm(\xi) = \pm\left[e^{i\frac{\pi}{2}\frac{d}{d\xi}} F_\pm(\xi)\right]^* . \tag{36}$$

Writing out the real and imaginary parts of both sides we find for <u>even</u> amplitudes the relation,

$$\mathrm{Im}\, F_+(\xi) = -\tan\left(\frac{\pi}{2}\,\frac{d}{d\xi}\right) \mathrm{Re}\, F_+(\xi) \tag{37}$$

and for <u>odd</u> amplitudes,

$$\mathrm{Re}\, F_-(\xi) = \tan\left(\frac{\pi}{2}\,\frac{d}{d\xi}\right) \mathrm{Im}\, F_-(\xi) . \tag{38}$$

These two formal equations were noted by John Bronzan in a talk at Argonne National Laboratory in March, 1973. Their application to the real world was impressed upon me by Gordon Kane. (They may be well known to Andre Martin and others.)

Before using (37) and (38) for p-p scattering I make a few observations. Firstly, for amplitudes having power-law behavior in ν these relations yield immediately the standard Regge phase of the amplitude, a result usually deduced from the Phragmén-Lindelöf theorem (e.g., Eden, 1967, p. 194). The reader can check that amplitudes varying as $\nu^\alpha(\ln \nu)^\beta$ have the standard phase with corrections or order $(\ln \nu)^{-1}$, as expected. The second observation is that if the functions on the right-hand sides of (37) and (38) are approximated by <u>finite</u> polynomials in ξ the infinitely many differentiations implied by

$$\tan\left(\frac{\pi}{2}\,\frac{d}{d\xi}\right) = \frac{\pi}{2}\,\frac{d}{d\xi} + \frac{1}{3}\left(\frac{\pi}{2}\right)^3 \frac{d^3}{d\xi^3} + \cdots$$

terminate in a finite number. Thus the nonlocality inherent in the equations (and equivalent to a dispersion relation) is replaced in practice by a local or semilocal connection. Note that with a quadratic approximation in ξ only the first derivative contributes. Since cross section data above the resonance region can invariably be approximated, at least locally, by a quadratic form in ξ or a power law in ν, Eqs. (37) and (38) yield simple connections between real and

imaginary parts.* A corollary is that the behavior of $\rho(\xi)$ at any energy is determined almost completely by the energy variation of σ_t in the immediate neighborhood. Nothing can be learned about asymptopia from the magnitude or energy dependence of $\rho(\xi)$ at finite energies.

For applications to scattering data it is convenient to introduce amplitudes $f_\pm$ that differ from the customary invariant amplitudes by one power of ν and are normalized so that

$$\sigma_t = \mathrm{IM}\, f \quad . \tag{39}$$

For proton-proton and antiproton-proton scattering we define $\sigma_\pm = \frac{1}{2}\left(\sigma_{\bar{p}p} \pm \sigma_{pp}\right)$ so that $\sigma_{pp} = \sigma_+ - \sigma_-$ and $\sigma_{\bar{p}p} = \sigma_+ + \sigma_-$. The corresponding amplitudes are denoted by $f_\pm(\xi)$. For the imaginary part of the odd amplitude (actually even under crossing because of our division by ν), we take the parametrization of Denisov et al. (1971):

$$\sigma_- = \mathrm{Im}\, f_- = A[P_{LAB}(\mathrm{GeV}/c)]^{-n}$$

with $a = 28.4 \pm 2.7$ mb and $n = 0.61 \pm 0.03$. Since $P_{Lab} \simeq \nu$ at Serpukhov energies this power-law behavior yields

$$\mathrm{Re}\, f_-(\xi) = \cot\left(\frac{\pi}{2} n\right) \sigma_-(\xi) \quad . \tag{40}$$

---

* The use of the approximate relations $\mathrm{Im}\, F_+ \simeq -\frac{\pi}{2}\frac{d}{d\xi}\mathrm{Re}\, F_+$ and $\mathrm{Re}\, F_- \simeq \frac{\pi}{2}\frac{d}{d\xi}\mathrm{Im}\, F_-$ resulting from keeping only the first term in the expansion of the tangent have been employed in the past, but not based on (37) and (38) and not with a clear explanation of what approximation was involved, at least to my knowledge.

For the amplitude $f_+(\xi)$ we use (38) to find*

$$\mathrm{Re}\, f_+(\xi) = \tan\left(\frac{\pi}{2}\frac{d}{d\xi}\right)\sigma_+(\xi) \quad . \tag{41}$$

With a quadratic form for σ_+,

$$\left.\begin{aligned} &\sigma_+(\xi) \simeq a + b\xi + c\xi^2 \,, \\ &\text{we have} \\ &\mathrm{Re}\, f_+(\xi) = \frac{\pi}{2}\frac{d}{d\xi}\sigma_+(\xi) = \frac{\pi}{2}(b + 2c\xi) \end{aligned}\right\} \quad . \tag{42}$$

Then we have the ratio of real to imaginary parts for proton-proton scattering given by

$$\rho_{pp}(\xi) = \frac{\frac{\pi}{2}(b + 2c\xi) - \cot\left(\frac{\pi n}{2}\right)\sigma_-(\xi)}{\sigma_+(\xi) - \sigma_-(\xi)} \quad . \tag{43}$$

The corresponding quantity for antiproton-proton scattering is

$$\rho_{\bar{p}p}(\xi) = \frac{\frac{\pi}{2}(b + 2c\xi + \cot\left(\frac{\pi n}{2}\right)\sigma_-(\xi)}{\sigma_+(\xi) + \sigma_-(\xi)} \quad . \tag{44}$$

---

* There is a subtlety here. The usual amplitude $F_+(\xi)$ satisfies (37). It is obvious that an additive real constant to F_+ will not affect the imaginary part calculated from (37). Correspondingly, the real part computed from (41) is uncertain by a term (c/ν). The ambiguity is equivalent to an unknown subtraction constant in a dispersion relation or in a parametrized form satisfying analyticity and crossing requirements (Bourrely and Fischer, 1973). Such a contribution vanishes exponentially (in ξ). Since we are concerned only with the high energy behavior we shall omit it.

The same general forms for $\rho(\xi)$ hold for π^+p and π^-p and K^+p and K^-p scattering as for pp and $\bar{p}p$. The behavior of the various $\rho(\xi)$ in the range from 5 to 70 GeV/c can now be understood. The "even" amplitude $f_+(\xi)$ is decreasing from the resonance region towards higher energies. The real part computed from (41) is therefore negative. For pp (and π^+p and K^+p) the two terms in the numerator in (43) are both negative, giving a negative $\rho(\xi)$ of appreciable magnitude. For $\bar{p}p$ (and π^-p and K^-p) on the other hand, the terms in the numerator tend to cancel, yielding a less negative (and perhaps even positive) value for $\rho(\xi)$.

Exercise: Take the available data on π^+p and π^-p total cross sections (from the various HERA and Particle Data Group complications) and determine $\rho(\xi)$ for each channel from 5 GeV/c to 200 GeV/c by the methods of this section. Compare the results with available data (Allaby, in Kiev 1970; Foley et al., 1969).

The results of a calculation using (42) and (43), with the Denisov parametrization for $\sigma_-(\xi)$, are shown in Figs. 13 and 14. Two quadratic forms in ξ for $\sigma_+(\xi)$ were fitted to a smoothed $\sigma_{pp}(\xi)$ plus $\sigma_-(\xi)$. The ratio $\rho(\xi)$ was then calculated using (43). The solid and dashed curves in Figs. 13 and 14 represent the two parametrizations. The available data for $\rho(\xi)$ above 10 GeV/c are shown in Fig. 14. The agreement between the curves and the data is quite satisfactory, showing the efficacy of our method. The whole calculation was an afternoon's work with an HP-35. The curves also agree in general trend with a recent dispersion relation calculation (Kroll, 1973) and the use of a parametrized analytic form (Bourrely and Fischer, 1973).

Shortly there should be results from the US-Soviet collaboration using a gas jet target at NAL. This experiment will span the gap between Serpukhov and the ISR. It should locate the cross-over point precisely (near 210 GeV, I hope!).

Since (37) and (38) are unfamiliar it is perhaps worthwhile to show explicitly the connection with dispersion relations. The odd amplitude $F_-(\nu)$, for example, satisfies a dispersion relation of the form of (10):

$$\mathrm{Re}\, F_-(\nu) = \frac{2}{\pi}\, \nu P \int_0^\infty d\nu' \, \frac{\mathrm{Im}\, F_-(\nu')}{\nu'^2 - \nu^2} \, .$$

If the variables are changed, with $\nu = \nu_0\, e^{\xi}$, $\nu' = \nu_0\, e^{\xi+\eta}$, this becomes

$$\mathrm{Re}\, F_-(\xi) = \frac{1}{\pi}\, P \int_{-\infty}^{\infty} \frac{\mathrm{Im}\, F_-(\xi + \eta)\, d\eta}{\sinh \eta} \, .$$

Unless $\mathrm{Im}\, F_-$ grows exponentially in η, as $e^{\lambda|\eta|}$ with $\lambda \geq 1$, the integral converges very rapidly away from $\eta = 0$. Excluding this circumstance, a Taylor series expansion of $\mathrm{Im}\, F_-(\xi + \eta)$ around $\eta = 0$ gives

$$\mathrm{Re}\, F_-(\xi) = \frac{2}{\pi} \sum_{n\ \mathrm{odd}} F_-^{(n)}(\xi)\, \frac{1}{n!} \int_0^\infty \frac{\eta^n\, d\eta}{\sinh \eta} \, ,$$

an expression that can be shown (exercise for the reader!) to be equivalent to (38).

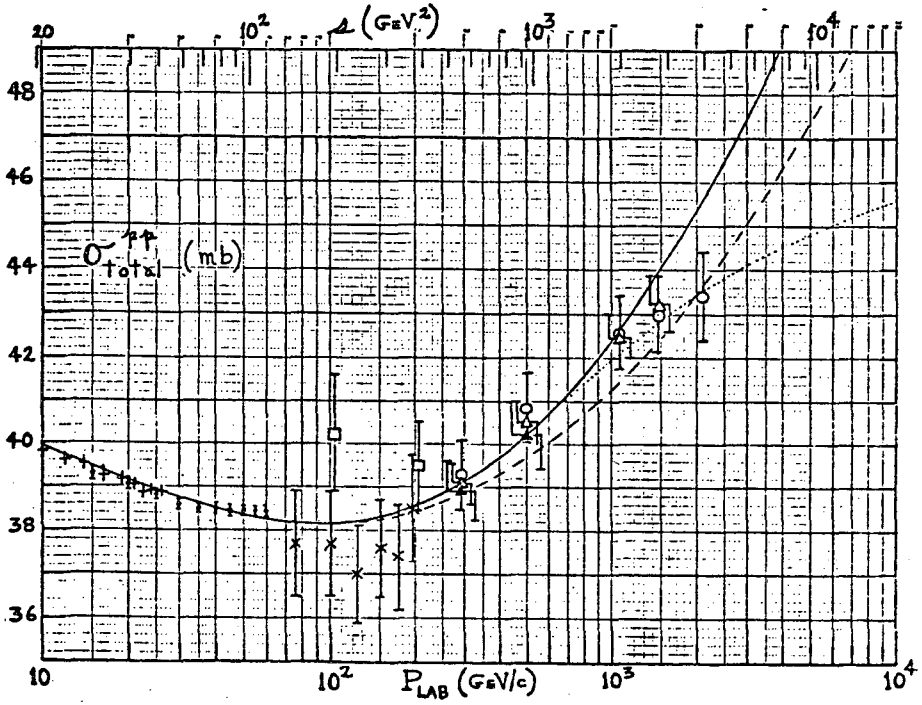

XBL 737-1006

Fig. 13. Total cross section data for p-p scattering from Fig. 2 replotted to show two quadratic parametrizations in $\xi = \ln \nu$. The dotted curve is yet another smooth behavior at higher energies.

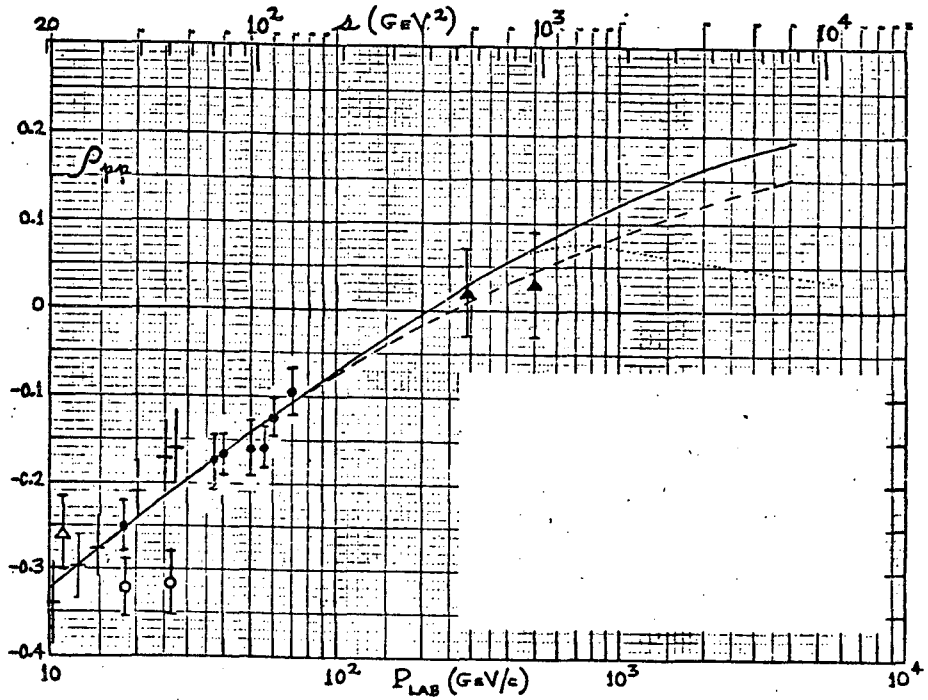

XBL 737-1005

Fig. 14. The ratio ρ of real to imaginary part of the forward nonflip amplitude for p-p scattering calculated by differentiation from the total cross section of Fig. 13. The solid, dashed and dotted curves here correspond to the solid, dashed and dotted curves in Fig. 13.

5. Partial Wave Distribution for Proton-Proton Scattering, MacDowell-Martin Bound on B(s)

In the previous two sections we have focussed on the p-p elastic amplitude at $t = 0$. Now we consider the question of the shape of the differential cross section. The discussion will be naive and schematic, neglecting spin completely.

The ISR data at $W \simeq 53$ GeV are shown in Fig. 5 as the stars with $E_{Lab} = 1480$ GeV indicated. At this energy the c.m.s. wave number is $k = W/2$ GeV $= 5.07\ W/2\ \mathrm{fm}^{-1} \simeq 134\ \mathrm{fm}^{-1}$. A slope parameter $B \simeq 10\ \mathrm{GeV}^{-2}$ (see Fig. 6) implies a mean square extent of ~ 0.9 fm. It can therefore be expected that of the order of 100 partial waves will be significant. The continuous impact parameter representation is quite appropriate.

(a) Partial wave distribution for pp scattering at ISR energies

The data of the ACGHT collaboration (Strolin, 1973) are replotted on a somewhat compressed vertical scale in Fig. 15. The data of this same group at very small $|t|$ values (Barbiellini et al., 1972) are not shown, but for $0.2(\mathrm{GeV}/c)^2 < |t| < 0.5(\mathrm{GeV}/c)^2$ they are consistent with an exponential in t with slope parameter $B \sim 10\text{-}11\ \mathrm{GeV}^{-2}$. At $|t| < 0.15(\mathrm{GeV}/c)^2$ the data show a steeper slope of order $B \sim 12\text{-}13\ \mathrm{GeV}^{-2}$, but this detail could not be seen in Fig. 15.

The dashed straight lines show that the data at small $|t|$ and for $2 < |t| < 4(\mathrm{GeV}/c)^2$ can be represented by exponentials in $|t|$. The dip at $|t| \sim 1.3(\mathrm{GeV}/c)^2$ implies an interference between two contributions to the amplitude. Since we know from Fig. 14 that at

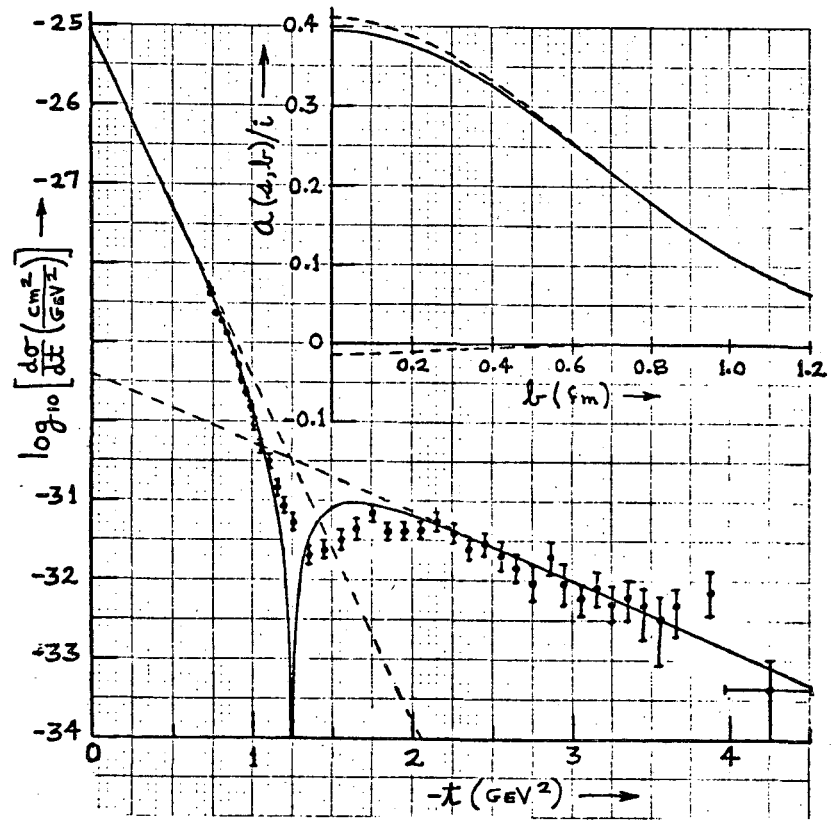

Fig. 15 Differential cross section for p-p elastic scattering at c.m.s. energy $W = 53$ GeV. Preliminary data of the ACGHT collaboration (Strolin, 1973). The dashed lines are proportional to $\exp(10t)$ and $\exp(2t)$. The solid curve is the cross section given by a purely imaginary nonflip amplitude whose partial wave profile is given by the solid curve in the inset at upper right.

$t = 0$ the real part of the nonspinflip amplitude is extremely small, we make the simplifying assumption that the amplitude is purely imaginary at all t values of interest. We are neglecting all other helicity amplitudes. Thus we fit the cross section with the expression,

$$\frac{d\sigma}{dt} = \frac{\sigma_t^2}{16\pi}\left|(1+\lambda)\, e^{B_1 t/2} - \lambda\, e^{B_2 t/2}\right|^2 . \qquad (45)$$

The coefficient $\sigma_t^2/16\pi$ is the optical theorem value of $d\sigma/dt$ at $t = 0$. The solid cross section curve in Fig. 15 is (45) with $\sigma_t = 40$ mb, $B_1 = 10\ \mathrm{GeV}^{-2}$, $B_2 = 2\ \mathrm{GeV}^{-2}$, and $\lambda = 7 \times 10^{-3}$. The numbers were chosen for their simplicity, rather than in any attempt to give a least squares fit. The integrated elastic cross section with these parameters is 8.0 mb, in rough agreement with the value of 7.6 ± 0.3 mb quoted by Amaldi et al. (1973b).

The partial wave (impact parameter) amplitude corresponding to the scattering amplitude in (45) can be obtained by the methods of Appendices B and C. The scattering amplitude $F(s,t)$ is

$$F(s,t) = i\, s\, \frac{\sigma_t}{8\pi}\left[(1+\lambda)e^{B_1 t/2} - \lambda\, e^{B_2 t/2}\right] \qquad (46)$$

and its partial wave projection, according to (B.24) and (C.16), is

$$a(s,b) = \frac{i\,\sigma_t}{8\pi}\left[\frac{(1+\lambda)}{B_1}\, e^{-b^2/2B_1} - \frac{\lambda}{B_2}\, e^{-b^2/2B_2}\right] . \qquad (47)$$

This partial wave profile (divided by i) is plotted as a function of impact parameter in fm in the inset of Fig. 15. The solid curve is the sum of the two terms in (47), while the dashed curves are the

separate contributions. The most remarkable thing is that the distribution need be only slightly flatter than a Gaussian in order to introduce the dip and secondary maximum. [A counter argument might be that the secondary maximum is only $\sim 10^{-6}$ times the forward cross section and hence should be generated by a change of the order of only 10^{-3} times a Gaussian and so should be within the thickness of the lines on the figure!] Similarly, the mentioned steeper slope of the cross section at $|t| < 0.15\ (\mathrm{GeV}/c)^2$ can be incorporated by a third term in (45) or (47) that will cause the partial wave profile to extend slightly farther out in the region beyond 1 fm. The calculation of this is left as an exercise for the reader.*

The simple description contained in Fig. 15 applies at one energy. It is important to ask about energy dependence. It is clear from Fig. 5 that from 20 GeV to 2000 GeV there is significant energy variation in the cross section at fixed t. It is less clear over the ISR range (500 to 2000 GeV lab equivalent). Any model based on the eikonal approximation (or something like it) and with a largely imaginary phase shift will have destructive interference between successive terms, as in our simple description (45), but different

---

* It is amusing to note that the sharper peak at very small $|t|$ can be generated by assuming $a(s,b)$ is purely imaginary, using (B.5) to solve for $\mathrm{Im}\, a = \frac{1}{2}\left(1 - \sqrt{1 - H}\right)$, and assuming that the overlap function H is a Gaussian in b (Heckman and Henzi, 1972). There is no a priori reason to favor at Gaussian for H, of course. See Barger, Phillips, and Geer (1972) for an example of a peripheral addition to the basic Gaussian for $a(s,b)$ and de Groot and Miettinen (1973) for a more elaborate analysis with the overlap function.

predictions about the energy dependences of the several contributing terms (Barger, Phillips, and Geer, 1973). In the Chou-Yang model* the eikonal phase shift is energy independent and so is $d\sigma/dt$. In the Regge eikonal model of Frautschi and Margolis the eikonal phase from the pomeron pole is (25) with $\alpha(0) = 1$. There is thus s-dependence of the phase through $B(s)$ provided $\alpha'(0) \neq 0$. According to (C.16) the nth power of the phase shift leads to a term in the scattering amplitude proportional to $B^{1-n}.\exp[Bt/2n]$. Thus the whole amplitude shrinks logarithmically, but successive terms involve relative powers of B^{-1} and so cause an energy dependence in the shape of the differential cross section, even when plotted versus $B(s)t$. There are other models, like the hybrid model of Chiu and Finkelstein, with features intermediate between these two and still others, like that of Cheng and Wu, with more drastic energy dependence at least asymptotically. Careful measurements at NAL energies and at the ISR should aid enormously in discriminating among models.

(b) MacDowell-Martin lower bound on the slope parameter B

While on the subject of partial wave distributions it is worthwhile to consider the following question: Given the total cross section and the integrated elastic cross section, can anything be said about the slope parameter B of the forward diffraction peak? Intuitively we expect a correlation. The larger the absorptive

---

* See Jackson (1970) for a description of this and the other models and also the appropriate references. Zachariasen (1971) also discusses the various models for diffraction scattering with emphasis on the J-plane structure.

diffracting object, the narrower in angle its diffraction pattern. This has already been remarked on in correlating the total cross sections of Fig. 1 with the differential cross sections of Figs. 4 and 5 (see also Fig. 9). We are thus not surprised to learn that the answer to the question is yes (MacDowell and Martin, 1964). We give a slightly simplified derivation of the MacDowell-Martin bound using the impact parameter description and also discuss its limitations as a tool for learning about the partial wave content of the scattering amplitude.

The bound is on the logarithmic derivative with respect to t of the absorptive part of the forward scattering amplitude $(F = D + iA)$,

$$A(s,t) = \frac{s}{2}\int_0^\infty db^2 \, \mathrm{Im}\, a(s,b)\, J_0(qb) \, . \tag{48}$$

The derivative of $A(s,t)$ with respect to $t = -q^2$ evaluated at $t = 0$ is

$$\left[\frac{dA(s,t)}{dt}\right]_{t=0} = \frac{s}{8}\int_0^\infty db^2 \, b^2 \, \mathrm{Im}\, a(s,b) \, . \tag{49}$$

The logarithmic derivative is thus

$$\left[\frac{1}{A}\frac{dA}{dt}\right]_{t=0} = \frac{\pi\int_0^\infty db^2 \, b^2 \, \mathrm{Im}\, a(s,b)}{4\pi\int_0^\infty db^2 \, \mathrm{Im}\, a(s,b)} \, . \tag{50}$$

Because of the optical theorem (B.25) the denominator in (50) is just the total cross section.

The existence of a lower bound on (50) stems from the unitarity requirement that $\mathrm{Im}\, a(s,b) \geq 0$. In fact, the imaginary part of $a(s,b)$ is constrained to the range,

$$0 \leq \mathrm{Im}\, a(s,b) \leq 1 \quad . \tag{51}$$

We are thus invited to consider a variational problem subject to some constraints. We define $b^2 = x$, $\mathrm{Im}\, a(s,b) = f(x)$, and introduce the absorptive contribution to the elastic cross section,

$$\sigma_{e\ell\ \mathrm{abs}} = 4\pi \int_0^\infty db^2 |\mathrm{Im}\, a(s,b)|^2 \quad . \tag{52}$$

Then we minimize (50) subject to the constraints,

$$\left.\begin{aligned} \sigma_t &= 4\pi \int_0^\infty f(x)dx \\ \sigma_{e\ell\ \mathrm{abs}} &= 4\pi \int_0^\infty [f(x)]^2\, dx \\ 0 &\leq f(x) \leq 1 \end{aligned}\right\} \quad . \tag{53}$$

This is a simple variational problem with Lagrange multipliers. The result is that (50) is minimized if

$$f(x) = \alpha\left(1 - \frac{x}{R^2}\right) \tag{54}$$

for $x < R^2$ such that $f(x) \leq 1$ and $f(x) = 1$ for smaller x. For all hadronic scattering processes at high energies $\sigma_{e\ell}/\sigma_t < 0.5$. From (54) we have

$$\frac{\sigma_{e\ell\ \mathrm{abs}}}{\sigma_t} = \frac{2}{3}\begin{cases} \alpha & \text{for } 0 \leq \alpha \leq 1 \\ \dfrac{3\alpha - 2}{2\alpha - 1} & \text{for } 1 < \alpha \quad . \end{cases}$$

Thus the range of interest is $\alpha < 1$ and the partial wave distribution (54) is linear in x or parabolic in b. For $\alpha \leq 1$, $\sigma_t = 2\pi R^2\alpha$, $\sigma_{e\ell\ \mathrm{abs}} = 4\pi R^2\alpha^2/3$, and $(A^{-1}\, dA/dt)_{t=0} = R^2/12$. The parameters R^2 and α can be eliminated to yield the bound,

$$\left(A^{-1}\frac{dA}{dt}\right)_{t=0} \geq \frac{\sigma_t^{\,2}}{36\pi\ \sigma_{e\ell\ \mathrm{abs}}} \geq \frac{\sigma_t^{\,2}}{36\pi\ \sigma_{e\ell}} \quad . \tag{55}$$

This is the MacDowell-Martin bound, apart from an insignificant and totally justified simplification.

With the knowledge that the forward amplitude is largely imaginary at high energies we can equate the logarithmic derivative of the absorptive part to one half of the slope parameter defined by (1). In this regime the MacDowell-Martin bound reads

$$B(s,0) \geq \frac{\sigma_t^{\,2}}{18\pi\ \sigma_{e\ell}} \quad . \tag{56}$$

Equation (56) is a nice bound, very solidly grounded in unitarity and nothing much else, but is it useful? Skeptics argue that no bound, even Froissart's, has ever had real practical use and the less assumptions needed to prove it, the less likely it is to be even vaguely useful. Certainly some bounds fall into this category

(see Roy, 1972, for the most recent and detailed compendium of all kinds). On the other hand, a bound is a definite statement and should at least be given a chance to prove itself. We test (56) against the data on p-p elastic scattering. In Fig. 16 we show a compilation of data on the ratio $\sigma_{e\ell}/\sigma_t$ for p-p and π^--p scattering. At

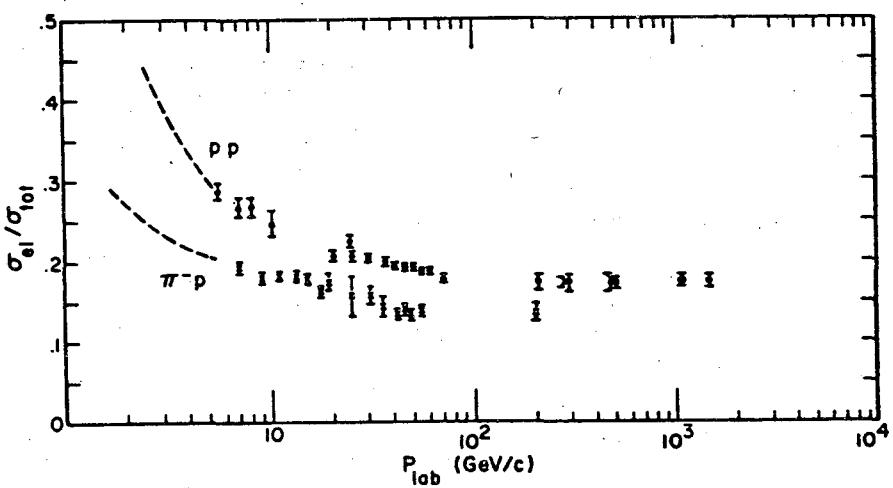

Fig. 16. The ratios of elastic to total cross sections for p-p and π^--p interactions versus laboratory momentum (from Jackson, 1973).

Serpukhov energies and above the p-p ratio is $\sigma_{e\ell}/\sigma_t \simeq 0.175$. Taking this value and the total cross sections from Fig. 2 or Fig. 13, we find $\sigma_t^2/18\pi\ \sigma_{e\ell} \simeq 10.1$ to $11.3\ (\mathrm{GeV/c})^{-2}$ from the bottom to the top of the ISR energy range. These lower bounds are to be compared with the experimental values of $B(s,0)$ from 11.5 ± 0.6 to 12.6 ± 0.8 over the same range. The experimental results are only slightly (10-15%) greater than the lower bound.

The closeness of experiment to the bound can be put in perspective by considering an example of an exponential fit for all t. The differential cross section is then

$$\frac{d\sigma}{dt}(s,t) = \frac{\sigma_t^2}{16\pi}(1+\rho^2)\exp[B_{eff}(s)t] \tag{57}$$

where we have explicitly exhibited the value at $t = 0$ via the optical theorem and the definition of ρ. Integration of (57) over t gives the relation,

$$B_{eff}(s) = \frac{\sigma_t^2(1+\rho^2)}{16\pi\ \sigma_{e\ell}} \quad . \tag{58}$$

Comparison of (58) with (56) shows that if ρ^2 is negligible then $B_{eff} = (9/8)B_{min}$. Since the differential cross section at small $|t|$ <u>is</u> fitted well by an exponential (or two exponentials of slightly different slopes) it is quite reasonable that the experimental slope parameter is just slightly larger than the theoretical lower bound. In fact, to the extent that the cross section is exponential in t over the range contributing significantly to the integral anything else is impossible.

At this point we are a little disappointed in the significance of the MacDowell-Martin bound. The closeness of the experimental slope to the bound is merely a consequence of an approximately Gaussian shape in impact parameter of $a(s,b)$. Of course, the fact that it is roughly Gaussian and not rectangular or some other strange shape is progress, isn't it? Yes, it is progress, but not because of the bound. One might think, as did MacDowell and Martin (apparently because of an arithmetic slip), that comparison of experiment with their bound could

distinguish between such grossly different partial wave distributions as a Gaussian and a rectangle. Not so. From (50) it is apparent that the slope parameter at $t = 0$ is determined by the average value of $x = b^2$. Requiring the first moment of a function to have a definite value constrains the function slightly, but still leaves almost unlimited freedom. To drive home this point I have constructed three different partial wave distributions, all having the following properties in common,

$$\sigma_t = 38.9 \text{ mb}$$

$$\sigma_{e\ell} = 6.8 \text{ mb}$$

$$B(s,0) = 11.4 \text{ GeV}^{-2}$$

and

$$\frac{B(s,0)}{B_{min}} = 1.125 \quad .$$

The cross section and slope values are appropriate to 300 GeV laboratory energy or $W \simeq 24$ GeV at the ISR. The choice $B/B_{min} = 9/8$ is consistent with experiment and contains the Gaussian and rectangular partial wave distributions as examples. The cross section for a Gaussian is (57); for the rectangle it is

$$\frac{d\sigma}{dt} = \frac{\sigma_t^{\,2}}{16\pi}\left|\frac{2J_1(qR)}{qR}\right|^2 \tag{59}$$

with $B(0) = R^2/4$. The third partial wave distribution is a "peripheral" one. The cross section is chosen to be of the form

$$\frac{d\sigma}{dt} = \frac{\sigma_t^{\,2}}{16\pi} J_0^{\,2}(qR)\, e^{-\lambda q^2} \quad . \tag{60}$$

The ratio $B(0)/B_{min}$ depends on the ratio of R^2/λ. For $R^2/\lambda = 7.0$ we have $B(0)/B_{min} = 9/8$. The purely imaginary partial wave distribution corresponding to (60) is

$$a(b) = i\,\frac{\sigma_t}{8\pi\lambda}\, I_0(Rb/\lambda)\, \exp[-(b^2 + R^2)/2\lambda] \tag{61}$$

where $I_0(z)$ is a modified Bessel function of the first kind and order zero.

The three partial wave distributions are shown in Fig. 17 and the differential cross sections in Fig. 18. The distributions in b are quite different in detail even though having the same $\langle x \rangle$ and the resulting cross sections are very different for $|t| > 0.1$, too! The message is, I hope, clear--nearness of the slope paramter $B(0)$ to the lower bound (56) establishes little about the partial wave distribution. The shape of $d\sigma/dt$ at $t \neq 0$ can, of course, furnish much information, as has been illustrated already in Fig. 15.

Lest I leave the impression of scorning bounds like the MacDowell-Martin bound let me remark that (56) is useful in correlating various asymptotic behaviors. If, for example, $\sigma_{e\ell}/\sigma_t \to$ constant and $\sigma_t \to C(\ell n\ s)^2$, (56) shows that the diffraction peak must exhibit rapid shrinkage with $B \sim (\ell n\ s)^2$ asymptotically. More on this in the next section.

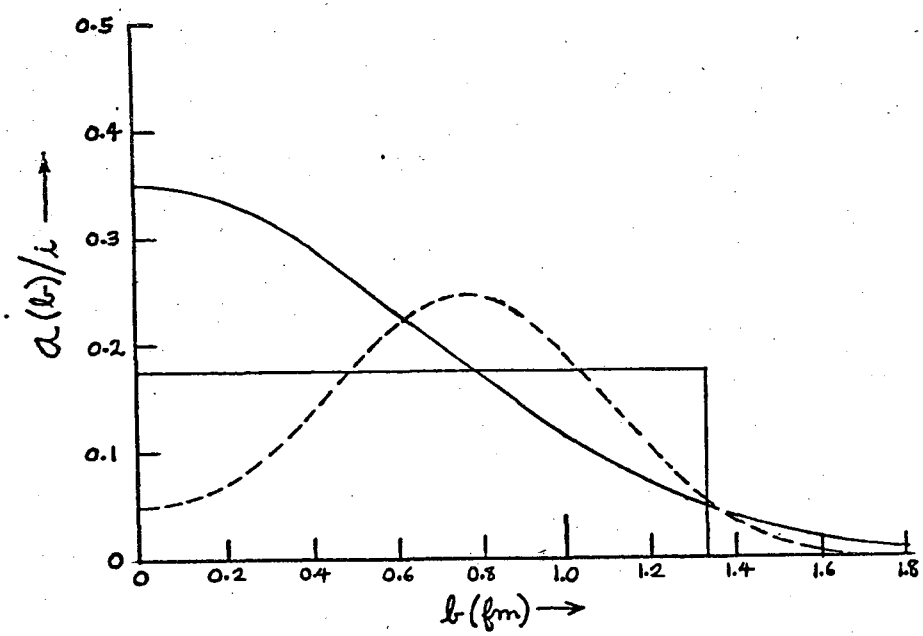

Fig. 17. Partial wave (impact parameter) distributions for p-p scattering. All three distributions give $\sigma_t = 38.9$ mb, $\sigma_{e\ell} = 6.8$ mb, $B(0) = 11.4\ \mathrm{GeV}^{-2}$ $\left(B(0)/B_{min} = 9/8\right)$.

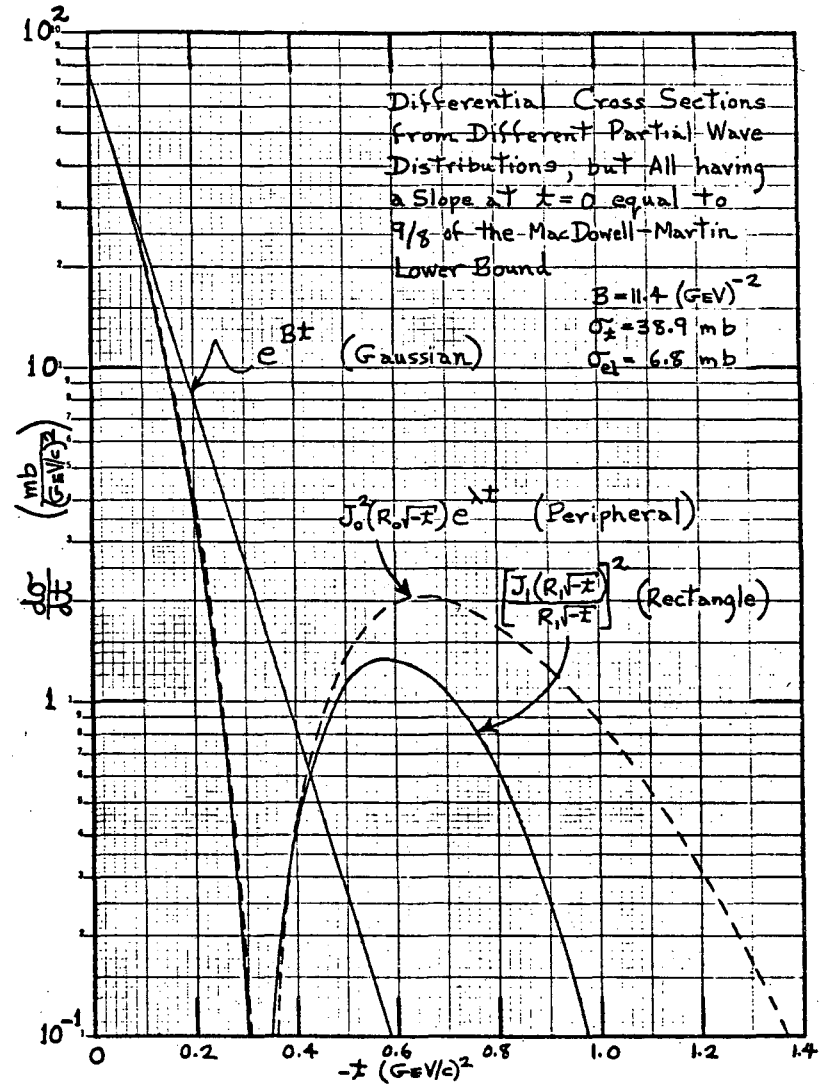

Fig. 18. Differential scattering cross sections from the partial wave distributions of Fig. 17. All three cross sections have the same slope at $t = 0$ and extrapolate to the same optical theorem point. For small $|t|$ they fit the p-p elastic data at ~ 300 GeV laboratory energy.

6. Asymptotics and J-plane Structure

Although various remarks have already been made about energy dependences of total and differential cross sections in both theory and experiment we summarize here and also discuss briefly the J-plane structure of some models. By J-plane structure we mean the singularity structure of the t-channel partial wave amplitude analytically continued to complex angular momentum j. The dependence of an amplitude on s for fixed t is related to the singularity structure in the J-plane through the Watson-Sommerfeld transformations of the t-channel partial wave series and the connection (11) between ν and $\cos\theta_t$ (See, for example, Collins and Squires, 1968). At high energies it is possible to replace the Froissart-Gribov formula for the analytically continued t-channel partial wave amplitude by the simpler Mellin transform formula,

$$\left.\begin{aligned} F(t,j) &= \int_1^\infty ds\, s^{-j-1} A(s,t) \\ &\text{with its inverse,} \\ A(s,t) &= \frac{1}{2\pi i}\int_{c-i\infty}^{c+i\infty} dj\, s^j F(t,j) \end{aligned}\right\} . \qquad (62)$$

In (62) c is any real number such that the vertical contour lies to the right of all the singularities of $F(t,j)$ and $A(s,t)$ is the s-channel absorptive part of the scattering amplitude (See Horn and Zachariasen, 1973, Appendix D, for the derivation and such details as signature.) To gain faith in (62), assume that $F(t,j)$ has a pole at $j = \alpha(t)$. The second relation then yields $A(s,t) \propto s^{\alpha(t)}$, as

expected for a Regge pole. A second order pole gives $A(s,t) \propto (\ln s)\, s^{\alpha(t)}$ and so on. It is left as an exercise for the reader to deduce the following examples:

$F(t,j)$	$A(s,t)$
$(j-\alpha)^{-1}$	s^α
$(j-\alpha)^{-2}$	$-s^\alpha \ln s$
$(j-\alpha)^n \ln(j-\alpha)$	$(-1)^n\, n!\, s^\alpha (\ln s)^{-n-1}$
$(j-\alpha)^\nu$	$-s^\alpha (\ln s)^{-\nu-1}/\Gamma(-\nu)$.

Here n is zero or a positive integer while ν is not an integer. The examples indicate some types of J-plane singularities and their associated s dependences. We saw that the successive terms in the Frautschi-Margolis (Regge eikonal) model had s-dependence $s^\alpha/(\ln s)^{n-1}$, $n = 1,2,\cdots$. The first term corresponds to a pole in the J-plane, while higher terms evidently correspond to logarithmic singularities with softer and softer discontinuities at the tip of the branch cut. There are, of course, considerably more complicated singularities possible in the J-plane.

Two examples with increasing total cross sections can be mentioned. One is the self-consistent solution of a multiperipheral model for diffractive scattering (Ball and Zachariasen, 1972). The scattering amplitude is

$$F(s,t) = i\beta R_0^{\,2} s\, \frac{J_1\left(qR_0 \ln(s/s_0)\right)}{q\, R_0} \qquad (63)$$

where $q^2 = -t$. The total cross section is $\sigma_t = 4\pi\beta R_0^2 \ln(s/s_0)$ so that the optical theorem point $\frac{d\sigma}{dt}(s,0)$ is proportional to $(\ln s)^2$. On the other hand, the diffraction pattern shrinks as $(\ln s)^2$ so that the integrated elastic scattering cross section is constant in energy. The J-plane structure is given by

$$F(t,j) = \frac{i\beta}{t}\left[\frac{j-1}{\sqrt{(j-1)^2 - tR_0^2}} - 1\right] . \qquad (64)$$

There are, for $t < 0$, complex conjugate branch points at $\alpha_c(t) = 1 \pm iqR_0$. For $t \to 0$ these coalesce to give a second order pole at $j = 1$, yielding $\sigma_t \propto \ln s$ according to our examples quoted above. In terms of s-channel partial waves the amplitude (63) has a rectangular distribution in impact parameter out to $b_{max} = R_0 \ln(s/s_0)$, with a magnitude that decreases as $(\ln s)^{-1}$. It corresponds classically to an absorbing disc with a logarithmically growing radius, but with a decreasing opacity.

The other example is an amplitude appropriate to any model that saturates the Froissart bound, e.g., the model of Cheng and Wu (1970). At sufficiently high energy the scattering amplitude is

$$F(s,t) = i\frac{R_0^2}{2} s(\ln s)^2 \frac{J_1(qR_0 \ln s)}{qR_0 \ln s} . \qquad (65)$$

The total cross section is $\sigma_t = 2\pi R_0^2(\ln s)^2$; $\sigma_{e\ell}/\sigma_t = 1/2$; the shrinkage of the diffraction peak is as $(\ln s)^2$. From (62) we find the J-plane projection to be

$$F(t,j) = \frac{R_0^2}{2}[(j-1)^2 - tR_0^2]^{-3/2} , \qquad (66)$$

with complex conjugate branch points $\alpha_c(t) = 1 \pm iqR_0$ for $t < 0$. The singularities become a third order pole at $t = 0$ and give $\sigma_t \propto (\ln s)^2$. The physical interpretation in the s-channel has already been discussed.

We summarize the asymptotic behavior of the various models in the following table:

Asymptotic Energy Dependence of Various Models

Model	σ_t	$\sigma_{e\ell}/\sigma_t$	B_{eff}	ρ
Pomeron pole + secondary poles	$a + bs^{-\frac{1}{2}}$	$(\ln s)^{-1}$	$\ln s$	$(-)s^{-\frac{1}{2}}$
Pomeron eikonal	$a - b(\ln s)^{-1}$	$(\ln s)^{-1}$	$\ln s$	$(+)(\ln s)^{-1}$
Ball-Zachariasen (second order pole at $t = 0$)	$\ln s$	$(\ln s)^{-1}$	$(\ln s)^2$	$(+)(\ln s)^{-1}$
Saturation of Froissart bound (third order pole at $t = 0$)	$(\ln s)^2$	1/2	$(\ln s)^2$	$(+)(\ln s)^{-1}$
Chou-Yang (fixed pole at $j = 1$)	constant	constant	constant	(0)

Comparison of the predictions of this table with the p-p data of Fig. 2 (σ_t), Fig. 16 ($\sigma_{e\ell}/\sigma_t$), Fig. 6 (B_{eff}), and Fig. 14 (ρ) shows several things. First of all, if one accepts the rising cross sections of Fig. 2 the simple Regge pole model and the Chou-Yang model are excluded. The other three models (and surely others) can accommodate the energy dependence of σ_t. Nothing can be said about

saturation of the Froissart bound unless we include the cosmic ray evidence (Yodh, Pal, and Trefil, 1972). Figure 16 is on the face of it peculiar. For both pp and $\pi^- p$ interactions the ratio $\sigma_{e\ell}/\sigma_t$ seems to become energy independent at high energies and be quite small (~ 0.175 for pp, ~ 0.135 for $\pi^- p$). For any of the models in the table, except Chou-Yang, we are asked to believe that this constancy is a transitional effect which will disappear at still higher energies. This is perhaps plausible for Cheng and Wu (although 0.5 is a long way off!), but less so for the Regge models. The third quantity, B_{eff}, displayed in Fig. 6 is also apparently in a transitional stage, at least for any model that saturates the Froissart bound. A steady growth with $\ell n\ s$ is consistent with the Regge pole and Regge eikonal models, although the inferred slope of the pomeron trajectory $\left(\alpha'(0) \simeq 0.3\right)$ is quite small. The evidence from Fig. 14 on $\rho(s)$ indicates that it is very far from its asymptotic behavior at ISR energies and so cannot be sensibly compared with the expectations of the table. Its crossover to positive values does, of course, support some models.

There once was a time when theorists stated that asymptotic behavior would occur at 5 or 10 GeV incident energy. From the evidence available today one might venture to say 5 or 10 TeV, but even that might be too low!

III. INCLUSIVE PROCESSES

1. Preamble

As already mentioned in the Introduction, inclusive processes of the type

$$a + b \rightarrow c + \text{anything}$$

or

$$a + b \rightarrow c + d + \text{anything}$$

(and in principle more complicated processes) have become an important aspect of high-energy experiment and theory. Partly this is by default--very many particle states, often with several unseen neutrals, are difficult if not impossible to study in complete detail. Partly, however, it is by design. We have learned that in some senses inclusive reactions are simple and amenable to theoretical analysis.

Though the basic concepts and ideas have been known for 10 years or more from the work of Amati, Stanghellini, and Fubini (1962), Fubini (1963), and from Wilson's Schladming lectures (1963), it is only in the past four years that intensive theoretical and experimental work has been done. The renewed interest on the theoretical side was prompted mainly by work of Feynman (1969a,b) and of Yang and collaborators (Benecke et al., 1969) with their ideas of scaling and of limiting fragmentation. The reasons for the experimental interest have already been discussed. By now hundreds of papers have been published; numerous conferences have been held; summaries of theory and of experiment exist in review journals and conference proceedings. Since these lectures are elementary and introductory I list a sampling of the reviews and conference reports where the hungry and/or dissatisfied reader can go for more or better information:

(a) Mostly experiment:

Wroblewski, 1970

Lander, 1971

Morrison, 1972

and the summary of contributed papers in Vol. 1 of the Proceedings of the Chicago-Batavia Conference (1972).

(b) Theory and experiment:

Quigg, 1971

Van Hove, 1971

Frazer et al., 1972

Horn, 1972

Jacob, 1972

Mueller, 1972 .

For entire conferences devoted to multiparticle production processes, see the proceedings of the Helsinki (1971) and the Zakopane (1972) meetings. Other lecturers here will carry on the list. In particular, the content of Wilson's hitherto unpublished Cornell report (Wilson, 1970) appears in these proceedings.

In this chapter we discuss the essential experimental facts and the general theoretical framework for inclusive processes. Most of the treatment is without bias towards any particular theoretical model, although some concepts, e.g., finite range correlations in rapidity, will be accepted as true without serious questioning. This facilitates establishing all the essential ideas and can be changed in the light of contrary facts without undue harm. The notation and kinematics of inclusive processes are described in Appendix D. Definitions of distributions, correlation of functions, multiplicity moments, and sum rules are given in Appendix E.

2. Basic Facts and Samples of Data

(a) Prong cross sections as functions of incident energy

As mentioned in the Introduction, increasing energy brings production of more and more particles, mostly pions but with some heavier particles as well. A measure of the particle production is afforded by the values of the topological or prong cross sections. These are the cross sections σ_n for a specific number n of charged particles in the final state (whose ionization produces prongs or tracks in a bubble chamber or emulsion), independent of how many neutrals are produced. At a given incident energy the prong cross sections are expected to be given by something like a Poisson distribution, with events having half as many or twice as many as the average number of prongs being fairly frequent.* Figure 19 shows a typical set of prong cross sections (Charlton et al., 1972). They happen to be from 205 GeV protons incident on the NAL 30" hydorgen bubble chamber; the results from 50 and 69 GeV at Serpukhov (Ammosov et al., 1972), 102 GeV at NAL (Chapman et al., 1972), and 303 GeV at NAL (Dao et al., 1972) are qualitatively similar. Later we will discuss the shape of the prong distributions in more detail, but now we turn to the energy dependence.

The prong cross sections for pp interactions at various energies are summarized in Fig. 20. The increasing numbers of

* Completely independent emission of particles would lead to a Poisson distribution in the number of charged prongs. Crude imposition of charge conservation by the assumption of pair production of positively and negatively charged particles leads to a Poisson distribution in the number of negative prongs (Wang, 1969).

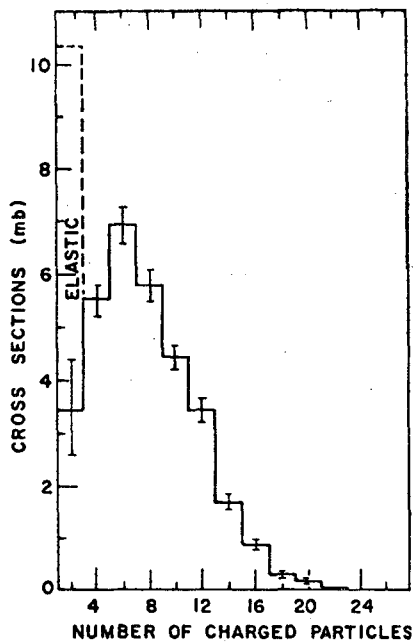

Fig. 19. Prong cross sections in millibarns versus prong number for 205 GeV pp interactions. The first and second moments are $\langle n_{ch} \rangle = 7.65 \pm 0.17$, $\langle n_{ch}^2 \rangle = 73.6 \pm 2.2$ (from Charlton et al., 1972).

particles produced as the energy increases is very evident. Not so dramatic but still evident is the peaking of a given cross section at some energy and then its decrease. The 2-, 4-, 6-, and even the 8-prong cross sections are decreasing at the highest energies. Whether these low prong number cross sections continue to decrease at higher energies or reach constant values is a point of considerable interest for "two-component" models of particle production. More later on this topic.

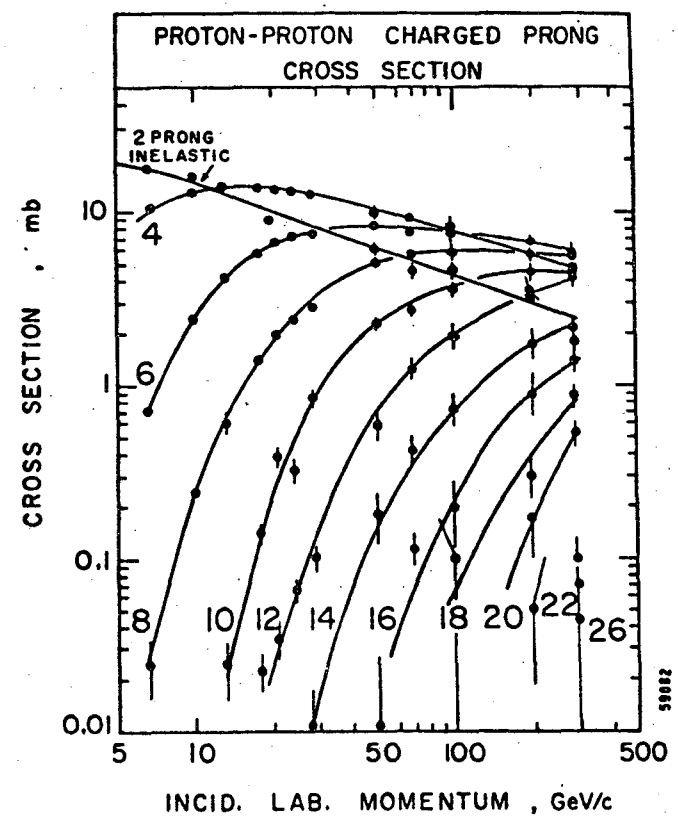

Fig. 20. Prong cross sections in millibarns versus incident laboratory momentum in GeV/c for pp interactions (Fig. 4.4 of Morrison, 1973).

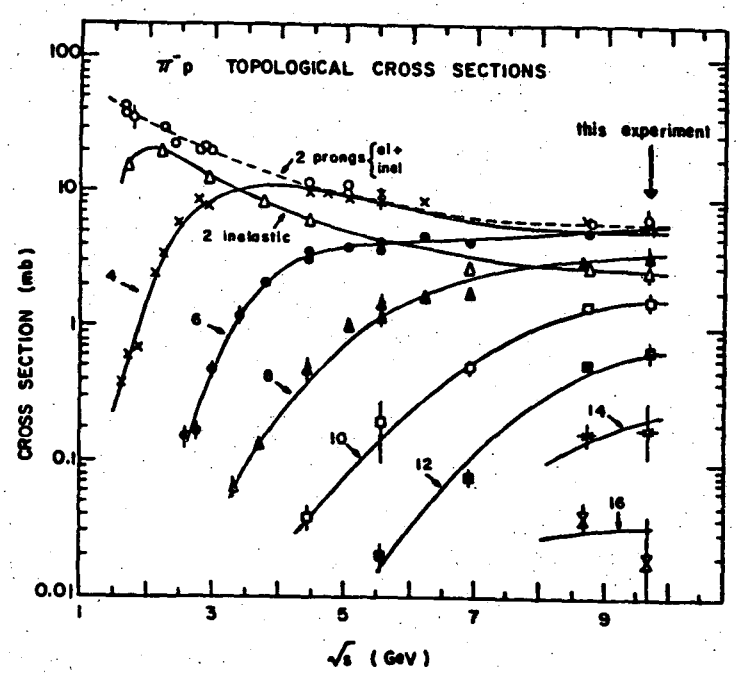

Fig. 21. Prong cross sections in millibarns versus center of mass energy $W = \sqrt{s}$ in GeV for $\pi^- p$ interactions. The highest energy ($W \simeq 9.7$) corresponds to 50 GeV/c laboratory momentum (from Ammosov et al., 1973).

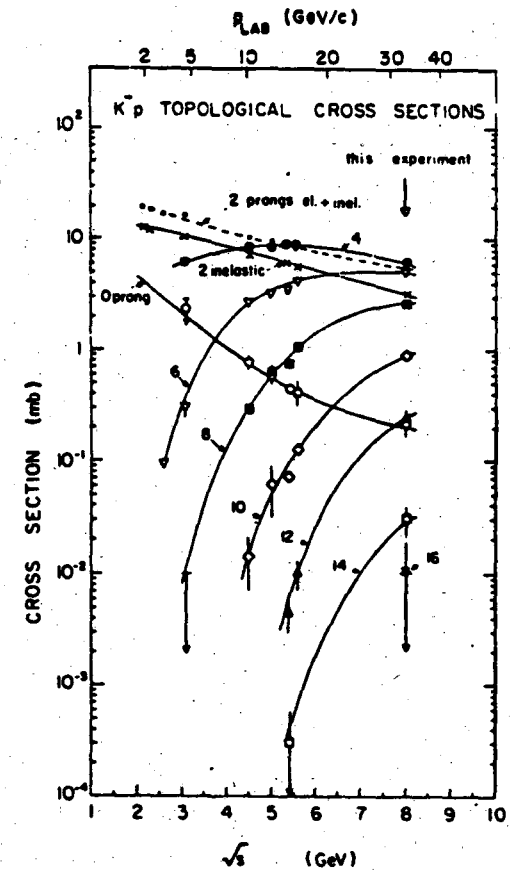

Fig. 22. Prong cross sections in millibarns versus center of mass energy $W = \sqrt{s}$ in GeV for $K^- p$ interactions. The highest energy ($W \simeq 8$ GeV) corresponds to 34 GeV/c laboratory momentum (from Ammosov et al., 1973).

For pions and K-mesons incident the data are not available at as high energies, only up to 34 GeV for K and 50 GeV plus the one set of data at 200 GeV (Huson, 1973) for pions, but the same trends and features are visible. Figures 21 and 22 show the presently existing results (without the 200 GeV π^- data).

(b) Average number of charged particles versus energy

The average number of charged particles per inelastic collision $\langle n_{ch} \rangle$ is defined by

$$\langle n_{ch} \rangle \sigma_{inel} = \sum_n{}' \, n \, \sigma_n \qquad (67)$$

where σ_n is the n-prong cross section and the prime on the sum means that the elastic scattering contribution (to the 2-prong cross section usually) is omitted. This quantity and higher moments defined analogously are a useful way of characterizing the prong distribution. It is obvious from Figs. 20-22 that $\langle n_{ch} \rangle$ is an increasing function of energy. It is popular to plot the data on $\langle n_{ch} \rangle$ versus s in the manner of Fig. 2 with a linear ordinate and a logarithmic abscissa. The data then show a roughly linear rise, at least at high energies, corresponding to

$$\langle n_{ch} \rangle \simeq a_0 + a_1 \, \ell n \, s \qquad (68)$$

with $a_0 \simeq -3.4$ and $a_1 \simeq 1.94$ for p-p interactions and similar values for π^-p and K^-p collisions. A logarithmic increase is expected on the basis of elementary considerations (see Section 3 below), but for the sake of perversity Fig. 23 displays the data for p-p interactions as a function of $Q^{\frac{1}{2}} = (W - 2m_p)^{\frac{1}{2}}$.

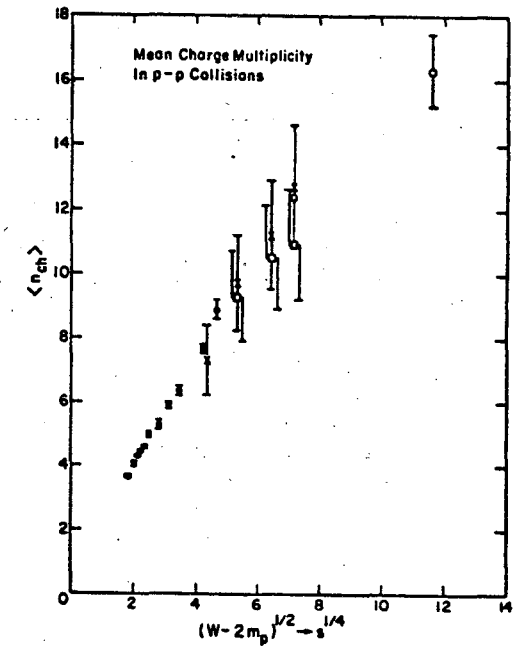

Fig. 23. Average charged particle multiplicity per inelastic p-p collisions versus $(W - 2m_p)^{\frac{1}{2}} \rightarrow s^{\frac{1}{4}}$ in $(\mathrm{GeV})^{\frac{1}{2}}$ (from Jackson, 1973). The highest point is an estimate from cosmic rays.

At high energies $Q^{\frac{1}{2}} \rightarrow s^{\frac{1}{4}}$. The data lie on a reasonable straight line, $\langle n_{ch} \rangle \simeq 1.85 \, Q^{\frac{1}{2}}$. This is an example of something known among my friends as Jackson's theorem (see Fig. 18 of Jackson, 1970), the point being that over a limited range a $\ell n \, s$ variation can be approximated by a power of s. Some models of multiparticle production, for example the hydrodynamic model of Landau, predict the $s^{\frac{1}{4}}$ variation of multiplicity.

(c) Average multiplicity of different types of particles as a function of energy

Figure 23 shows that the average number of charged particles per inelastic p-p collision is of the order of 10 to 13 at ISR energies. We expect that these are predominantly pions, but it is obviously of interest to learn the composition in detail. For example, are the proportions of K-mesons and/or antiprotons relative to pions constant in energy, even though the total number of charged particles increases? Or is some (all?) of the increase above some energy accounted for by an increased production of $K^{\pm}$ and $\bar{p}$? A summary of available data is shown in Fig. 24. Several features are worthy of note. At low energies the charged multiplicity is built up with protons and to a lesser extent positive and then negative pions. Soon, however, the pions take over the bulk of the multiplicity and rise in proportion to the total. The average number of protons decreases slightly, from slightly less than 2 at low energies to ~ 1.3 at ISR energies. The K^+, K^-, and $\bar{p}$ average multiplicities are quite small at low energies and have a steeper energy dependence than the pions. Nevertheless, even at ISR energies $(s \sim 10^3 - 3 \times 10^3\ \mathrm{GeV}^2)$, their average numbers per collision are still small:

$$\langle n_{K^+} \rangle \simeq 0.4\text{-}0.5, \qquad \langle n_{K^-} \rangle \simeq 0.3\text{-}0.4, \qquad \langle n_{\bar{p}} \rangle \simeq 0.10\text{-}0.15.$$

There is some indication that the relative proportions of K^+ and K^- may be becoming s-independent at the highest energies, but the average number of $\bar{p}$ is still growing relative to $\langle n_{ch} \rangle$.

All of this makes most reasonable sense on the naive grounds of energetics, with the more massive objects being produced with

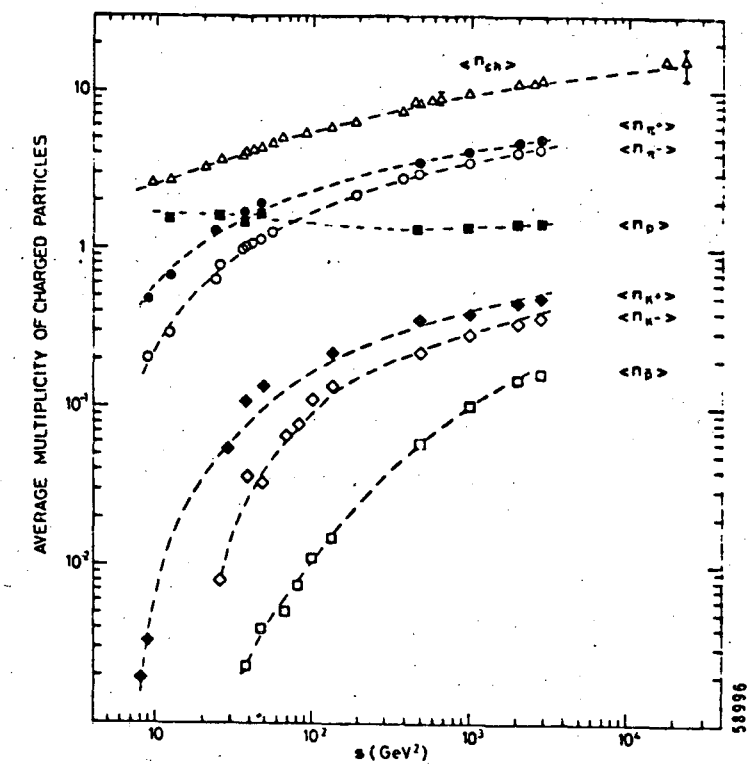

Fig. 24. Average multiplicity of various charged particles per inelastic p-p collisions versus s in $(\mathrm{GeV})^2$ on a log-log plot. The top points and curve are for all charged particles. In order on the right from the top are π^+, π^-, p, K^+, K^-, $\bar{p}$ multiplicities. (Figure from Antinucci et al., 1973.)

greater difficulty. One can ask, of course, whether the range of s shown in Fig. 24 is plausible, or whether one might have expected a more rapid rise from threshold and earlier development of an asymptotic behavior. After all, at $s \simeq 3000$ GeV it is energetically possible to make 28 nucleon-antinucleon pairs! (or ~ 380 pions!). The relatively expanded scale in Fig. 24 over which the multiplicities rise can be explained in part at least by the small inelasticity of the collisions. The collision partners, perhaps with their charges changed, carry off an appreciable fraction of the available energy. This "leading particle" effect is exhibited in more detail in item (e) below.

(d) Limited transverse momentum

One of the most striking features of multiparticle reactions at high energies is the limited extent of the transverse momenta, i.e., the magnitude of the component of momentum perpendicular to the beam direction. On a Peyrou plot of $p_{\parallel}$ vs $p_{\perp}$, with the kinematic boundary a circle with radius, $p \simeq W/2$, events cluster along the x-axis. This behavior has been known for a long time in cosmic rays (see, for example, Feinberg, 1972, and earlier references cited there). Two examples from recent experiments at accelerators are given in Figs. 25 and 26. The data shown in Fig. 25 are inclusive distributions in $p_{\perp}^2$ for π, K^0, and Λ from K^--p interactions at 13 GeV/c (Barletta et al., 1973). The results in Fig. 26 are from the ISR and show the inclusive invariant cross sections for π^+, π^-, K^+, K^-, p, and $\bar{p}$ at fixed $p_{\parallel}$ ($x = 0.16$) versus $p_{\perp}$ (Bertin et al., 1972). Independently of whether one fits with an exponential in $p_{\perp}$ or $p_{\perp}^2$ one finds mean values of transverse momenta of the

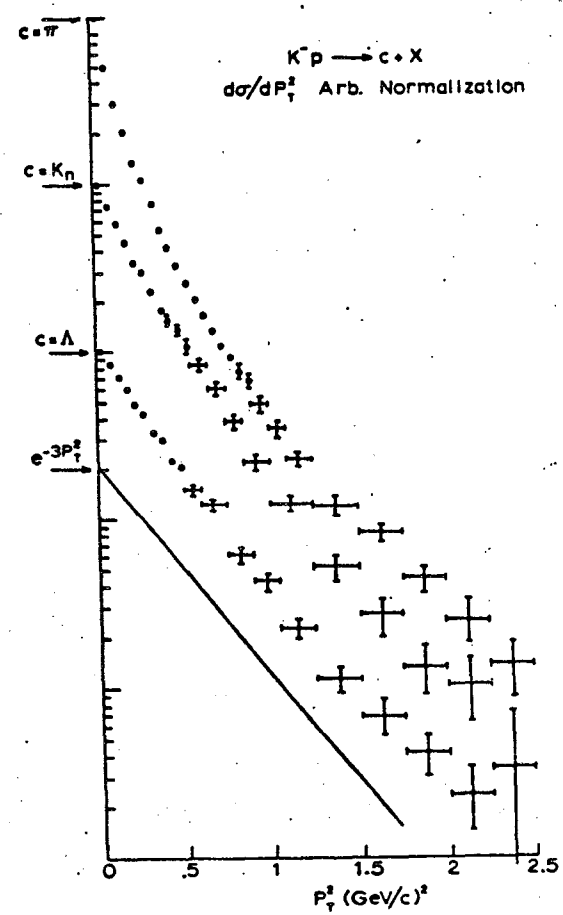

Fig. 25. Distributions in $p_{\perp}^2$ for pions, neutral K-mesons and Λ hyperons from K^-p interactions at 13 GeV/c (from Barletta et al., 1973). $(p_{\perp}^2)_{max} \simeq 6.4$ (GeV/c)^2.

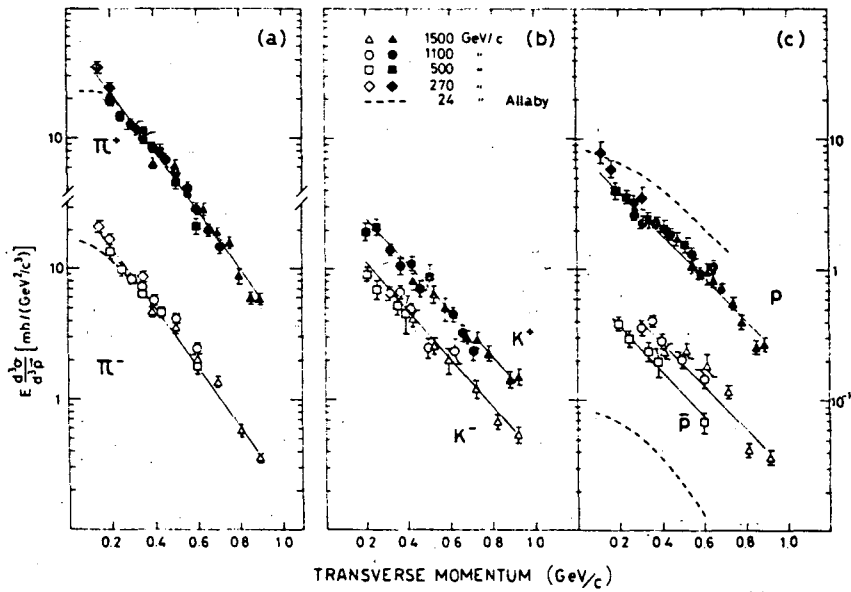

Fig. 26. Invariant cross sections $E(d^3\sigma/dp^3)$ for π^+, π^-, K^+, K^-, p, and $\bar{p}$ produced in p-p collisions at ISR energies as functions of $p_\perp$ in GeV/c at $x = 0.16$. The solid lines are exponential fits to the ISR data. The dashed lines show the trends of 24 GeV/c data from CERN. (Figure from Bertin et al., 1972.)

order of $\langle p_\perp \rangle \simeq 0.33$ GeV/c for pions and $\langle p_\perp \rangle \simeq 0.4$-$0.5$ GeV/c for $K^\pm$ or $p^\pm$. There is very little variation in $\langle p_\perp \rangle$ with bombarding energy from ~ 10 GeV to cosmic ray energies well above the ISR. There is some variation of $\langle p_\perp \rangle$ with $p_{||}$ at a given energy. This

can be understood in terms of the constraints imposed by the kinematic boundary.*

The smallness of $\langle p_\perp \rangle$ is another manifestation of a property of hadronic interactions already seen in the collimated character of elastic scattering where $\langle -t \rangle \simeq B^{-1} \sim 0.1\ (\mathrm{GeV/c})^2$. Hadrons are extended objects and their interactions are peripheral with the exchange of "soft" quanta as the dominant mechanism. Multiparticle production apparently proceeds in the same way. The multiperipheral model (Amati, Stanghellini, and Fubini, 1962, and hundreds of subsequent papers by others) is one explicit realization of this.

(e) Longitudinal behavior (in $p_{||}$, x, or y) of inclusive distributions

The other kinematic dimension to be considered is the longitudinal momentum $p_{||}$ or the equivalent variables x or y [see Appendix D, Eqs. (D.4) and (D.8)]. While in the transverse direction all types of particles tend to be limited in $p_\perp$, in the beam direction there are significant differences depending on particle type and the relation to the incident collision partners. Figure 27 shows some typical inclusive distributions in x for fixed $p_\perp = 0.8$ GeV/c at the ISR (Albrow et al., 1973). The data span the range of $0.2 < x < 1.0$. This may appear to be nearly the whole range of x, but the region $0 \leq x \leq 0.2$ is more important than it seems because of

* There was for a time interest in something called the "seagull effect", namely a dip in $\langle p_\perp \rangle$ as a function of x at $x = 0$. If one evaluates $\langle p_\perp \rangle$ from the invariant cross section $d^3\sigma/dyd^2p_\perp$ at fixed y instead, then $\langle p_\perp \rangle$ versus y shows a more or less monotonic behavior away from $y = 0$. See, for example, Figs. 12 and 13 of Bosetti et al. (1973).

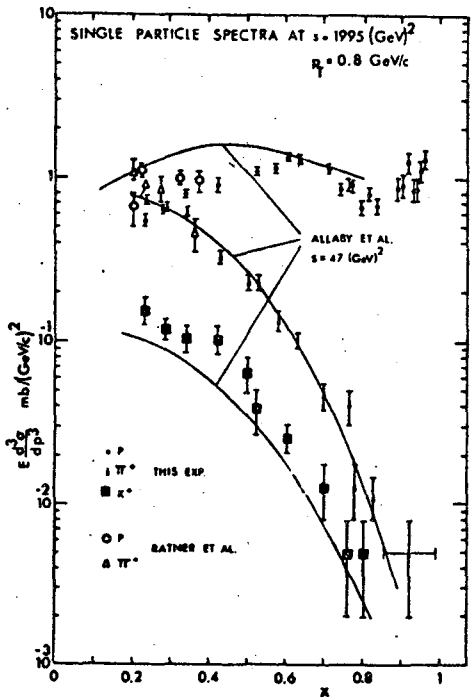

Fig. 27. Inclusive invariant cross sections $Ed^3\sigma/dp^3$ for $p + p \to c$ + anything where $c = p, \pi^+, K^+$ at $s = 1995\ (\mathrm{GeV})^2$ and $p_\perp = 0.8$ GeV/c versus $x = 2p_{\parallel}^*/\sqrt{s}$. The curves show the trend of CERN data at 24 GeV/c incident laboratory momentum $[s = 47\ (\mathrm{GeV})^2]$. Figure from Albrow et al. (1973).

the phase space dx/x [see (D.32)]. Rapidity phase space does not have any weighting factor; rapidity thus shows more clearly the fraction of available phase space covered. From (D.27) we deduce that at $p_\perp = 0.8$ GeV/c, $x = 0.2$ corresponds to $\Delta y \simeq 1.5$, 1.6, and 1.9 for π, K, and p respectively. Comparison with $\Delta y = Y/2 \simeq 3.8$ for the range $0 < x < 1$ shows that the particles in Fig. 27 come from regions

of phase space close to, or at least not remote from, the incident proton. They are all in the "fragmentation region" of Benecke et al. (1969).

The shapes of the spectra in Fig. 27 are characteristic of inclusive distributions at any energy. The protons are relatively flat (on a logarithmic scale) and persist up to $x = 1$. In fact the elastic peak and its tail of diffractively produced resonances and continuum in missing mass M^2 are not visible because of a broadened resolution and elimination of elastic events. The region near $x = 1$ for the protons is discussed in detail by Sens in these proceedings. The pion and K-meson spectra are typical of particles different from the incident ones. The distributions peak near $x = 0$ and fall more or less exponentially in $|x|$ away from that point, with negligible yields at the kinematic boundary $(x = 1)$. Corresponding features for π^+ interactions at 8 and 16 GeV/c, this time integrated over all $p_\perp^2$, are shown in Fig. 28. The "leading particle" effect is visible in the data on the left, $\pi^+p \to \pi^+X$. For negative x both distributions fall rapidly as $x \to -1$. This is expected because $x \to -1$ is the proton end of the scale. The inclusive proton spectra (not shown) peak at $x \simeq -1$ and fall monotonically with increasing x, being ~0.1 in relative size at $x \simeq 0$ and still smaller for $x > 0$.

(f) Scaling

Feynman (1969a,b) gave a description of hadronic interactions that leads to the conclusion that as $s \to \infty$ the inclusive cross section, expressed in terms of $p_\perp^2$ and $x = 2p_{\parallel}^*/\sqrt{s}$, should be independent of s. This is called Feynman scaling. At more or less the same time Yang and collaborators (Benecke et al., 1969) from a rather different point of view suggested the hypothesis of limiting

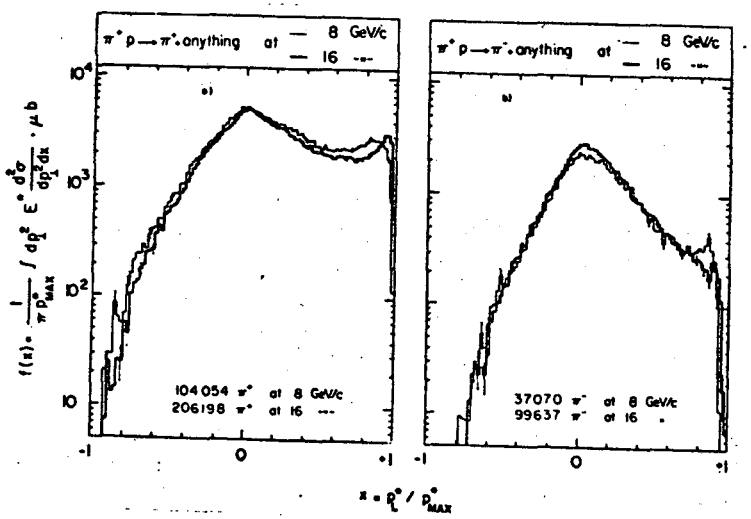

Fig. 28. Invariant inclusive cross sections, integrated over $p_\perp^2$ for $\pi^+p \to \pi^\pm X$ at 8 and 16 GeV/c versus x. Left-hand figure, π^+; right-hand figure, π^- (from Bosetti et al., 1973).

fragmentation whereby at high enough energies the inclusive cross section for the production of a particle c from a target (or projectile) should be independent of the incident energy and type of the other collision partner provided the momentum of c is finite in the rest frame of the target (or projectile). For x away from x = 0, these two kinds of scaling are equivalent, as will be shown below.

Tests of scaling or the approach to scaling abound in the literature (see the references cited at the beginning of this chapter). We refer only to Figs. 27 and 28 for an indication. The solid curves in Fig. 27 are representations of 24 GeV/c ($s = 47$ GeV^2) data from CERN while the points are ISR data at $s \simeq 2000$ GeV^2. For the π^+

data scaling is satisfied to within 10-20% accuracy. For the protons and K^+ scaling over such a wide range in s does not occur. The K^+ cross sections are rising from $s \simeq 50$ to $s \simeq 2000$, while the proton inclusive cross section falls slightly. Over the ISR range $s \simeq 500$ to $s \simeq 3000$ GeV^2 the data on $p + p \to c$ + anything, $c = \pi^+, \pi^-, K^+, K^-$, show scaling in the fragmentation region ($|x| > 0.2$) to an accuracy of 10-15% (see Prof. Sens's lectures for examples). Only the $p + p \to \bar{p}$ + anything fails to scale at ISR energies. This is consistent with the behavior of $\langle n_{\bar{p}} \rangle$ shown in Fig. 24.

Figure 28 shows $\pi^+p \to \pi^\pm$ + anything at 8 and 16 GeV/c laboratory momentum. These energies are very low compared to the ISR energies, but the approach to scaling is visible. Details of the s dependence of the different regions of x need not concern us. These energies are sufficiently low that kinematic effects (e.g., in $\pi^+p \to \pi^-$ only events with four or more charged prongs can contribute) can still have undue influence.

(g) Quantum number transfer

An interesting aspect of multiparticle production is the extent of transfer of additive quantum numbers such as charge, hypercharge, or baryon number from the region of phase space occupied by the initial particles to other regions in the final state. If we think of the colliding hadrons as extended bodies of hadronic matter making rather peripheral collisions with a relatively small fraction of the total energy going into particle production, we might expect that the "leading particles" would largely preserve their quantum numbers. In the multiperipheral model this naive expectation occurs because of the correlation between the size of possible rapidity gaps and the Regge

intercepts of the links. Crudely speaking the higher the intercept the larger the gap. Empirically (and dynamically in the models) the highest trajectories carry the fewest nonvacuum quantum numbers. Thus baryon number, for example, has difficulty migrating very far down the rapidity axis in such models.

Let Q be one of the additive quantum numbers such as charge. Then we define the differential distribution in rapidity dQ/dy by

$$\sigma_{inel} \frac{dQ}{dy} = \sum_c{}' Q_c \int \frac{d\sigma_{ab}{}^c}{dy\, d^2p_\perp} d^2p_\perp \qquad (69)$$

Figs. 29 and 30 show differential distributions in rapidity for electric charge. The data of Fig. 29 are from π^+p and π^-p interactions at 16 GeV/c. These data show no narrow spikes at the extremities of the plot with zero or very small values between. Rather, there is a gradual change from one end to the other, with the negative charge (belonging initially to the incident pion) being spread out somewhat more than the proton's positive charge. This can be accounted for by the lighter mass of the pion and its greater mobility in rapidity. The data of Fig. 30 are perhaps more revealing. These are from p p interactions at various energies and show the anticipated tendency as the rapidity interval widens to have the charge cling to its initial part of the rapidity phase space. While by no means localized precisely, the charge does tend to stay within one or two units in rapidity of the ends of the plot. This behavior is consistent with and lends some support to the idea of a finite correlation length in rapidity.

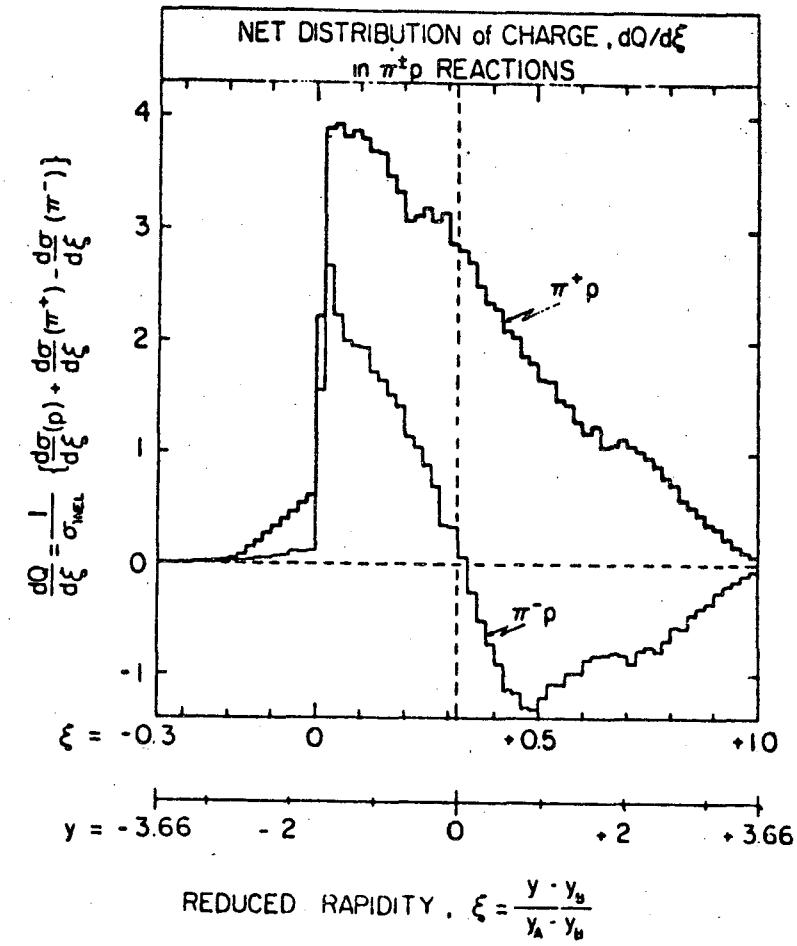

Fig. 29. Differential distribution in rapidity of electric charge for π^+p and π^-p interactions at 16 GeV/c (Data from the ABCCHW and ABBCCHW collaborations; figure from Morrison, 1972).

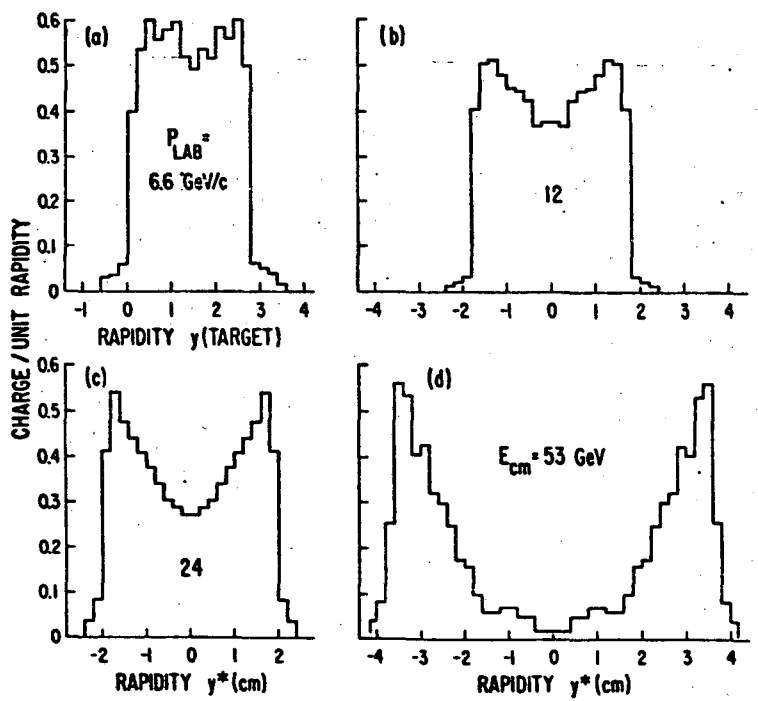

Fig. 30. Differential distribution in rapidity of electric charge for $p\,p$ interactions at P_{lab} = 6.6, 12, 24 GeV/c and W = 54 GeV ($P_{lab} \simeq$ from 1500 GeV/c) (from Sivers, 1973).

3. Theoretical framework assuming a finite correlation length: Feynman-Wilson "gas"

A very useful conceptual framework for inclusive processes is the fluid analogy, often called the Feynman-Wilson gas. The idea is that, since phase-space can be written $dy\, d^2p_\perp$ and the kinematics limits the possible range of y, while the dynamics effectively limits

the range of $p_\perp$, the particles in a multiparticle production process can be viewed as a fluid confined in a bottle in the $y - \vec{p}_\perp$ space. As $s \to \infty$, the bottle becomes very long and the "motion" inside is essentially one-dimensional. Figure 31 is a schematic diagram of the envisioned situation. The normalized n-particle distributions defined

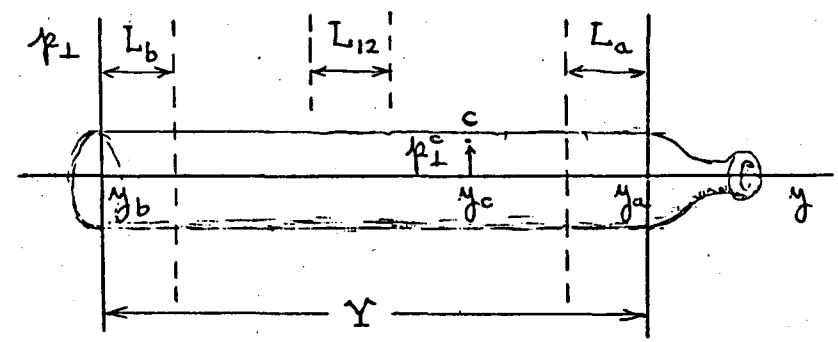

Fig. 31. Feynman-Wilson gas picture. The "gas" of produced particles is confined in phase space to the general region of the "bottle". The length of the bottle is determined by the kinematics, while its radius is governed by the dynamic limitation of $p_\perp$. The finite correlation lengths at each end and in the center are indicated by L_a, L_b, and L_{12}.

by (E.5) are thought of in much the same way as the corresponding densities in a real fluid. In particular, the essential working hypothesis is that the correlation length in rapidity over which a given particle can be influenced by another is finite. We see immediately that a number of important results follow directly from

this hypothesis. The idea of a finite correlation length and its consequences is contained in the work of Amati, Stanghellini, and Fubini (1962) on the multiperipheral model and in the papers of Wilson (1963, 1970). Wilson attributes the fluid analogy to Feynman.

(a) Limiting fragmentation and scaling at finite x

Consider the single particle inclusive density,

$$\rho_{ab}{}^{c} = \rho_{ab}{}^{c}(y_a - y_b, y_c - y_a, \vec{p}_\perp) . \tag{70}$$

In general it depends on the indicated three variables, the first being equivalent to the c.m.s. energy W and the second and third to the momentum $\vec{p}$ of particle c in a frame related to the incident particles. Suppose now that particle c is produced "in the vicinity" of particle a, that is, the rapidity difference $(y_c - y_a)$ is finite as $s(Y) \to \infty$. The assumption of a finite range of correlation implies that at large enough energies particle c cannot "know" what type or where particle b is on the rapidity axis. In this circumstance the density (70) must become independent of $Y = y_a - y_b$ and also of particle b:

$$\lim_{\substack{Y\to\infty \\ y_c - y_a \text{ fixed}}} \rho_{ab}{}^{c} = f_a{}^{c}(y_c - y_a, \vec{p}_\perp) = g_a{}^{c}(x, \vec{p}_\perp) . \tag{71}$$

The first form in (71) can be recognized as a statement of limiting fragmentation of particle a (Benecke et al., 1969), while the second, equivalent [because of Eq. (D.27)], form is a statement of Feynman scaling (Feynman, 1969a,b) in the region $x > 0$.

If particle c is produced "in the vicinity" of particle b then the limit corresponding to (71) has $a \to b$ and $x < 0$.

(b) Central plateau

Suppose that particle c is produced in the central region of Fig. 31, that is, many correlation lengths L away from either end. Then it will be unaware of the identity or position in rapidity of either a or b. The density (70) then becomes independent of Y and y and is only a function of $\vec{p}_\perp$:*

$$\lim_{\substack{Y\to\infty \\ y_c - y_b \gg L_b \\ y_a - y_c \gg L_a}} \rho_{ab}{}^{c} = h^{c}(\vec{p}_\perp) . \tag{72}$$

The invariant cross section in this so-called central region is flat in rapidity and depends on the incident particles a and b only through the factor σ_{ab}.

For p-p interactions at ISR energies the apparent development of a central plateau, as well as evidence for limiting fragmentation, is shown in Fig. 32. Data from a number of experiments at different c.m.s. energies, but all at $p_\perp = 0.4$ GeV/c, are plotted as a function of $y_{Lab} = y_c - y_a$. Limiting fragmentation to an accuracy of 10-20% over the ISR range can be seen from the data at $y_{Lab} < 3$ for all particles except possibly antiprotons. Comparison of the dashed lines with the ISR points indicates departures from scaling at $W = 6.8$ GeV. The central plateau for $\pi^{\pm}$, $K^{\pm}$, and p seems established although a plot of the data versus y^* instead of y_{Lab} would indicate some

* One might think that there could be a possible dependence on y, independent of y_a and y_b, but the Lorentz invariance of $\rho_{ab}{}^{c}$ requires that it be a function of $y - y_a$ and $y - y_b$.

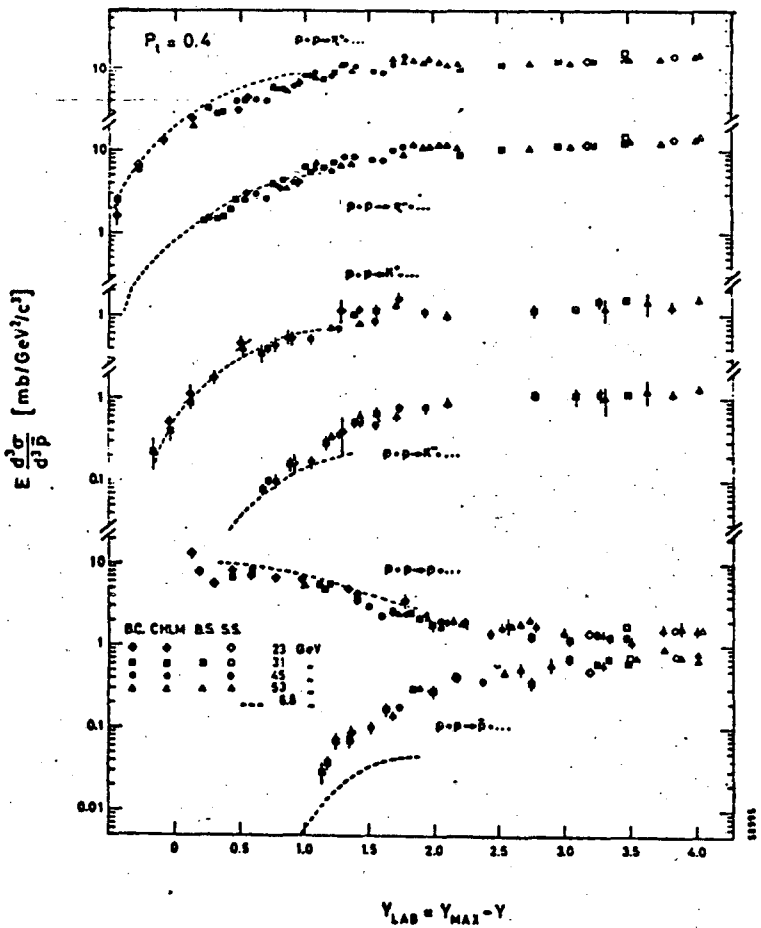

Fig. 32. Compilation of single particle inclusive invariant cross sections in $mb/(GeV)^2$ at $p_\perp = 0.4$ GeV/c for $p + p \to c$ + anything with $c = \pi^+, \pi^-, K^+, K^-, p, \bar{p}$ at various ISR energies (and 24 GeV/c in the lab) as functions of $y_{Lab} = y_c - y_a$. Note the displaced ordinate scales. The center of the rapidity scale $(y_a + y_b)/2$ is at $y_{Lab} = 2.0^-$, 3.2, 3.5, 3.9^-, and 4.0^+ for $W = 6.8$, 23, 31, 45, and 53 GeV, respectively. (Figure from Bussiere, 1973.)

tendency for the plateau to rise with increasing energy by 10-20%. The logarithmic scales in Fig. 32 and the scatter of the data points makes this difficult to see. The conclusion from Fig. 32 is that (71) and (72) are verified, at least at the 10-15% level.*

(c) Growth of multiplicity and correlation parameters with energy

The existence of a central plateau over all but finite regions at either end of the total rapidity interval Y implies that as $s \to \infty$ the multiplicity must grow logarithmically:

$$\langle n_c \rangle = \int \rho_{ab}{}^c \, d\phi_c \simeq \text{const.} + \ln(s/m_a m_b) \int \rho_{ab}{}^c(y^* = 0, \vec{p}_\perp) d^2p_\perp .$$

Thus the coefficient a_1 in (68) is given by

$$a_1 = \sum_{c \text{ charged}} \int \rho_{ab}{}^c(y^* = 0, \vec{p}_\perp) d^2p_\perp \qquad (73)$$

Direct computation of the right-hand side of (73) from the charged particle distributions at $\theta_{cms} = 90°$ at the ISR gives numbers in

---

* In his lectures at Middleton Hall Prof. Sens reported more recent results with greater accuracy ($\sim$ 3-5%) that seem to show the various inclusive cross sections following universal curves in $y_{Lab} = y_c - y_a$, with a continued steady rise as $(y_{Lab})_{max} = Y/2$ increases. Such behavior is inconsistent with the short-range correlation picture, provided we are in the asymptotic domain. With $L \sim 2$ and $Y/2 \sim 4$ we might expect deviations of the order of $\exp(-Y/2L) \simeq e^{-2} \simeq 0.1^+$. Thus asymptopia may not be available quite yet at the ISR.

reasonable agreement with a_1, as inferred from the multiplicity as a function of energy.

Stodolsky (1973) has remarked on the connection between the coefficient a_1 and the limitation on $p_\perp$. In essence he employs the conservation of energy sum rule (E.19). For simplicity consider that only one kind of particle is produced, that its $p_\perp$ distribution is more or less independent of y^* and that its distribution in y^* can be approximated by a rectangle on the range, $-\frac{Y}{2}+\Delta < y^* < \frac{Y}{2}-\Delta$. Then (E.19), evaluated in the c.m.s. for $\mu_a = 0$, reads

$$W = \int \omega \cosh y^* \, \rho(Y,y^*,\vec{p}_\perp) dy \, d^2p_\perp$$

$$\simeq 2\langle\omega\rangle \, a_1 \sinh\left(\frac{Y}{2}-\Delta\right)$$

$$\simeq \langle\omega\rangle \, a_1 \exp\left(\frac{Y}{2}-\Delta\right) = \frac{\langle\omega\rangle \, a_1}{m_N} W e^{-\Delta} \qquad (74)$$

where $\langle\omega\rangle$ is the average value of the transverse mass (D.5) and we have assumed nucleon-nucleon collisions. From (74) we have

$$\langle\omega\rangle \simeq \frac{m_N e^{\Delta}}{a_1} \quad . \qquad (75)$$

Empirically $a_1 \simeq 2^-$ for charged particles. If most particles are pions and all three charged states are produced equally, we can expect the total multiplicity to have $a_1 \simeq 3$. With $|\Delta| \ll 1$, we find $\langle\omega\rangle \simeq 0.3$ GeV, in good agreement with the observed value of $\langle p_\perp\rangle$ for pions. It can be argued that (75) is just an expression of conservation of energy and therefore a definition of Δ in terms of a_1 and $\langle\omega\rangle$. Nevertheless, it is an explicit demonstration of the connection

between the multiplicity and the extension of the inclusive cross section in transverse momentum and in rapidity.

The asymptotic energy dependence of the correlation parameters f_k (E.13) in the finite correlation length picture follows in the same way as for the multiplicity. Consider the two-particle correlation function $C(1,2)$. As indicated schematically in Fig. 31, $C(1,2)$ falls rapidly to zero for $|y_1 - y_2| \gg L_{12}$. Thus in the integral (E.16) defining f_2 integration over $(y_1 - y_2)$ with y_2 fixed will give a finite Y-independent value. The subsequent integration over y_2 will effectively multiply by a factor Y and $f_2 \propto Y = \ln(s/m_a m_b)$. This same behavior occurs for higher correlation parameters, with all but the last integration yielding a Y-independent result asymptotically and the final integration introducing a factor of Y. Thus the hypothesis of finite range correlations leads to the asymptotic energy dependence,

$$f_k \propto \ln s \qquad (76)$$

for all k. Present energies may not be sufficiently large to test this sort of asymptotic statement, especially for the higher correlation parameters. In Sec. 5 we discuss a mixed description of production that differs in its predictions from (76).

4. Relation of the Feynman-Wilson gas to a Regge description, the approach to scaling

The framework of Sec. 3 is an asymptotic one expected to be valid as $s \to \infty$, or better, as $Y \gg L$. At finite energies (5 GeV/c - 500 GeV/c lab momentum) we expect to see departures from the predictions of (71) and (72). The energy dependences of the

nonscaling contributions can be anticipated by invoking a Regge description in analogy with the Regge theory of $2 \to 2$ processes. It is customary to speak of the Mueller-Regge description because of Mueller's important paper relating one-particle inclusive cross sections to the discontinuity in M^2 of the forward $3 \to 3$ amplitude (Mueller, 1970). This subject is dealt with in detail by other lecturers and in the references cited at the beginning of this Chapter. I restrict my explicit discussion of Muellerism to Fig. 33 where the standard set of diagrams are displayed. For the theorists who wish to know about the firmness of the theoretical foundations there are papers by Stapp (1971), Tan (1971), and Polkinghorne (1972). Our brief treatment below is based on heuristic arguments of power-law behavior in the various subenergies with little reference to the details of Regge theory.

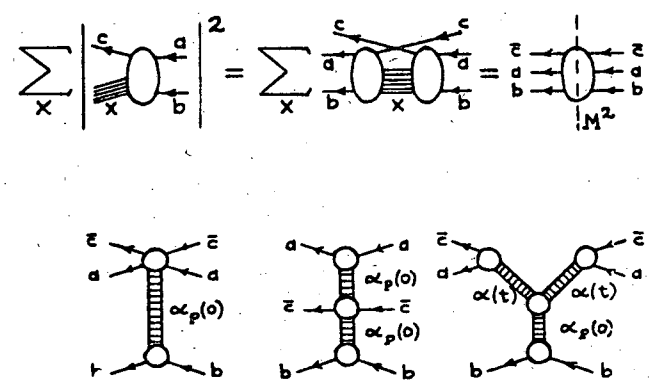

Fig. 33 Schematic diagrams for Regge analysis of inclusive processes. Top line: Conversion of the inclusive cross section for $a + b \to c$ + anything, via unitarity and analytic continuation, into a discontinuity (in M^2, the mass squared of X) of the forward 6-particle amplitude for $ab\bar{c} \to ab\bar{c}$. Bottom line: Various assumed Regge limits, single Regge (limiting fragmentation region), double Regge (central or pionization region), triple Regge limit.

(a) Fragmentation region, triple Regge region

Equation (71) is the statement of scaling in the fragmentation region of a. In Regge language the energy dependence of the cross section is expected to be $s^{\alpha(0)-1}$ and the absence of any energy variation is attributed to exchange of the Pomeranchuk trajectory with $\alpha(0) = \alpha_P(0) = 1$. At finite energies other Regge singularities with smaller intercepts will contribute. Thus (71) is generalized to

$$\lim_{\substack{y_c - y_a \text{ fixed} \\ Y \gg 1}} \rho_{ab}{}^{c} = \sum_k \left(\frac{s}{s_0}\right)^{\alpha_k(0)-1} g_k(x,\vec{p}_\perp) \quad . \tag{77}$$

Note that in (77) we can if we wish replace the variable x with s/M^2 according to (D.29). On the basis of $2 \to 2$ phenomenology where the dominant nondiffractive Regge exchanges have $\alpha(0) \simeq 1/2$ we expect that in the fragmentation region a good description of the s dependence will be given by

$$\rho_{ab}{}^{c} \simeq g_0(x,\vec{p}_\perp) + \left(\frac{s_0}{s}\right)^{\frac{1}{2}} g_1(x,\vec{p}_\perp) \quad . \tag{78}$$

For the reaction $pp \to p$ + anything (78) has been tested over the range from 40 to 400 GeV incident energy at NAL (Sannes et al., 1973, and private communication). In the range $0.75 < x < 0.95$ and $0.2 < |t| < 0.5$ Eq. (78) is quite consistent with the data; furthermore, the functions g_0 and g_1 seem to have closely the same shape in x and in $p_\perp^2$.

The triple-Regge region indicated by the lower right-hand diagram of Fig. 33 is a subset of the fragmentation region correspondin to s/M^2 large, as well as s and M^2. Since $M^2 \simeq s(1 - x)$, the

region of large s/M^2 has $x \simeq 1^-$. As $s \to \infty$ this means that there is a large rapidity gap between c and the nearest particle in "anything". Regge behavior as $s^{\alpha_i(t)}$, where $t = (p_a - p_c)^2$, is expected. The cross section will thus vary as $s^{2\alpha_i(t)-1}$ for fixed M^2, with the s^{-1} factor coming from division by the incident flux. But if M^2 is also large we expect a Regge description in terms of M^2, i.e., $(M^2)^{\alpha_k(0)}$. In order to be a special form of (77) there must be additional M^2 dependence in the form of a factor $(M^2)^{-2\alpha_i(t)}$, leading to the expression

$$\rho_{\text{Triple Regge}} \simeq \frac{1}{s} \sum_{i,j,k} \beta_{ijk}(t) \left(\frac{s}{M^2}\right)^{\alpha_i(t)+\alpha_j(t)} (M^2)^{\alpha_k(0)} . \tag{79}$$

In (79) we have generalized somewhat by replacing $2\alpha_i(t)$ by $\alpha_i(t) + \alpha_j(t)$ to allow for interference terms and summing over i,j,k. The scaling contribitions in (79) come from $\alpha_k(0) = 1$ independently of $\alpha_i(t)$ and $\alpha_j(t)$. The dependence on s/M^2 or x is, or course, dependent on $\alpha_i(t)$ and $\alpha_j(t)$ as well as $\alpha_k(0)$.

The triple-Regge region is of great interest both theoretically and experimentally, as is discussed in detail by other lecturers.

(b) Central region

For particle c in the central region of Fig. 31 Eq. (72) is the scaling statement. At finite energies we expect secondary contributions depending on the two rapidity differences $y_c - y_b$ and $y_a - y_c$, or equivalently on the subenergies s_{bc} and s_{ac} [see Eq. (D.17)]. The general behavior in s will be $(s_{bc})^{\alpha(0)-1} \propto \exp([\alpha(0) - 1](y_c - y_b))$ and similarly for s_{ca}. Keeping only the leading secondary contributions, as in (78), we find

$$\lim_{\substack{y_a-y_c \gg 1 \\ y_c-y_b \gg 1}} \rho_{ab}{}^{c} \simeq h_0(\vec{p}_\perp) + e^{-(y_c-y_b)/2} h_1^{(1)}(\vec{p}_\perp) + e^{-(y_a-y_c)/2} h_1^{(2)}(\vec{p}_\perp) \tag{80}$$

where the secondary functions $h_1^{(i)}(\vec{p}_\perp)$ depend on the Regge couplings of $\bar{b}b \to$ Reggeon $\to c$ and $\bar{a}a \to$ Reggeon $\to c$. For a symmetric situation such as $pp \to c +$ anything, (80) can be written conveniently in terms of c.m.s. rapidity as

$$\rho_{\text{central}}(s,y^*,\vec{p}_\perp) \simeq h_0(\vec{p}_\perp) + \left(\frac{s_0}{s}\right)^{\frac{1}{4}} h_1(\vec{p}_\perp) \cosh y^*/2 . \tag{81}$$

There are two observations here. The first is that the s dependence of the approach to scaling is $s^{-\frac{1}{4}}$, rather than $s^{-\frac{1}{2}}$. This follows immediately from the fact that the relevant rapidity difference is $Y/2$, not Y. The second observation is that the sign of $h_1(\vec{p}_\perp)$ governs the curvature in rapidity away from $y = 0$. If the approach to the scaling limit in the central region is from above (below) then the curvature of the distribution in y^* is concave upwards (downwards). Experiment for pions or all charged particles shows a rise with increasing energy at $y^* = 0$ and concavity downwards away from $y^* = 0$ (see Fig. 32). This behavior is quite consistent with (81). The rise shown by a combination of data at $P_{lab} < 30$ GeV and early ISR data was compatible with a $s^{-\frac{1}{4}}$ variation (Ferbel, 1972). More recently, however, the simple behavior of (81) has been cast in doubt by more extensive data from the ISR. These results at $y^* \simeq 0$ in combination with lower energy data are more consistent with $s^{-\frac{1}{2}}$ than $s^{-\frac{1}{4}}$ (Jarlskog, 1973).

The question of the approach to scaling is obviously an interesting one. The above simple remarks are just the beginnings. Duality and exchange degeneracy arguments can be brought to bear in order to estimate the expected sizes of the secondary contributions. This subject is dealt with in some detail by Roberts in his lectures. There is also the "threshold" aspect exhibited in Fig. 24 wherein appreciable production of heavier particles begins at higher s values and takes longer to approach an approximately scaling limit. The effect at $y^* \simeq 0$ is even more pronounced than in the integrated results shown in Fig. 24. While smallest for pions, this threshold effect is undoubtedly present at a level such that plots of data at $y^* \simeq 0$ from $P_{lab} < 30$ GeV to ISR energies against $s^{-\frac{1}{4}}$ or $s^{-\frac{1}{2}}$ are of dubious value. Some theoretical support for the importance of a threshold effect comes from application of two-component duality to inclusive distributions with the consequence that the nonleading $(s^{-\frac{1}{4}})$ contributions in (81) must be positive.

(c) Factorization

The finite-range correlation picture for the n-particle distributions has implicit in it the idea of factorization. Thus, in (71) the normalized density depends on a and c, but not on b, and in (72) is independent of both a and b. This means that the inclusive cross section in these regions depends on b (or on a and b) only through the multiplicative factor σ_{ab}. In Regge language this is a natural consequence of the assumption of Pomeranchuk-singularity dominance of the total cross sections and the appearance of the $P - \bar{b}b$ and $P - \bar{a}a$ vertices in the $3 \to 3$ amplitude, as shown in Fig. 33.

These factorization properties have been tested extensively for the fragmentation region, mostly at energies below 30 GeV incident in the laboratory (Chen et al., 1971; Lander, 1971; Berger, Oh, and Smith, 1972; Miettinen, 1972; Lam, 1972; Fry et al., 1972). The overall conclusion is that factorization holds for the scaling contribution in the fragmentation region to 10-15%. There is also some evidence for factorization of secondary contributions (Miettinen, 1972) and for two-particle distributions (Lam, 1972).

Factorization for the central region is tested only roughly by the analysis of the approach to scaling of Ferbel (1972). More detailed checks will be possible with Serpukhov and NAL data on reactions initiated by pions, K-mesons and antiprotons, as well as protons. There is a high probability that factorization will fail to hold at the level of a few percent because of the presence of Regge cuts or, in other terms, from the existence of a diffractive contribution associated with the incident particles, as well as a finite-correlation length contribution. See the next section and, in much more detail, Harari's lectures. See also Wilson (1970).

5. Brief remarks on a two-component description

There have been various specific models devised to describe multiparticle reactions. These are described and references to the literature are given in Frazer et al. (1972) and Horn (1972). The short-range correlation picture with its explicit realization in the multiperipheral model of Amati, Stanghellini, and Fubini (1962) and many subsequent versions is perhaps one extreme. At the opposite extreme is the diffractive model in its recent realizations of Adair (1972), Hwa (Hwa, 1971; Hwa and Lam, 1971), and Jacob and Slansky

(Jacob and Slansky, 1972; Jacob, Slansky, and Wu, 1972; Berger, Jacob, and Slansky, 1972) in which all the production is assumed to occur by excitation of the incident particles into fireballs or nova that subsequently decay. A more reasonable view is that nature elects to make use of both dynamical mechanisms (Wilson, 1970). There is now support for the presence of a "diffractive" as well as a "multiperipheral" component in a number of experiments. Professor Sens discusses one of these--the correlation of a proton near $x = 1^-$ with the angular distribution of charged particles. Another is the behavior of the prong cross sections at different energies (Figs. 20-22) or equivalently $\langle n \rangle$ and f_2. We will comment briefly on this aspect. It is dealt with in more depth by Harari.

The two-component or two-mechanism model for prong cross section in its simplest form assumes an incoherent superposition of a "diffractive" cross section and a "multiperipheral" cross section for each n value. It is further assumed that the diffractive part contributes most importantly to the low multiplicities and is independent of energy in each topology, while the multiperipheral part is perhaps Poisson-like in its distribution over topologies with a mean multiplicity that grows with energy, but whose total contribution to the inelastic cross section is an energy-independent fraction. Different versions of this two-component model have been discussed by many authors (Bialas, Fiałkowski and Załewski, 1972; Fiałkowski, 1972; Fiałkowski and Miettinen, 1973; Frazer et al., 1973; Harari and Rabinovici, 1973; Quigg and Jackson, 1972; Van Hove, 1973). The variants differ in detail, but agree on the essentials. There is a relatively small, but important, diffractive component that amounts to 20 ± 5% of the inelastic cross section, with the remainder as

multiperipheral. The consequences for the prong cross sections are sketched in Fig. 34 at the bottom. At high energies there should be seen a clear distinction between the constant diffractive component at low prong number and the multiperipheral component that moves out in n roughly proportional to $\ln s$. Estimates indicate that at the highest ISR energy there might be signs of a shoulder at small n.

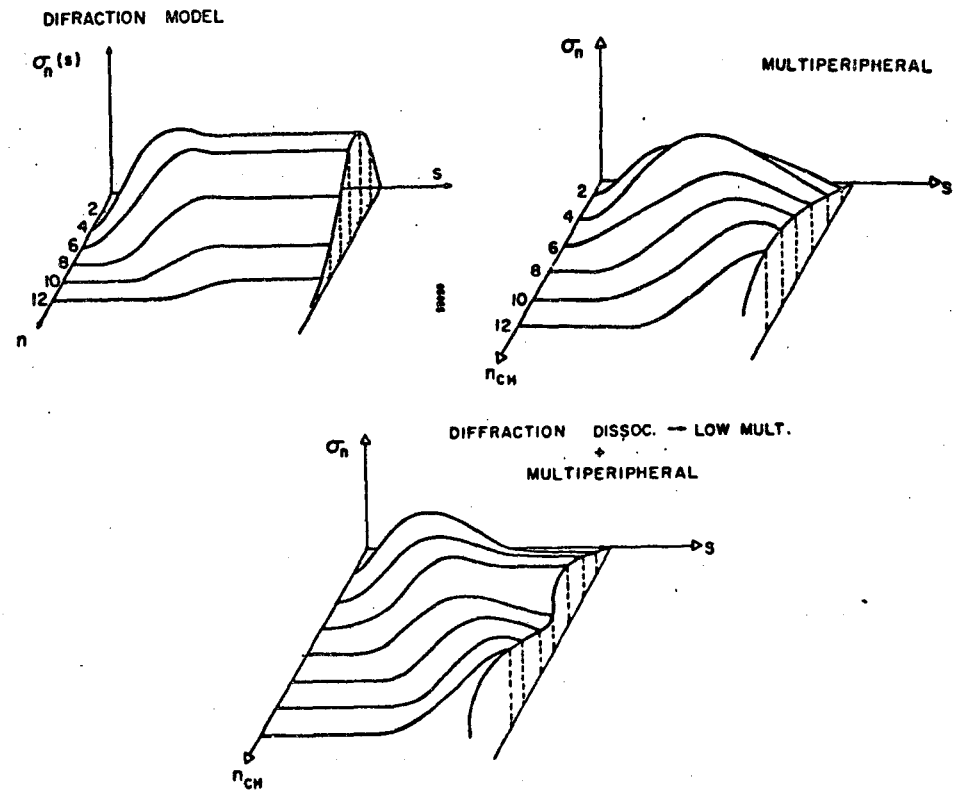

Fig. 34. Prong cross sections as functions of n and s. The expected behavior for diffractive, multiperipheral and two-component models are shown at upper left, upper right, and lower center, respectively (from Morrison, 1973).

The behavior of correlation parameters in a two-component model is of interest. First we note that in the extreme diffractive model the logarithmically growing multiplicity is generated by assuming

$$\sigma_n \propto \frac{1}{n^2} \qquad \text{for} \quad n < N \tag{82}$$

where $N \propto s^{\frac{1}{2}}$ (or some more modest power of s). The correlation parameter f_2 involves the sum of $n(n-1)\sigma_n$ and so behaves asymptotically as $f_2 \propto N \propto s^{\frac{1}{2}}$. This is in marked contrast to the result (76) of the multiperipheral (finite-range correlation) model. The purely diffractive model, while in reasonable accord with the data on f_2 in pp collisions at Serpukhov energies and below is in gross disagreement with the NAL bubble chamber data at 200 and 300 GeV.

In the two-component model the diffractive part is confined to low multiplicities and is s-independent. Thus its contributions to $\langle n \rangle$ and f_2 are constant in energy. All the energy dependence is by hypothesis in the other component. Let α_d and $\alpha_m = 1 - \alpha_d$ be the fractions of the two components in the inelastic cross section and let $\langle n \rangle_d$, $\langle n \rangle_m$, f_{2d}, f_{2m} be the mean multiplicities and correlation parameters for each component separately (normalized to the diffractive and multiperipheral parts of the inelastic cross section, respectively). In the two-component model without interference it is easy to show that the multiplicity and the correlation parameter are given by

$$\begin{aligned} \langle n \rangle &= \alpha_d \langle n \rangle_d + \alpha_m \langle n \rangle_m \\ f_2 &= \alpha_d f_{2d} + \alpha_m f_{2m} + \alpha_d \alpha_m (\langle n \rangle_m - \langle n \rangle_d)^2 . \end{aligned} \tag{83}$$

Now suppose that $\langle n \rangle_d$, f_{2d} are independent of energy, while $\langle n \rangle_m$, f_{2m} grow asymptotically as $\ln s$. Then we find from (83) the asymptotic behavior,

$$\begin{aligned} \langle n \rangle &\propto \ln s \\ f_2 &\propto (\ln s)^2 . \end{aligned} \tag{84}$$

[For higher correlation parameters one finds $f_k \propto (\ln s)^k$.] The cross term in f_2 (83)--a long-range correlation effect--produces $f_2 \propto (\ln s)^2$, even though the ingredients varied as $\ln s$ at most. The two humps developing in Fig. 34 for increasing s are, of course, just a different manifestation and source of this phenomenon. The many versions of the two-component model have little difficulty fitting the observed correlation parameters f_2 up to the highest NAL energies.

As a final remark on evidence in support of two operative mechanisms in multiparticle production we mention briefly the rapidity correlations observed in pp interactions at ISR energies between charged particles and photons (Dibon et al., 1973). The correlation functions $R(y_1,y_2)$ defined by Eq. (E.18) for these data are displayed in Fig. 35. The distributions at the different ISR energies are qualitatively and even quantitatively similar. The open circles show the correlation as a function of y^*_{photon} for $y^*_{ch} = 0$. There appears to be a fairly important short-range correlation centered about $y^*_{photon} \simeq y^*_{ch}$ and having a range of the order of $L \sim 2\text{-}3$. The solid points are for $y^*_{ch} = -2.5$. They exhibit a smaller short-range effect centered at $y^*_{photon} \simeq y^*_{ch}$ and also a long-range correlation whose existence is clear, but whose actual magnitude is

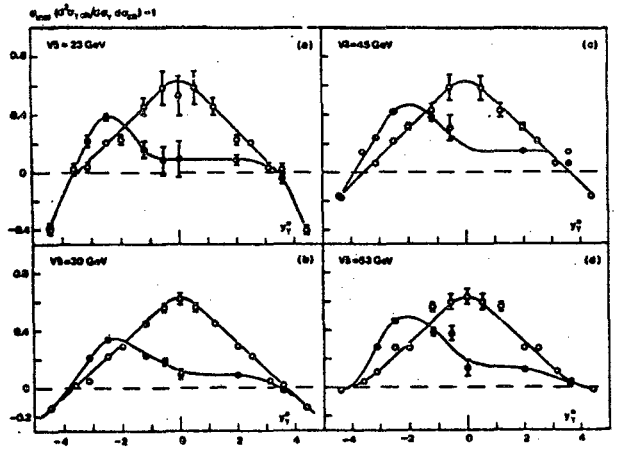

Fig. 35. Rapidity correlation functions $R(y_1,y_2)$ defined by (E.18) for photon-charged particle correlations in pp collisions at ISR energies (W = 23, 30, 45, and 53 GeV) as functions of y^*_{photon}. The solid points correspond to $y^*_{ch} = 0$ and the open circles to $y^*_{ch} = -2.5$ (from Dibon et al., 1973).

probably not easy to establish with certainty because of errors in normalization of the various cross sections. In spite of such uncertainties the presence of a long-range correlation component in the data is certain. Integration of such a contribution leads to $f_2 \propto (\ell n\ s)^2$, as we have already seen.

APPENDIX A

S-matrix formulas, cross sections, two-body kinematics

In what follows the usual units for relativistic particle physics and quantum theory are used: $\hbar = c = 1$; masses, momenta, and energies are expressed in GeV; cross sections are calculated in units of $M^{-2} = (\mathrm{GeV})^{-2}$ and are converted to millibarns by multiplication by the magic factor 0.389. Free particle states are normalized to one particle per unit volume. The phase space for a single particle is thus $d^3p/(2\pi)^3$. The convention on 4-vectors is indicated by $p_\mu = (E, p_x, p_y, p_z)$ and $a\cdot b = a_0 b_0 - \underset{\sim}{a}\cdot\underset{\sim}{b}$.

1. Invariant or Feynman amplitude $\mathcal{M}$

The invariant amplitude $\mathcal{M}$ is related to the S-matrix through the relation,

$$S_{\beta\alpha} = \delta_{\beta\alpha} - i(2\pi)^4\,\delta^{(4)}(p_\beta - p_\alpha)\,\mathcal{M}_{\beta\alpha}/\sqrt{\prod_i (2E_i)} \qquad (A.1)$$

where α and β are the labels for the initial and final states and the product of factors $(2E_i)$ is over all the particles in both initial and final states. Implicit in the S-matrix element are the conservation of energy and momentum delta functions. The invariant amplitude has these factors extracted. Its various arguments are thus to be taken as evaluated taking the conservation laws into account. With the presence of the square root of the product of factors $(2E_i)$ and the single particle normalization stated above, the invariant amplitude is Lorentz invariant, as its name implies.

2. Decay processes $\alpha \to (1,2,\cdots,n)$

The transition probability is

$$dw_{\beta\alpha} = \frac{(2\pi)^4}{2E_\alpha}|\mathcal{M}_{\beta\alpha}|^2 \prod_{i=1}^{n} \frac{d^3p_i}{(2\pi)^3(2E_i)}\cdot\delta^{(4)}(p_1 + p_2 + \cdots + p_n - p_\alpha). \qquad (A.2)$$

For a two-particle final state, in the rest frame of α,

$$dw_{\beta\alpha} = \frac{1}{32\pi^2}|\mathcal{M}_{\beta\alpha}|^2 \frac{p_{cms}\, d\Omega_{cms}}{m_\alpha^2} \qquad (A.3)$$

where

$$\left(\frac{p_{cms}}{m_\alpha}\right)^2 = \frac{1}{4}\left[1 - \left(\frac{m_1 + m_2}{m_\alpha}\right)^2\right]\cdot\left[1 - \left(\frac{m_1 - m_2}{m_\alpha}\right)^2\right].$$

If some observables, e.g., spins, are not detected, averages of the initial state and sums over the final state are understood.

3. Two-particle collision cross section $\alpha = (1,2)$; $\beta = (3,4,\cdots,n+2)$

The projectile is labelled #1 and the target #2 in what follows. The differential cross section is

$$d\sigma_{\beta\alpha} = \frac{(2\pi)^4|\mathcal{M}_{\beta\alpha}|^2}{4\sqrt{(p_1\cdot p_2)^2 - m_1^2 m_2^2}}\cdot\prod_{i=3}^{n+2}\frac{d^3p_i}{(2\pi)^3(2E_i)}\cdot\delta^{(4)}\left(\sum_i p_i - p_\alpha\right). \qquad (A.4)$$

In this form the cross section is manifestly Lorentz invariant. The factor $\sqrt{(p_1\cdot p_2)^2 - m_1^2 m_2^2}$ is called the

flux factor*. It is obviously invariant and has the useful values,

$$\sqrt{(p_1\cdot p_2)^2 - m_1^2 m_2^2} = \begin{cases} m_2 p_1 & \text{(laboratory or target rest frame)} \\ W p_{cms} & \text{(center of mass frame)} \end{cases} \tag{A.5}$$

where W is the total energy in the cms.

For a two-body final state $(m_1 + m_2 \to m_3 + m_4)$, the cms differential cross section is

$$\frac{d\sigma}{d\Omega_{cms}} = \frac{1}{64\pi^2 s}\frac{p'_{cms}}{p_{cms}}|\mathcal{M}_{\beta\alpha}|^2 \tag{A.6}$$

where $s = m_1^2 + m_2^2 + 2m_2(E_1)_{lab}$ is the square of the total energy W in the cms. The ratio of the final to initial cms momenta is

$$\frac{p'_{cms}}{p_{cms}} = \sqrt{\frac{[s - (m_3 + m_4)^2][s - (m_3 - m_4)^2]}{[s - (m_1 + m_2)^2][s - (m_1 - m_2)^2]}} .$$

The differential cross section expressed per unit interval in invariant momentum transfer $t = (p_1 - p_3)^2 = (p_2 - p_4)^2$ is

* With the advent of colliding beam machines, in which the target is in motion and not necessarily in head-on collision with the projectile, there has arisen some question about the appropriateness of this flux factor. See Newton (1966), p. 220-1, for the generally accepted view and Martin and Spearman (1970), p. 153-4, for a different, non-invariant convention as well as the standard result.

$$\frac{d\sigma}{dt} = \frac{\pi}{p'_{cms}\, p_{cms}}\cdot\frac{d\sigma}{d\Omega_{cms}} = \frac{1}{64\pi\, s\, p_{cms}^2}|\mathcal{M}_{\beta\alpha}|^2 . \tag{A.7}$$

Note that $s\, p_{cms}^2$ is just the square of the invariant flux factor (A.5).

For elastic scattering the standard cms scattering amplitude f_{cms} is related to the invariant amplitude by

$$f_{cms} = \frac{-1}{8\pi W}\mathcal{M} . \tag{A.8}$$

For inelastic two-body processes conventions vary, but usually an additional factor of $\sqrt{p'_{cms}/p_{cms}}$ appears on the right-hand side of (A.8). Then the differential cross section (A.6) is given by the absolute square of f_{cms}.

4. Optical theorem

The optical theorem that follows from conservation of probability (unitarity of the S matrix) is

$$-\frac{1}{2}\,\mathrm{Im}\,\mathcal{M}_{\alpha\alpha} = \sqrt{(p_1\cdot p_2)^2 - m_1^2 m_2^2}\;\sigma_{total} \tag{A.9}$$

where σ_{total} is the total cross section for the channel α. This can be written in a more familiar form,

$$\sigma_{total} = \frac{4\pi}{p_1}\,\mathrm{Im}\, f(0°) \tag{A.10}$$

where $f(0°)$ is the forward scattering amplitude (whose square gives the differential elastic scattering cross section per unit solid angle) in any frame moving parallel to the incident particle's direction and p_1 is the incident particle's momentum in that frame.

5. Two-body kinematics

Some kinematic variables have already been defined. We gather here a summary of useful two-body quantities. The general notation is indicated in Fig. A.1 for the process,

$$m_1 + m_2 \rightarrow m_3 + m_4 \quad . \tag{A.11}$$

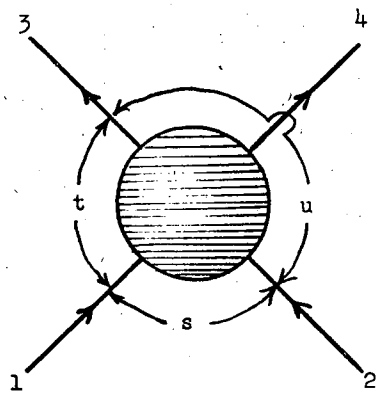

Fig. A.1

The invariant variables s,t,u are defined by

$$\begin{aligned} s &= (p_1 + p_2)^2 = (p_3 + p_4)^2 \\ t &= (p_1 - p_3)^2 = (p_2 - p_4)^2 \\ u &= (p_1 - p_4)^2 = (p_2 - p_3)^2 \end{aligned} \tag{A.12}$$

with the constraint equation,

$$s + t + u = m_1^2 + m_2^2 + m_3^2 + m_4^2 \quad . \tag{A.13}$$

In terms of laboratory quantities (the laboratory is the frame where particle 2 is at rest) the invariants are

$$\begin{aligned} s &= m_1^2 + m_2^2 + 2m_2(E_1)_{lab} \\ t &= m_2^2 + m_4^2 - 2m_2(E_4)_{lab} \\ u &= m_2^2 + m_3^2 - 2m_2(E_3)_{lab} \quad . \end{aligned} \tag{A.14}$$

For elastic scattering or reactions in which $m_4 = m_2$ the momentum transfer t simplifies to $t = -2m_2(T_4)_{lab}$, where T_4 is the kinetic energy of the recoiling particle #4.

The invariants can also be expressed in terms of the center of mass (c.m.s.) variables. Let the c m.s. energies and momenta of the particles be E_1, E_2, E_3, E_4 and $p_1 = p_2 = p$, $p_3 = p_4 = p'$. Then $s \equiv W^2 = (E_1 + E_2)^2 = (E_3 + E_4)^2$ is the square of the total c.m.s. energy and

$$\left.\begin{aligned} E_1 &= \frac{W^2 + m_1^2 - m_2^2}{2W} , \qquad E_2 = \frac{W^2 + m_2^2 - m_1^2}{2W} \\ E_3 &= \frac{W^2 + m_3^2 - m_4^2}{2W} , \qquad E_4 = \frac{W^2 + m_4^2 - m_3^2}{2W} \\ \text{and} \qquad & \\ p^2 &= \frac{1}{4s}\left[s^2 - 2(m_1^2 + m_2^2)s + (m_1^2 - m_2^2)^2\right] \\ p'^2 &= \frac{1}{4s}\left[s^2 - 2(m_3^2 + m_4^2)s + (m_3^2 - m_4^2)^2\right] \end{aligned}\right\} . \tag{A.15}$$

The two momentum transfer variables are

$$t = t_{min} - 2pp'(1 - \cos\theta_{cms})$$
$$u = u_{min} - 2pp'(1 + \cos\theta_{cms}) \qquad (A.16)$$

where θ_{cms} is the angle between $\vec{p}_1$ and $\vec{p}_3$ in the c.m.s. and

$$t_{min} = (E_1 - E_3)^2 - (p - p')^2$$
$$u_{min} = (E_1 - E_4)^2 - (p - p')^2 \quad . \qquad (A.17)$$

At high energies $(W \gg m_i)$ some useful approximations are

$$p \simeq \frac{W}{2}\left(1 - \frac{m_1^2 + m_2^2}{W^2} - \frac{2m_1^2 m_2^2}{W^4} + \cdots\right)$$
$$p' \simeq \frac{W}{2}\left(1 - \frac{m_3^2 + m_4^2}{W^2} - \frac{2m_3^2 m_4^2}{W^4} + \cdots\right) \qquad (A.18)$$

$$t_{min} \simeq -\frac{1}{s}\left[(m_1^2 - m_3^2)(m_2^2 - m_4^2) + \frac{1}{s}(m_1^2 m_2^2 - m_3^2 m_4^2) \times (m_1^2 + m_2^2 - m_3^2 - m_4^2) + \cdots\right]$$

and u_{min} has $m_3 \longleftrightarrow m_4$. Note that if $m_1 = m_3$ <u>or</u> $m_2 = m_4$ $t_{min} \propto s^{-2}$ and so approaches zero very rapidly at high energies. For elastic scattering $t_{min} \equiv 0$, of course, and $u_{min} = (m_1^2 - m_2^2)^2/s$ without approximation.

The three-dimensional scalar product of the c.m.s. momenta $\vec{p}_1$ and $\vec{p}_3$ can be expressed in terms of the invariants s,t,u:

$$4p_s p'_s \cos\theta_s = t - u + \frac{(m_1^2 - m_2^2)(m_3^2 - m_4^2)}{s} \qquad (A.19)$$

where we have changed the notation slightly in order to discuss channels other than the s-channel of Fig. A.1. For the t- and u-channel processes, where t and u are, respectively, the squares of the total c.m.s. energies in the two channels and the other invariants are momentum transfers, the corresponding expressions are

$$4p_t p'_t \cos\theta_t = s - u + \frac{(m_1^2 - m_3^2)(m_2^2 - m_4^2)}{t} \qquad (A.20)$$

$$4p_u p'_u \cos\theta_u = t - s + \frac{(m_1^2 - m_4^2)(m_3^2 - m_2^2)}{u} \quad . \qquad (A.21)$$

The angle θ_t is the angle between $\bar{2}$ and 1 in the t-channel c.m.s. of the process $1 + \bar{3} \to \bar{2} + 4$; θ_u is the angle between $\bar{1}$ and $\bar{3}$ in the process $\bar{3} + 2 \to \bar{1} + 4$. The various momenta are the c.m.s. values in each channel, obtained from (A.15) by substitution.

APPENDIX B

Partial Waves, Helicity Amplitudes, Impact Parameter Representation

The material in this appendix is well known. It is brought together here mostly to fix notation, not to give derivations.

1. Partial wave decompositions

Because of the convenience of dealing with a Lorentz invariant amplitude we define the scattering (or two-body reaction) amplitude $F_{\beta\alpha}(s,t)$ by

$$F_{\beta\alpha}(s,t) = \frac{-1}{8\pi} \mathcal{M}_{\beta\alpha}(s,t) \tag{B.1}$$

where $\mathcal{M}_{\beta\alpha}$ is the invariant amplitude in (A.1). From (A.7) the differential cross section is

$$\frac{d\sigma_{\beta\alpha}}{dt} = \frac{\pi}{sp^2} |F_{\beta\alpha}(s,t)|^2 \quad . \tag{B.2}$$

For particles without spin $F_{\beta\alpha}(s,t)$ has the Rayleigh-Faxen-Holtsmark partial wave expansion,

$$F_{\beta\alpha}(s,t) = \left(\frac{s}{pp'}\right)^{\frac{1}{2}} \sum_{\ell=0}^{\infty} (2\ell + 1)\, a_\ell^{(\beta\alpha)}(s)\, P_\ell(\cos\theta) \tag{B.3}$$

where $\cos\theta$ is related to t via (A.16) and $a_\ell^{(\beta\alpha)}(s)$ is called the partial wave amplitude.

The optical theorem (A.9) can be translated into a statement about the partial wave amplitudes:

$$\mathrm{Im}\, a_\ell^{(\alpha\alpha)}(s) = \sum_\beta |a_\ell^{(\beta\alpha)}(s)|^2 + G_\ell^{(\alpha)}(s) \tag{B.4}$$

where the sum over β is over all the kinematically allowed two-body channels and the function $G_\ell^{(\alpha)}(s)$ represents the contribution from the open channels with more than two particles. Sometimes (B.4) is written

$$\mathrm{Im}\, a_\ell^{(\alpha\alpha)}(s) = |a_\ell^{(\alpha\alpha)}(s)|^2 + \frac{1}{4} H_\ell^{(\alpha)}(s) \tag{B.5}$$

where $H_\ell(s)$ contains all the contributions to the unitarity sum except for the elastic scattering part. $H_\ell(s)$ is the partial wave projection of the so-called overlap function (Van Hove, 1964). If the elastic scattering partial wave amplitude is written as

$$a_\ell^{(\alpha\alpha)}(s) = \frac{1}{2i}\left(e^{2i\delta_\ell(s)} - 1\right) \quad , \tag{B.6}$$

then (B.5) implies that

$$\left|e^{2i\delta_\ell(s)}\right|^2 = 1 - H_\ell^{(\alpha)}(s) \quad . \tag{B.7}$$

If only elastic scattering can occur, $H_\ell = 0$ and the phase shift δ_α is real. If other channels are open then δ_α is complex, with positive imaginary part. The partial wave amplitude (B.6) thus lies on the boundary of or inside the unitarity circle, a circle on an Argand diagram of radius $1/2$ centered at the point $i/2$.

2. Helicity amplitudes

If the particles possess spin a convenient set of amplitudes are the helicity amplitudes of Jacob and Wick (1959). The initial and final states are specified by the usual kinematic variables of Appendix (A.5) and also by the helicities λ_j of the particles. The generalization of (B.2) for unpolarized beams is

$$\frac{d\sigma}{dt} = \frac{\pi}{sp^2}\cdot\frac{1}{(2s_1+1)(2s_2+1)}\sum_{\{\lambda\}}|\langle\lambda_3\lambda_4|F(s,t)|\lambda_1\lambda_2\rangle|^2 . \quad (B.8)$$

The generalization of the partial wave expansion (B.3) is

$$\langle\lambda_3\lambda_4|F(s,t)|\lambda_1\lambda_2\rangle = \left(\frac{s}{pp'}\right)^{\frac{1}{2}}\sum_j (2j+1)\langle\lambda_3\lambda_4|a_j(s)|\lambda_1\lambda_2\rangle d_{\lambda\mu}{}^j(\theta) \quad (B.9)$$

where $d_{\lambda\mu}{}^j(\theta)$ is a Wigner notation function (see the Appendix of Jacob and Wick, 1959) and $\lambda = \lambda_1 - \lambda_2$, $\mu = \lambda_3 - \lambda_4$, while j is the angular momentum.

3. Helicity amplitudes for $0^- + \frac{1}{2}^+ \to 0^- + \frac{1}{2}^+$ processes

An important special case of helicity amplitudes is for the reaction, $0^- + \frac{1}{2}^+ \to 0^- + \frac{1}{2}^+$ or $M + B \to M' + B'$, where M stands for meson and B for baryon. To reduce the number of subscripts we introduce a change in notation from Appendix (A.5). We put

$$\left.\begin{array}{llll} m_1 = \mu, & m_2 = m, & m_3 = \mu', & m_4 = m' \\ E_1 = \omega, & E_2 = E, & E_3 = \omega', & E_4 = E' \\ \vec{p}_1 = \vec{q}, & \vec{p}_2 = \vec{p}, & \vec{p}_3 = \vec{q}', & \vec{p}_4 = \vec{p}' \end{array}\right\} \quad (B.10)$$

In the c.m.s. we have $\vec{p} = -\vec{q}$ and $\vec{p}' = -\vec{q}'$.

The invariant spinor amplitude $F_{\beta\alpha}(s,t)$ is

$$F_{\beta\alpha}(s,t) = \bar{u}_\beta(\vec{p}')[A(s,t) + \tfrac{1}{2}(\not{q} + \not{q}')\, B(s,t)]\, u_\alpha(\vec{p}) \quad (B.11)$$

where $\bar{u}_\alpha u_\alpha = 2m$, $\bar{u}_\beta u_\beta = 2m'$, and $A(s,t)$, $B(s,t)$ are two scalar invariant amplitudes. The convention on gamma matrices is that of Bjorken and Drell (1964). A straightforward Pauli reduction leads to the form,

$$F_{\beta\alpha}(s,t) = \langle\chi'_{\lambda'}|f_1(s,t) + f_2(s,t)\,\vec{\sigma}\cdot\hat{p}'\,\vec{\sigma}\cdot\hat{p}|\chi_\lambda\rangle \quad (B.12)$$

where

$$\left.\begin{array}{l} f_1 = \sqrt{(E+m)(E'+m')}\left[A + \left(W - \frac{m+m'}{2}\right)B\right] \\ f_2 = \sqrt{(E-m)(E'-m')}\left[-A + \left(W + \frac{m+m'}{2}\right)B\right] \end{array}\right\} . \quad (B.13)$$

The helicity amplitudes $F_{\lambda'\lambda}$ are explicitly

$$\begin{aligned} F_{++} &= F_{--} = (f_1 + f_2)\cos\frac{\theta}{2} \\ F_{+-} &= -F_{-+} = (f_1 - f_2)\sin\frac{\theta}{2} . \end{aligned} \quad (B.14)$$

(In these expressions as in all our helicity amplitudes we have specialized the azimuthal angle to $\phi = 0$.)

The differential cross section and polarization are

$$\left.\begin{array}{l} \frac{d\sigma}{dt} = \frac{\pi}{sp^2}\left(|F_{++}|^2 + |F_{+-}|^2\right) \\ P = \frac{2\,\mathrm{Im}(F_{++}F_{+-}{}^*)}{|F_{++}|^2 + |F_{+-}|^2} \end{array}\right\} \quad (B.15)$$

Each of the helicity amplitudes $F_{\lambda'\lambda}$, called s-channel helicity amplitudes to distinguish them from t-channel helicity amplitudes obtained by taking helicity projections in the process $M\bar{M}' \to \bar{B}B'$, has a partial wave expansion of the form (B.9).

4. Impact parameter representation

At high enough energies, where very many partial waves are important, the partial wave series (B.3) and (B.9) can be converted into more convenient and intuitive integrals over impact parameter. For large j and not too large angles the Wigner rotation functions are approximately,

$$d_{\lambda\mu}{}^{j}(\theta) \simeq J_n\left((2j+1)\sin\frac{\theta}{2}\right) \tag{B.16}$$

where $J_n(z)$ is the nth order Bessel function and $n = \mu - \lambda = (\lambda_3 - \lambda_4 - \lambda_1 + \lambda_2)$ is the net helicity flip. With the approximation of replacing the sum in (B.9) by an integral over $(j + \frac{1}{2})$ and the use of (B.16) we obtain

$$\langle\lambda_3\lambda_4|F(s,t)|\lambda_1\lambda_2\rangle \simeq \left(\frac{s}{pp'}\right)^{\frac{1}{2}} \int 2(j+\tfrac{1}{2})\, d(j+\tfrac{1}{2})$$

$$\times \langle\lambda_3\lambda_4|a(s,j+\tfrac{1}{2})|\lambda_1\lambda_2\rangle\, J_n\left(2(j+\tfrac{1}{2})\sin\frac{\theta}{2}\right) .$$

At high energies where t_{min} is negligible, (A.16) shows that

$$-t \equiv q^2 \simeq 4pp'\sin^2\frac{\theta}{2} . \tag{B.17}$$

We therefore define the impact parameter b by

$$\sqrt{pp'}\, b = j + \frac{1}{2} \tag{B.18}$$

and write the agrument of the Bessel function as

$$2(j+\tfrac{1}{2})\sin\frac{\theta}{2} = qb .$$

The integral over $(j + \frac{1}{2})$ then becomes the <u>impact parameter representation</u>,

$$\langle\lambda_3\lambda_4|F(s,t)|\lambda_1\lambda_2\rangle \simeq 2(spp')^{\frac{1}{2}} \int_0^\infty b\, db\, J_n(qb)\langle\lambda_3\lambda_4|a(s,b)|\lambda_1\lambda_2\rangle . \tag{B.19}$$

For particles with no spin the representation corresponding to (B.3) is

$$F_{\beta\alpha}(s,t) \simeq 2(spp')^{\frac{1}{2}} \int_0^\infty b\, db\, J_0(qb)\, a_{\beta\alpha}(s,b) . \tag{B.20}$$

The "partial wave" projection formulas complementary to (B.19) and (B.20) are

$$\langle\lambda_3\lambda_4|a(s,b)|\lambda_1\lambda_2\rangle = \frac{1}{2(spp')^{\frac{1}{2}}} \int_0^\infty q\, dq\, J_n(qb)$$

$$\times \langle\lambda_3\lambda_4|F(s,t=-q^2)|\lambda_1\lambda_2\rangle \tag{B.21}$$

and

$$a_{\beta\alpha}(s,b) = \frac{1}{2(spp')^{\frac{1}{2}}} \int_0^\infty q\, dq\, J_0(qb)\, F_{\beta\alpha}(s,t=-q^2) . \tag{B.22}$$

In these integrals over momentum transfer it is assumed that the amplitude falls off rapidly enough in $q = \sqrt{-t}$ that the integrals converge. From (A.18) it can be seen that at high energies where (B.19) and (B.20) are likely to be useful the coefficient of the integrals is

$$2(spp')^{\frac{1}{2}} = s\left(1 - \frac{m_1^2 + m_2^2 + m_3^2 + m_4^2}{2s} + \cdots\right) \simeq s \,. \qquad (B.23)$$

It is sometimes useful to replace (B.20) and (B.22) by an equivalent two-dimensional Fourier transform representation,

$$\left.\begin{aligned} F_{\beta\alpha}(s,t) &= \frac{s}{2\pi}\int d^2b\; e^{i\vec{q}\cdot\vec{b}}\, a_{\beta\alpha}(s,b) \\ &\text{and its inverse,} \\ a_{\beta\alpha}(s,b) &= \frac{1}{2\pi s}\int d^2q\; e^{-i\vec{q}\cdot\vec{b}}\, F_{\beta\alpha}(s,t=-q^2) \end{aligned}\right\} \,. \qquad (B.24)$$

Here $\vec{q}$ and $\vec{b}$ are two-dimensional transverse vectors. We have used (B.23) to simplify slightly.

For elastic scattering of spinless particles the representation (B.20) leads [via integration of (B.2) over all q^2 and by means of the optical theorem (A.9)] to the following expressions for the elastic and total cross sections:

$$\begin{aligned} \sigma_{e\ell} &= 4\pi\int_0^\infty d(b^2)\,|a(s,b)|^2 \\ \sigma_t &= 4\pi\int_0^\infty d(b^2)\;\mathrm{Im}\; a(s,b) \,. \end{aligned} \qquad (B.25)$$

If $a(s,b)$ is written in a form equivalent to (B.6):

$$a(s,b) = \frac{1}{2i}\left(e^{2i\delta(s,b)} - 1\right) \qquad (B.26)$$

and the complex phase shift $\delta(s,b)$ is given by $\delta = \alpha + i\beta$, then the total, elastic and inelastic cross sections become

$$\left.\begin{aligned} \sigma_t &= 2\pi\int_0^\infty d(b^2)[1 - e^{2\beta}\cos 2\alpha] \\ \sigma_{e\ell} &= 4\pi\int_0^\infty d(b^2)\left[e^{-2\beta}\sin^2\alpha + \tfrac{1}{4}(1 - e^{-2\beta})^2\right] \\ \sigma_{inel} &= \pi\int_0^\infty d(b^2)[1 - e^{-4\beta}] \end{aligned}\right\} \,. \qquad (B.27)$$

APPENDIX C

Eikonal Approximation

For short-wavelengths scattering can be described in terms of a semi-classical trajectory (localized wave packets) and impact parameters. For the Schrödinger equation this leads to the eikonal approximation for the phase shift as a function of energy and impact parameter. The standard derivation of the eikonal approximation is given in many places (e.g., Gottfried, 1966, p. 113ff; Glauber , 1959, p. 315ff). The eikonal approximation to the wave function leads at high energies to

$$\psi_k(\vec{x}) \simeq \psi_k^{(0)}(\vec{x})\cdot\exp\left[\frac{-i}{\hbar v}\int_{-\infty}^{z} V(\vec{b},z')\,dz'\right] \qquad (C.1)$$

where $\vec{b}$ is the impact parameter of the incident particle and $V(\vec{x})$ is the scattering potential. The exponent represents the phase accumulated up to the point $(\vec{b},z)$ by the action of the potential. Straightforward calculation of the scattering amplitude leads to the approximate expression,

$$f(\vec{k}',\vec{k}) \simeq \frac{k}{2\pi i}\int d^2b\; e^{-i(\vec{k}'-\vec{k})_\perp\cdot\vec{b}}\left[e^{2i\Delta(\vec{b})} - 1\right] \qquad (C.2)$$

where

$$\Delta(\vec{b}) = -\frac{1}{2\hbar v}\int_{-\infty}^{\infty} V(\vec{b},z)\,dz \qquad (C.3)$$

is the eikonal approximation to the phase shift. For a spherically symmetric potential integration over azimuth in (C.2) leads to an

expression equivalent to (B.20) with (C.3) as an approximation to the phase in (B.26).

The lowest order approximation to (C.2) in powers of the potential is obtained by expanding the exponential in the integrand. This gives

$$f^{(1)}(\vec{k}',\vec{k}) = -\frac{1}{4\pi}\int d^3x\; e^{-i(\vec{k}'-\vec{k})_\perp\cdot\vec{x}}\,\frac{2m}{\hbar^2}\,V(\vec{x}) \qquad (C.4)$$

which, for small angle scattering where $\vec{k}'-\vec{k}$ is perpendicular to the incident direction, is just the first Born approximation.

An alternative derivation of (C.2) and (C.3) with closer connection to the relativistic problem is based on the Born series of which (C.4) is the first term. With the definition $U(\vec{x}) = -2m\,V(\vec{x})/\hbar^2$, and its Fourier transform,

$$U(\vec{q}_1,\vec{q}_2) = \int d^3x\; e^{-i\vec{q}_1\cdot x}\,U(\vec{x})\,e^{i\vec{q}_2\cdot\vec{x}}\;, \qquad (C.5)$$

the $(\underline{n+1})$th term in the Born series,

$$f(\vec{k}',\vec{k}) = \sum_{n=1}^{\infty} f^{(n)}(\vec{k}',\vec{k})\;, \qquad (C.6)$$

can be written formally

$$4\pi\, f^{(n+1)}(\vec{k}',\vec{k}) = \langle\vec{k}'|UGUG\cdots GU|\vec{k}\rangle$$

where there $n+1$ factors of U and n Green functions G. More explicitly, this reads

$$4\pi\, f^{(n+1)} = \left[\frac{1}{(2\pi)^3}\right]^n \int d^3q_1 \int d^3q_2 \cdots \int d^3q_n\, U(\vec{k}',\vec{q}_1)$$

$$\cdot \frac{1}{q_1^{\,2} - k^2 - i\epsilon} \cdot U(\vec{q}_1,\vec{q}_2) \cdot \frac{1}{q_2^{\,2} - k^2 - i\epsilon} \cdots \frac{1}{q_n^{\,2} - k^2 - i\epsilon} \cdot U(\vec{q}_n,\vec{k}) \quad . \tag{C.7}$$

Each potential factor in (C.7) is replaced by its representation (C.5). Then the eikonal approximation is made by approximating the intermediate momentum factors in all the Green function propagators as follows. Choose the z-axis for all integrations as the incident direction $\vec{k}$ [or the average direction $(\vec{k} + \vec{k}')/2$] and define parallel and perpendicular components of every vector: $\vec{x} = (\vec{x}_\perp, z)$, $\vec{q}_n = (\vec{q}_{n\perp}, q_{n\parallel})$. A typical propagator is then approximated by neglecting $q_\perp^{\,2}$:

$$(q^2 - k^2 - i\epsilon)^{-1} \equiv (q_\perp^{\,2} + q_\parallel^{\,2} - k^2 - i\epsilon)^{-1} \simeq (q_\parallel^{\,2} - k^2 - i\epsilon) \; .$$

The amplitude (C.7) then becomes

$$4\pi\, f^{(n+1)} \simeq \int d^3x\, e^{-i\vec{k}'\cdot\vec{x}}\, U(\vec{x}_\perp, z) \prod_{j=1}^{n} (2\pi)^{-3} \int d^2x_{j\perp} \int dz_j$$

$$\cdot U(\vec{x}_{j\perp}, z_j) \int dq_{j\parallel} \frac{1}{q_{j\parallel}^{\,2} - k^2 - i\epsilon} \cdot \int d^2q_{j\perp}$$

$$\times\; e^{i\vec{q}_{j\perp}\cdot(\vec{x}_{j-1} - \vec{x}_j)_\perp + iq_{j\parallel}(z_{j-1} - z_j)} \cdot e^{i\vec{k}\cdot\vec{x}_n} \quad .$$

The integrals over the transverse components of each intermediate momentum $d^2q_{j\perp}$ can now be performed to yield the product of two-dimensional delta functions,

$$\prod_{j=1}^{n} (2\pi)^2\, \delta^{(2)}\left(\vec{x}_{(j-1)\perp} - \vec{x}_{j\perp}\right) \quad .$$

This is equivalent to the semi-classical straight line path implicit in (C.1). The integrations over the (n+1) different $d^2x_{j\perp}$ are thus reduced to only one:

$$4\pi\, f^{(n+1)} = \int d^2x_\perp \int dz\, e^{-i\vec{k}'\cdot\vec{x}}\, U(\vec{x}_\perp, z) \cdot \prod_{j=1}^{n} (2\pi)^{-1} \int dz_j\, U(\vec{x}_\perp, z_j)$$

$$\cdot \int dq_{j\parallel} \frac{e^{iq_{j\parallel}(z_{j-1} - z_j)}}{q_{j\parallel}^{\,2} - k^2 - i\epsilon} \cdot e^{i\vec{k}\cdot\vec{x}_n} \quad . \tag{C.8}$$

The integral over $dq_{j\parallel}$ can be done by contour integration to yield

$$\int dq\, \frac{e^{iq(z_{j-1} - z_j)}}{q^2 - k^2 - i\epsilon} = \frac{\pi i}{k}\, e^{ik|z_{j-1} - z_j|} \quad . \tag{C.9}$$

Inspection of the remaining integrals over dz_j in (C.8) with (C.9) inserted shows that each integrand oscillates rapidly at high energies and thus will give a negligible result unless in each successive integral $(z_{j-1} - z_j) \geq 0$. With the approximation to small angle scattering, (C.8) can thus be written

$$4\pi\, f^{(n+1)} \simeq \left(\frac{i}{2k}\right)^n \int d^2x_\perp\, e^{i\vec{q}\cdot\vec{x}_\perp} \prod_{j=0}^{n} \int dz_j\, U(\vec{x}_\perp, z_j)$$

$$\times\; \Theta(z_0 - z_1)\, \Theta(z_1 - z_2) \cdots \Theta(z_{n-1} - z_n) \tag{C.10}$$

where $\vec{q} = \vec{k} - \vec{k}'$ is the vectorial momentum transfer. The restriction on the ranges of integration has a familiar counterpart in the limitations on the time integrations in the expansion of the S matrix in quantum field theory. Because of the symmetry of the integrand of the (n+1)-dimensional integral the ranges of all the z integrations can be extended to the interval $(-\infty,\infty)$ provided we divide by $(n+1)!$. Thus (C.10) becomes

$$f^{(n+1)} = \frac{k}{2\pi i}\cdot\frac{1}{(n+1)!}\int d^2x_\perp\, e^{i\vec{q}\cdot\vec{x}_\perp}\left[\frac{i}{2k}\int_{-\infty}^{\infty} dz\, U(\vec{x}_\perp,z)\right]^{n+1} . \tag{C.11}$$

With the definition of $U(\vec{x})$ and the Born series (C.6) it is directly evident that (C.11) is the (n+1)st term in the expansion of the eikonal formula (C.2).

The derivation of the eikonal approximation in relativistic field theories seems possible in some theories and not in others (See, for example, Abarbanel and Itzykson, 1969; Lévy and Sucher, 1969; Tiktopoulos and Treiman, 1971; Fried, 1971; Cheng and Wu, 1972; Swift, 1972). In spite of the uncertainty of its fundamental basis the eikonal method is an extremely plausible and simple way to impose the requirements of unitarity in the direct channel. The standard recipe for "eikonalization" relies on the connection (C.4) of the lowest order exchange amplitude (the first Born approximation) with the two-dimensional Fourier transform of the phase shift $\Delta(\vec{b})$. Explicitly, if the lowest order relativistic amplitude is $F_{Born}(s,t)$, then the relativistic eikonal phase is [in the notation of (B.24) and (B.26)]

$$\delta_{eikonal}(s,b) = \frac{1}{2\pi s}\int d^2q\, e^{-i\vec{q}\cdot\vec{b}}\, F_{Born}(s,t=-q^2) \tag{C.12}$$

and the relativistic eikonal amplitude is

$$F_{eikonal}(s,t) = \frac{s}{4\pi i}\int d^2b\, e^{i\vec{q}\cdot\vec{b}}\left(e^{2i\delta_{eikonal}(s,b)} - 1\right) . \tag{C.13}$$

The eikonal phase (C.12) is in general complex and describes elastic scattering in the presence of competing processes. In nonrelativistic problems this situation is normally described by a complex optical model potential.

For reference we quote some simple examples of $F_{Born}(s,t)$ and its two-dimensional Fourier transform, $s\,\delta_{eikonal}(s,b)$:

$$\frac{F_{Born}(s,t=-q^2)}{A(s)(q^2+\mu^2)^{-1}} \qquad \frac{s\,\delta_{eikonal}(s,b)}{A(s)\,K_0(\mu b)} \tag{C.14}$$

$$A(s)(q^2+\mu^2)^{-2} \qquad A(s)\mu^{-2}\cdot\mu b\, K_1(\mu b) \tag{C.15}$$

$$A(s)\,\exp[-B(s)q^2/2] \qquad A(s)\big(B(s)\big)^{-1}\exp[-b^2/2B(s)] \tag{C.16}$$

$$\frac{[A(s)]^2}{q(q^2+4\mu^2)^{\frac{1}{2}}}\,\ln\left(\frac{\sqrt{q^2+4\mu^2}+q}{\sqrt{q^2+4\mu^2}-q}\right) \qquad [A(s)\,K_0(\mu b)]^2 . \tag{C.17}$$

APPENDIX D

Kinematics of Inclusive Processes

The process $a + b \to c$ + anything is indicated diagramatically in Fig. D.1. With the masses of a, b, and c given and unpolarized beams, there are three

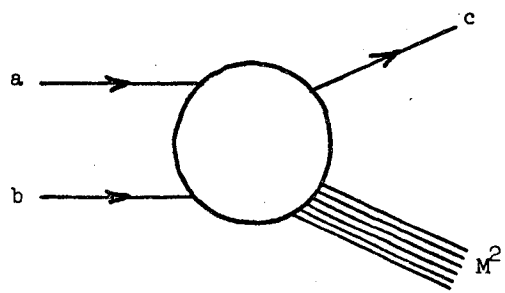

Fig. D.1

kinematic variables, plus a trivial one (e.g., the azimuthal angle of the momentum of c in the c.m.s.) needed to describe the cross section. These can be simply the total c.m.s. energy W and the components of the momentum of c parallel and perpendicular to the incident beam, $p_{||}$ and $p_{\perp}$. This is one more variable than in the $2 \to 2$ process of Appendix (A.5) because the missing mass M is variable, not fixed by $M = m_4$. Nothing more really need be said, but in describing inclusive processes several different choices of variable are made and it is necessary to move from one to the other. We summarize in this Appendix the more important sets of variables and their connections. An exhaustive compilation of inclusive kinematics can be found in Kasman (1972).

1. (s, t, u, M^2)

The obvious and direct extension of the two-body kinematics is the use of any three of s, t, u, M^2 as variables. The definitions of s, t, u are given in (A.12), which in the present notation are

$$s = (p_a + p_b)^2 , \qquad t = (p_a - p_c)^2, \qquad u = (p_c - p_b)^2 \tag{D.1}$$

and

$$M^2 = (p_a + p_b - p_c)^2 . \tag{D.2}$$

The constraint equation (A.13) reads

$$s + t + u - M^2 = m_a^{\,2} + m_b^{\,2} + m_c^{\,2} . \tag{D.3}$$

2. $(s, p_{\perp}, x)$

In discussing scaling Feynman (1969a,b) introduced a reduced longitudinal momentum variable called x. In the c.m.s. frame let the momentum $\vec{p}$ of particle c have components parallel and perpendicular to the incident direction (that of particle a) denoted by $p^*_{||}$ and $\vec{p}_{\perp}$. Then Feynman's x is defined as either

$$x = \frac{p^*_{||}}{p^*_{max}} \quad \underline{\underline{\text{OR}}} \quad x = \frac{2p^*_{||}}{\sqrt{s}} \tag{D.4}$$

where p^*_{max} is the maximum momentum permitted c in the c.m.s. The two definitions are equivalent at high energies. For simplicity and definiteness we use the second form throughout.

The variables $s, p_{\perp}, x$ (plus the azimuth of $\vec{p}_{\perp}$) are an equivalent set for inclusive processes. Note one peculiarity of the x variable. If $p_{||}$ is finite then as $s \to \infty$, $x \to 0$ independent of the particular value of $p_{||}$. This means that for $s \to \infty$ a finite part

of phase space is mapped into $x = 0$. This can cause some conceptual problems, as we will discuss below when we consider cross section formulas.

3. $(s, p_\perp, y)$

In the c.m.s. or any other frame K moving uniformly parallel to the incident direction (z-axis) particle c has momentum $\vec{p}$ with components $p_{||}$ and $\vec{p}_\perp$. There is another Lorentz frame K' moving with a relative velocity $\vec{\beta}$ parallel to the z-axis in which particle c has only transverse components of momentum, i.e., $\vec{p}' = \vec{p}_\perp$. In that frame, the energy of particle c is $E' = \omega_c$, where

$$\omega_c = \sqrt{p_\perp^2 + m_c^2} \tag{D.5}$$

is sometimes called the transverse or the longitudinal mass and is denoted by m_T, μ, κ by other authors. The energy and momentum of particle c in the frame K can evidently be expressed in terms of $p_\perp$ and β according to

$$\left.\begin{aligned} \vec{p}_\perp &= \vec{p}_\perp \\ p_{||} &= \omega \sinh y \\ E &= \omega \cosh y \end{aligned}\right\} \tag{D.6}$$

where ω is given by (D.5) and the longitudinal boost or <u>rapidity</u> y is related to β by

$$y = \tanh^{-1} \beta \, . \tag{D.7}$$

Thus $p_{||}$ can be replaced by y, and $(s, p_\perp, y)$ can be used as the three kinematic variables. For reference we record two more expressions for y:

$$y = \left\{ \begin{aligned} &\frac{1}{2} \ln\left(\frac{E + p_{||}}{E - p_{||}}\right) \\ &\ln\left(\frac{E + p_{||}}{\omega}\right) \end{aligned} \right\} \, . \tag{D.8}$$

The above expressions define the rapidity y in the frame K. What about different frames, e.g., c.m.s. and laboratory? The laws of Lorentz transformations are such that the rapidity y_1 in frame K_1 differs by a constant from the rapidity y_2 in frame K_2, the constant being the longitudinal boost that takes one from K_1 to K_2 according to (D.7). This translation by a constant amount in going from one Lorentz frame to another (along the beam direction) is one of the attractive features of rapidity.

4. <u>Rapidity and related angular variables</u>

If $p_\perp^2 \gg m^2$ the expression (D.8) for y can be approximated by

$$y \simeq \ln\left(\cot \frac{\theta}{2}\right) - \frac{m^2}{2p_\perp^2} \cos \theta \tag{D.9}$$

where $\tan \theta = p_\perp / p_{||}$. Thus in the c.m.s. the rapidity is approximately equal to the cosmic ray angular variable,

$$\eta = \ln\left(\cot \frac{\theta_{cms}}{2}\right) \, . \tag{D.10}$$

Another cosmic ray angular variable is

$$\eta' = - \ln(\tan \theta_{Lab}) \tag{D.11}$$

where Θ_{Lab} is the angle of emission of particle c in the laboratory. If c is relativistic in the lab and the c.m.s. motion is also relativistic in the lab, then the two angular variables are related by

$$\eta' = \eta + \ln(\gamma_{cms}) \tag{D.12}$$

where $\gamma_{cms} = (1 - \beta_{cms}^2)^{-1/2} \simeq W/2m_b$.

5. Invariant sub-energies in terms of rapidity differences, s and Y

The invariant sub-energy of particles 1 and 2 is

$$s_{12} = (p_1 + p_2)^2 \quad . \tag{D.13}$$

Using (D.6) to represent the momenta and energies this can be written

$$s_{12} = m_1^2 + m_2^2 + 2\omega_1\omega_2 \cosh(y_1 - y_2) - 2\vec{p}_{1\perp}\cdot\vec{p}_{2\perp} \quad . \tag{D.14}$$

Similarly, the invariant momentum transfer,

$$t_{12} = (p_1 - p_2)^2 \ , \tag{D.15}$$

can be written

$$t_{12} = m_1^2 + m_2^2 - 2\omega_1\omega_2 \cosh(y_1 - y_2) + 2\vec{p}_{1\perp}\cdot\vec{p}_{2\perp} \quad . \tag{D.16}$$

If the rapidity difference $y_1 - y_2$ is large, then

$$s_{12} \simeq -t_{12} \simeq \omega_1\omega_2 \exp|y_1 - y_2| \quad . \tag{D.17}$$

If we specialize to the incident particles a and b then we have

$$s = m_a^2 + m_b^2 + 2m_a m_b \cosh Y \tag{D.18}$$

where $Y = y_a - y_b$ is the laboratory rapidity of particle a. At high energies, Y is given approximately by

$$Y \simeq \ln(s/m_a m_b) + O(\tfrac{1}{s}) \quad . \tag{D.19}$$

In this limit the rapidity of the c.m.s. is

$$Y_{cms} \simeq \tfrac{1}{2}(Y - \Delta) \tag{D.20}$$

and the rapidities of particles a and b in the c.m.s. are

$$y_a^* \simeq \tfrac{1}{2}(Y + \Delta) \ , \qquad y_b^* \simeq -\tfrac{1}{2}(Y - \Delta) \tag{D.21}$$

where

$$\Delta = \ln(m_b/m_a) \quad .$$

This is indicated in Fig. D.2 for $\Delta > 0$. The maximum rapidity interval

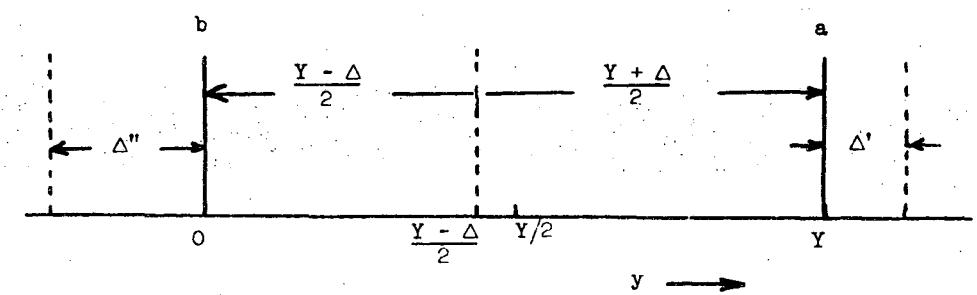

Fig. D.2

available to particle c is approximately Y, but depending on its mass it may be slightly larger or smaller than this. If c is

lighter than both a and b then the maximum and minimum rapidities for c are indicated on Fig. D.2 with

$$\Delta' = \ln(m_a/m_c)$$

$$\Delta'' = \ln(m_b/m_c) = \Delta + \Delta' .$$

This corresponds to an absolute maximum c.m.s. rapidity for particle c of

$$|y_c^*|_{max} = \ln(W/m_c) . \tag{D.22}$$

The value (D.22) is attained at $p_\perp = 0$. If particle c has a non-vanishing value of $p_\perp$ the maximum allowed rapidity is smaller. The range of rapidity is restricted to

$$-y^*_{max}(p_\perp) \le y_c^* \le y^*_{max}(p_\perp)$$

where at high energies and for $p_\perp \ll W/2$ the extreme is given by

$$y^*_{max}(p_\perp) \simeq \ln(W/\omega_c) .$$

Since most particles have relatively small $p_\perp$ this value is typically smaller than (D.22) by less than unity. At large $p_\perp$, of course, it causes an appreciable shortening of the range of rapidity.

6. Phase space and invariant cross section

The single-particle inclusive cross section is given by (A.4), integrated over all final state momenta except particle c and summed over all final states β that contain c and are kinematically allowed. The cross section this appears schematically as

$$d\sigma_{ab}{}^c = \frac{(\text{Lorentz invariant})}{(\text{Flux factor})} \cdot \frac{d^3p_c}{E_c} \tag{D.23}$$

where the flux factor is given by (A.5). It is useful to define the invariant differential cross section for $a + b \to c$ + anything as

$$E_c \frac{d^3\sigma_{ab}{}^c}{d^3p_c} = F_{ab}{}^c . \tag{D.24}$$

It is easy to show that the invariant phase space d^3p/E can be written in terms of $\vec{p}_\perp$ and y as

$$\frac{d^3p}{E} = d^2p_\perp \frac{dp_\parallel}{E} = d^2p_\perp dy . \tag{D.25}$$

Thus the invariant differential cross section is sometimes written as

$$F_{ab}{}^c = \frac{d^3\sigma}{d^2p_\perp dy} . \tag{D.26}$$

7. Relations between variables

We have the three major sets of variables $(s, p_\perp, y)$, $(s, p_\perp, x)$, and (s, t, M^2). We give here the relations among these variables in the high energy limit where terms of order $1/s$ relative to the leading contributions are neglected.

(a) Rapidity y and Feynman's x

For finite $|x|$ (not of order $1/\sqrt{s}$), fixed moderate $p_\perp$, and large s the relation between x and y is

$$x = \begin{cases} \frac{\omega}{m_a} \exp(y_c - y_a) , & x > 0 \\ -\frac{\omega}{m_b} \exp(y_b - y_c) , & x < 0 \end{cases} \tag{D.27}$$

where ω is given by (D.5) and $x > 0$ means that particle c is in the same hemisphere as particle a in the c.m.s. For fixed $p_\perp$ the differentials are related by $dy = dx/x$, as follows from (D.25) when E^* is approximated by $p_{||}^*$.

(b) Relations between (t, M^2) and $(p_\perp, x)$

For finite $|x|$, moderate $p_\perp$, and large s the invariant momentum transfer t can be written in terms of $p_\perp$ and x as

$$t = m_a^2(1 - x) + m_c^2\left(1 - \frac{1}{x}\right) - \frac{p_\perp^2}{x} \tag{D.28}$$

provided $x > 0$. For $x < 0$, the connection is

$$t = -s|x| + m_a^2 + m_c^2\left(1 - \frac{1}{|x|}\right) + m_b^2|x| - \frac{p_\perp^2}{|x|} \quad . \tag{D.28'}$$

Exactly at $x = 0$, i.e., for $p_{||}^* = 0$, the relation is

$$t = m_a^2 + m_c^2 - \omega_c\sqrt{s} \quad . \tag{D.28''}$$

Similarly, the square of the missing mass is

$$M^2 = s(1 - |x|) + m_c^2\left(1 - \frac{2}{|x|}\right) - \frac{2p_\perp^2}{|x|} \tag{D.29}$$

provided $|x|$ is finite. For $p_{||}^* = 0$, we have instead

$$M^2 = s - 2\sqrt{s}\,\omega_c + m_c^2 \quad . \tag{D.29'}$$

It is worthwhile to note that for a given x the minimum t value (obtained by putting $p_\perp = 0$ m (D.28) is

$$t_{min} = m_a^2(1 - x) + m_c^2\left(1 - \frac{1}{x}\right) \quad . \tag{D.30}$$

If we use $x = 1 - M^2/s$ from (D.29), t_{min} can be written alternatively as

$$t_{min} \simeq \begin{cases} (m_a^2 - m_c^2)M^2/s \ , & m_a \neq m_c \\ -m^2(M^2/s)^2 \ , & m_a = m_c = m \ . \end{cases} \tag{D.31}$$

These last expressions can also be obtained from (A.18) with appropriate approximations. They do not hold too near $x = 1$, i.e., where M^2 is not large compared to the other masses.

(c) Relations between (t, M^2) and $(p_\perp, y)$

From (D.16) it follows that the invariant momentum transfer is given in terms of rapidity by

$$t = m_a^2 + m_c^2 - 2m_a\omega_c \cosh(y_c - y_a) \quad . \tag{D.32}$$

For large $|y_c - y_a|$ this becomes

$$t \simeq m_a^2 + m_c^2 - m_a\omega_c \exp|y_c - y_a| \quad . \tag{D.32'}$$

The square of the missing mass can be found in the high energy limit from (D.29) and (D.27) to be approximately

$$M^2 \simeq \begin{cases} s\left[1 - \frac{\omega}{m_a}\exp(y_c - y_a)\right] \ , & y_c^* > 0 \\ s\left[1 - \frac{\omega}{m_b}\exp(y_b - y_c)\right] \ , & y_c^* < 0 \ . \end{cases} \tag{D.33}$$

(d) Phase space connections and invariant cross sections

In the high energy limit the differentials of the three sets of variables are related as follows:

$$dy dp_\perp^2 \simeq \frac{dx}{x} dp_\perp^2 \simeq dx\, dt \simeq \frac{1}{s} dM^2\, dt \qquad (D.34)$$

This means that the invariant cross section can be written in the alternative forms,

$$F_{ab}{}^c = \frac{d^3 \sigma_{ab}{}^c}{dy\, d^2p_\perp} \simeq x \frac{d^3 \sigma_{ab}{}^c}{dx\, d^2p_\perp} \simeq \frac{1}{\pi} \frac{d\sigma_{ab}{}^c}{dx\, dt} \simeq \frac{s}{\pi} \frac{d\sigma_{ab}{}^c}{dM^2\, dt} \quad . \qquad (D.35)$$

The factors of π in the last two forms are present to give cross sections per unit azimuthal angle.

The approximate phase space in terms of x and $p_\perp^2$ in (D.34) is singular at $x = 0$. The exact expression is $dx\, dp_\perp^2/x_0$ where $x_0 = \left(x^2 + \frac{4\omega^2}{s}\right)^{\frac{1}{2}}$ is the scaled energy. For $|x| \gg 2\omega/\sqrt{s}$, $x_0 \simeq |x|$ and the expressions in (D.34) and (D.35) are accurate. As $|x| \to 0$, however, the distinction between $|x|$ and x_0 must be made. Note that in integrating $F_{ab}{}^c$ over any finite interval of some variable one must multiply by the relevant phase space differential from (D.34). Thus the number of particles seen in the interval $\Delta(p_\perp^2)$ and Δx, integrated over azimuth, is

$$\Delta N = (\text{Flux}) \times (\text{Time}) \times F_{ab}{}^c \times \pi \times \Delta(p_\perp^2) \frac{\Delta x}{x_0} \quad . \qquad (D.36)$$

As $s \to \infty$, this number is almost singular at $x = 0$ if $F \neq 0$ there.

APPENDIX E

Distributions, Correlations, Moments, Sum Rules in Inclusive Processes

We have defined the kinematics of inclusive processes in Appendix D. Here we put down definitions of the normalized distributions, correlation functions, moments, and sum rules.

1. Normalized distributions

The n-particle inclusive invariant cross section for the process,

$$a + b \rightarrow (1 + 2 + \cdots + n) + \text{anything} \tag{E.1}$$

is defined in conformity to the single particle cross section (D.24) as

$$E_1 E_2 \cdots E_n \frac{d^{3n}\sigma_{ab}(1,2,\cdots,n)}{d^3p_1 d^3p_2 \cdots d^3p_n} \quad . \tag{E.2}$$

In order to compress the notation somewhat it is convenient to adopt the notation

$$d\phi_i = \frac{d^3p_i}{E_i} \quad , \tag{E.3}$$

for the Lorentz invariant phase space. Then the invariant cross section (E.2) is

$$\frac{d^n\sigma_{ab}(1,2,\cdots,n)}{d\phi_1 d\phi_2 \cdots d\phi_n} \quad . \tag{E.4}$$

It is also convenient to introduce the normalized distributions,

$$\rho_{ab}(1,2,\cdots,n) = \frac{1}{\sigma_{ab}} \frac{d^n\sigma_{ab}(1,2,\cdots,n)}{d\phi_1 d\phi_2 \cdots d\phi_n} \quad . \tag{E.5}$$

In (E.5) sometimes σ_{ab} is the inelastic, rather than total, cross section if the elastic scattering contribution is omitted from the appropriate inclusive cross sections. In what follows we will generally omit the subscripts ab. The incident particles will be understood to be given.

2. Multiplicities and Higher Moments

The average number of particles of type i is given by the integral over all phase space of the normalized single-particle inclusive distribution for particles of type i:

$$\langle n_i \rangle = \int \rho(i) d\phi_i \quad . \tag{E.6}$$

Higher moments are defined similarly by integrals over all phase space of 2-particle and higher distributions. For example, the second moments are given by

$$\langle n_i n_j - \delta_{ij} n_i \rangle = \int \rho(i,j) d\phi_i d\phi_j \quad . \tag{E.7}$$

The presence of $\langle n(n-1) \rangle$ for $i = j$ stems from the definition of the inclusive cross section--if there are n particles of type i in a given event, the first one can be picked out in n different ways and the second in $(n - 1)$. The third moment is given by

$$\langle n_i n_j n_k - \delta_{ij} n_i n_k - \delta_{ik} n_i n_j - \delta_{jk} n_i n_j + 2\delta_{ij}\delta_{jk} n_i \rangle$$

$$= \int \rho(i,j,k) d\phi_i d\phi_j d\phi_k \qquad (E.8)$$

and so on.

The analog in inclusive distributions of the prong cross sections discussed in Sec. III.2(a) are the n-charged particle distributions summed over all types of charged particles. We denote these normalized distributions by $\rho_{ch}(1,2,\cdots,n)$, but it should be remembered that 1 stands for <u>any</u> charged particle in the phase space element $d\phi_1$, and similarly for the other particles. The various charged particle moments can be defined either through the prong cross sections:

$$\langle n^k \rangle = \sum_n n^k \sigma_n/\sigma \quad , \qquad (E.9)$$

or in terms of integrals over the various normalized distributions

$$\left.\begin{aligned} \langle n_{ch} \rangle &= \int \rho_{ch}(1)\, d\phi_1 \\ \langle n_{ch}(n_{ch} - 1) \rangle &= \int \rho_{ch}(1,2)\, d\phi_1 d\phi_2 \end{aligned}\right\} \qquad (E.10)$$

and so on.

3. <u>Correlation coefficients, correlation functions</u>

The idea of totally uncorrelated production of particles would lead to the prediction that the n-particle distribution is given by

$$\rho(1,2,\cdots,n) = \rho(1)\,\rho(2)\cdots\rho(n) \quad . \qquad (E.11)$$

This is not actually attainable on kinematic grounds alone (see Sec. 4 below), but is a useful norm from which to measure correlations. The analog for the prong cross sections is a Poisson distribution,

$$\frac{\sigma_n}{\sigma} = \frac{\langle n \rangle^n}{n!} e^{-\langle n \rangle} \quad . \qquad (E.12)$$

From (E.11) or (E.12) and the definitions of the moments in Sec. 2 above it can be shown quite simply that the integral correlation coefficient for charged particles,

$$f_k = \langle n_{ch}(n_{ch} - 1)\cdots(n_{ch} - k + 1) \rangle - \langle n \rangle^k \qquad (E.13)$$

vanishes for uncorrelated charged particle production. The correlation coefficients f_k are thus useful as empirical quantities measuring the character of the n-particle distributions. Equation (E.13) defines f_k for the charged particles, but there are obvious generalizations for other situations, e.g., charged and neutral, π^+, K^+, and p, etc.

Sometimes moments for negative prongs instead of all charged prongs are presented. These moments are trivially related to the moments for all charged prongs because of charge conservation. Let Q be the total charge in units of the proton's charge in the initial state. Then for an event with n charged prongs, the number n_- of negative prongs is $n_- = (n - Q)/2$. This leads to the relations,

$$\begin{aligned} \langle n_- \rangle &= \tfrac{1}{2}\langle n \rangle - \tfrac{Q}{2} \\ f_2^- &= \tfrac{1}{4} f_2 - \tfrac{\langle n \rangle}{4} + \tfrac{Q}{2} \end{aligned} \qquad (E.14)$$

and corresponding linear combinations for higher moments.

The integral correlation coefficients f_k have their differential counterparts constructed from the normalized n-particle inclusive distributions $\rho(1,2,\cdots,n)$. The most commonly used one is the two-particle correlation function $C(1,2)$:

$$C(1,2) = \rho(1,2) - \rho(1)\,\rho(2) \,. \tag{E.15}$$

Evidently, the integral of $C(1,2)$ over phase space gives f_2:

$$f_2 = \int C(1,2)\, d\phi_1\, d\phi_2 \,. \tag{E.16}$$

Because of limited statistics, often correlations ar given in only one variable, say rapidity. The two-particle rapidity correlation function is defined by

$$\bar{C}(y_1,y_2) = \int C(1,2)\, d^2p_\perp^{(1)}\, d^2p_\perp^{(2)} \,. \tag{E.17}$$

From the experimental point of view it is more convenient to define a correlation function $R(y_1,y_2)$ as the ratio of $\bar{C}$ to the integral of $\rho(1)\,\rho(2)$ over $d^2p_\perp^{(1)}\, d^2p_\perp^{(2)}$. Thus the function $R(y_1,y_2)$ is

$$R(y_1,y_2) = \frac{\int \rho(1,2)\, d^2p_\perp^{(1)}\, d^2p_\perp^{(2)}}{\int \rho(1)\, d^2p_\perp^{(1)} \int \rho(2)\, d^2p_\perp^{(2)}} - 1 \,. \tag{E.18}$$

The advantage of $R(y_1,y_2)$ is that it measures the fractional correlation and so treats favored and unfavored portions of phase space equally, whereas $C(1,2)$ given by (E.15) or $\bar{C}(y_1,y_2)$ given by (E.17) can be small because $\rho(1,2)$ and $\rho(1)\,\rho(2)$ are small, even though $\rho(1,2)/\rho(1)\,\rho(2) \neq 1$.

4. Energy-Momentum and Other Sum Rules

The strict requirement of conservation of 4-momentum between the initial and final state in every collision event leads to a family of "sum rules" involving inclusive cross sections or normalized densities (Chou and Yang, 1970; DeTar, Freedman, and Veneziano, 1971; Predazzi and Veneziano, 1971). The simplest of these involves the single-particle densities. The 4-momentum of theinitial state can be written as

$$(p_a + p_b)^\mu = \sum_{(i)} p_i^{\,\mu}\, \rho(i)\, d\phi_i \tag{E.19}$$

where the sum is over all contributing types of particles and $\mu = 0,1,2,3$. The right-hand side of (E.19) is just the summing up of all the momenta in the final state. If we multiply both sides by σ_{ab} we see that (E.19) is a relation between the 0-particle inclusive cross section and an integral over the 1-particle inclusive cross section. There is a fairly obvious generalization relating the n-particle inclusive cross section to the $(n + 1)$-particle ones. Consider the process $a + b \to (1 + 2 + \cdots + n) +$ anything with its cross section $d^n\sigma(1,2,\cdots,n)/d\phi_1 d\phi_2 \cdots d\phi_n$. For fixed momenta $p_1,p_2,\cdots,p_n$, the momentum of "anything", namely $P = p_a + p_b - (p_1 + p_2 + \cdots + p_n)$, can be thought of as being built up in the manner of (E.19) by a sum of integrals over the various inclusive cross sections for $(n + 1)$ particles in the reaction, $a + b \to \big(1 + 2 + 3 + \cdots + n + (n + 1)\big) +$ anything. Thus we have the general sum rule,

$$(p_a + p_b - p_1 - p_2 - \cdots - p_n)^\mu \rho_{ab}(1,2,\cdots,n)$$

$$= \sum_{(n+1)} \int (\rho_{n+1})^\mu \rho_{ab}(1,2,\cdots,n,n+1) d\phi_{n+1} \qquad \text{(E.20)}$$

where the sum is over the different particle types chosen as the $(n+1)$st particle. Evidently, (E.19) is (E.20) for $n = 0$.

The most useful of these sum rules are the $n = 0$ and $n = 1$ forms. The $n = 0$ one is (E.19). The $n = 1$ expression is

$$(p_a + p_b - p_1)^\mu \rho_{ab}(1) = \sum_{(2)} \int (p_2)^\mu \rho_{ab}(1,2) d\phi_2 .$$

This can be written in terms of the correlation function (E.15) with the aid of (E.19):

$$- p_1^\mu \rho_{ab}(1) = \sum_{(2)} \int p_2^\mu C_{ab}(1,2) d\phi_2 . \qquad \text{(E.21)}$$

The existence of a nonvanishing value on the left-hand side of (E.21) shows that $C_{ab}(1,2)$ cannot be identically zero. Particle production cannot be completely uncorrelated emission. Some correlations are imposed merely by energetics.

Similar sum rules can be written for any conserved additive quantity. Denoting such a quantity by Q (Q = electric charge, z-component of isospin, hypercharge, baryon number, etc.), the sum rule reads

$$Q_a + Q_b = \sum_{(i)} \int Q_i \rho(i) d\phi_i . \qquad \text{(E.22)}$$

The manner in which different regions of phase space contribute to the sum on the right-hand side is discussed for electric charge in Sec. III.2(f).

REFERENCES

1. Conferences and Summer School Proceedings

Proceedings of the 4th Scottish Universities' Summer School, Edinburgh, July 28-August 17, 1963, Strong Interactions and High Energy Physics, ed. R. G. Moorhouse (Oliver and Boyd, Edinburgh and London, 1964).

Proceedings of the 7th Scottish Universities' Summer School, Edinburgh, August 1-20, 1966, Particle Interactions at High Energies, eds. T. W. Preist and L. L. J. Vick (Oliver and Boyd, Edinburgh and London, 1967).

Proceedings of the Third International Conference on High-Energy Collisions, Stony Brook, September 5-6, 1969, High Energy Collisions, ed. C. N. Yang et al. (Gordon and Breach, N.Y., 1969).

Proceedings of the XV International Conference in High Energy Physics, Kiev, August 26-September 4, 1970, ed. V. Shelest et al. ("Naukova Dumka", Kiev, 1972).

Proceedings of the Colloquium on Multiparticle Dynamics, Helsinki, May 25-28, 1971, ed. E. Byckling, K. Kajantie, H. Satz, and J. Tuominiemi (Research Institute for Theoretical Physics, Helsinki, Finland).

Proceedings of the Rochester Meeting of the Division of Particles and Fields of the American Physical Society, Rochester, August 30-September 12, 1971, Particles and Fields - 1971, ed. A. C. Melissinos and P. F. Slattery (A.I.P. Conference Proceedings No. 2, Particles and Fields Subseries No. 1, American Institute of Physics, N.Y., 1971).

Proceedings of the Fourth International Conference on High-Energy Collisions (Stony Brook Series), Oxford, April 5-7, 1972, ed. J. R. Smith (Rutherford High Energy Laboratory, Chilton, Didcot, Berkshire, U.K., 1972).

Proceedings of the IIIrd International Colloquium on Multiparticle Reactions, Zakopane, June 20-24, 1972 (Institute of Nuclear Research, Warsaw, Report "P" NR 1421/V1/PH).

Proceedings of the XVIth International Conference on High-Energy Physics, Chicago-Batavia, September 6-13, 1972, eds. J. D. Jackson, A. Roberts, R. Donaldson (National Accelerator Laboratory, Batavia, Illinois, 1973).

Proceedings of the International Conference on New Results from Experiments on High Energy Particle Collisions, Vanderbilt, March 26-28, 1973, ed. Robert S. Panvini (A.I.P. Conference Proceedings No. 12, Particles and Fields Subseries No. 4, American Institute of Physics, N.Y., 1973).

2. References

Abarbanel, H. D. I. and C. Itzykson, 1969, Phys. Rev. Letters 23, 53.

Adair, R. K., 1972, Phys. Rev. D5, 1105.

Albrow, M. G. et al., 1973, Nucl. Phys. B51, 388.

Allaby, J. V., 1970, Kiev, p. 11-40.

Amaldi, U., 1973, "ISR results on Proton-proton elastic scattering and total cross-sections", in Highlights in Particle Physics, ed. A. Zichichi (Editrice Compositori, Bologna, 1973).

Amaldi, U. et al., 1973a, Phys. Letters 43B, 231.

Amaldi, U. et al., 1973b, Phys. Letters 44B, 112.

Amati, D., A. Stanghellini, and S. Fubini, 1962, Nuovo Cimento 26, 896.

Amendolia, S. R. et al., 1973, Phys. Letters 44B, 119.

Ammosov, V. V. et al., 1972, Phys. Letters 42B, 519.

Ammosov, V. V. et al., 1973, CERN/C. Ph.II/Phys. 73-5 (12.2.1973).

Antinucci, M. et al., 1973, Lett. Nuovo Cimento 6, 121.

Ball, J. S. and F. Zachariasen, 1972, Phys. Letters 40B, 411.

Barbiellini, G. et al., 1972, Phys. Letters 39B, 663.

Barger, V., R. J. N. Phillips, and K. Geer, 1972, Nucl. Phys. B47, 29.

Barger, V., R. J. N. Phillips, and K. Geer, 1973, Nucl. Phys. B54, 463.

Barletta, W. et al., 1973, Phys. Rev. D7, 3233.

Barloutaud, R., 1973, Oxford, Vol. 1, p. 215.

Benecke, J. et al., 1969, Phys. Rev. 188, 2159.

Berger, E. L., M. Jacob, and R. Slansky, 1972, Phys. Rev. D6, 2580.

Berger, E. L., B. Y. Oh, and G. A. Smith, 1972, Phys. Rev. Letters 28, 322.

Bertin, A., 1972, Phys. Letters 42B, 493.

Bialas, A., K. Fialkowski, and K. Zalewski, 1972, Nucl. Phys. B48, 237.

Bjorken, J. D. and S. D. Drell, 1964, Relativistic Quantum Mechanics (McGraw-Hill, N.Y.), Appendix A.

Blatt, J. M. and V. F. Weisskopf, 1952, Theoretical Nuclear Physics (Wiley, N.Y.).

Bosetti, P. et al., 1973, Nucl. Phys. B54, 141.

Bourrely, C. and J. Fischer, TH.1652-CERN, 12 April/73.

Bracci, E. et al., 1972a, Compilation of Cross Sections I - π^- and π^+ Induced Reactions, CERN/HERA 72-1, May 1972.

Bracci, E. et al., 1972b, Compilation of Cross Sections II - K^- and K^+ Induced Reactions, CERN/HERA 72-2, October 1972.

Braccini, P., 1973, Vanderbilt, p.

Bussiere, A., 1973, Vanderbilt, p.

Chabaud, V. et al., 1972, Phys. Letters 38B, 441, 445, 449.

Chapman, J. W. et al., 1972, Phys. Rev. Letters 29, 1686.

Charlton, G. et al., 1972, Phys. Rev. Letters 29, 515.

Chen, M.-S. et al., 1971, Phys. Rev. Letters 26, 1583.

Cheng, H. and T. T. Wu, 1970, Phys. Rev. Letters 24, 1456.

Cheng, H. and T. T. Wu, 1972, Phys. Rev. D5, 3170.

Cheng, H., J. K. Walker, and T. T. Wu, 1973a, Phys. Letters B44, 97.

Cheng, H., J. K. Walker, and T. T. Wu, 1973b, Phys. Letters B44, 283.

Chiu, C. B., 1972, in Annual Review of Nuclear Sciences, Vol. 22, ed. E. Segré, J. R. Grover, and H. P. Noyes (Annual Reviews, Palo Alto, California).

Chou, T. T. and C. N. Yang, 1970, Phys. Rev. Letters 25, 1072.

Collins, P. B. D. and E. J. Squires, 1968, Regge Poles in Particle Scattering, Springer Tracts in Modern Physics, Vol. 45, ed. G. Hohler (Springer-Verlag, Berlin).

Cornille, H. and A. Martin, 1972, Phys. Letters 40B, 671.

Dao, F. T. et al., 1972, Phys. Rev. Letters 29, 1627.

Denisov, S. P. et al., 1971, Phys. Rev. Letters 36B, 415, 528.

de Groot, see under "G".

De Tar, C. E., D. Z. Freedman, and G. Veneziano, 1971, Phys. Rev. D4, 906.

Dibon, H. et al., 1973, Phys. Letters 44B, 313.

Diddens, A. N., 1972, Oxford, Vol. 1, p. 127.

Eden, R. J., 1967, High Energy Collisions of Elementary Particles, Cambridge University Press.

Eden, R. J., 1971, Rev. Mod. Phys. 43, 15.

Feinberg, E. L., 1972, Physics Reports (Phys. Letters C) 5, 237.

Ferbel, T., 1972, Phys. Rev. Letters 29, 448.

Feynman, R. P., 1969a, Stony Brook, p. 237.

Feynman, R. P., 1969b, Phys. Rev. Letters 23, 1415.

Feynman, R. P., 1972, Photon-Hadron Interactions (W. A. Benjamin, Reading, Mass.).

Fialkowski, K., 1972, Phys. Letters 41B, 379.

Fialkowski, K. and H. I. Miettinen, 1973, Phys. Letters 43B, 61.

Foley, K. J. et al., 1969, Phys. Rev. 181, 1775.

Fox, G. C. and C. Quigg, 1973, in Annual Review of Nuclear Science, Vol. 23, ed. E. Segré, J. R. Grover, and H. P. Noyes (Annual Reviews, Palo Alto, California).

Frazer, W. R. et al., 1972, Rev. Mod. Phys. 44, 284.

Frazer, W. R. et al., 1973, Phys. Rev. D7, 2647.

Fried, H. M., 1971, Phys. Rev. D3, 2010.

Froissart, M., 1961, Phys. Rev. 123, 1053.

Fry, J. R. et al., 1973, Nucl. Phys. B58, 420.

Fubini, S., 1963, Edinburgh, p. 259.

Giacomelli, G., 1972, Chicago-Batavia, Vol. 3, p. 219.

Glauber, R. J., 1959, Lectures in Theoretical Physics, Vol. 1, W. E. Brittin, ed. (Interscience, N.Y.).

Gottfried, K., 1966, Quantum Mechanics, Vol. 1 (W. A. Benjamin, Reading, Mass.).

de Groot, E. H. and H. I. Miettinen, 1973, R.H.E.L. preprint RL-73-003 (April 1973).

Grunberg, G. and T. N. Truong, 1973, Phys. Rev. Letters 31, 63.

Harari, H. and E. Rabinovici, 1973, Phys. Letters 43B, 49.

Heckman, P. and R. Henzi, 1972, Phys. Letters 41B, 189.

Horn, D., 1972, Physics Reports (Phys. Letters C) 4, 1.

Horn, D. and F. Zachariasen, 1973, Hadron Physics at Very High Energies, (W. A. Benjamin, Reading, Mass.).

Huson, F. R., 1973, Vanderbilt, p.

Hwa, R. C., 1971, Phys. Rev. Letters 26, 1143.

Hwa, R. C. and C. S. Lam, 1971, Phys. Rev. Letters 27, 1098.

Jackson, J. D., 1970, Rev. Mod. Phys. 42, 12.

Jackson, J. D., 1973, Vanderbilt, p.

Jacob, M., 1972, Chicago-Batavia, Vol. 3, p. 373.

Jacob, M. and R. Slansky, 1972, Phys. Rev. D5, 1847.

Jacob, M., R. Slansky, and C.-C. Wu, 1972, Phys. Rev. D6, 2444.

Jacob, M. and G. C. Wick, 1959, Annals of Physics (N.Y.) 7, 404.

Jarlskog, G., 1973, Vanderbilt, p.

Jin, Y. S. and A. Martin, 1964, Phys. Rev. 135B, 1375.

Kasman, J., 1972, in M. E. Law et al., A Compilation of Data on Inclusive Reactions, Lawrence Berkeley Laboratory Report LBL-80, August, 1972, Part III.

Khuri, N. N. and T. Kinoshita, 1965, Phys. Rev. 137B, 720; 140B, 706.

Kroll, P., Karlsruhe preprint TKP7/73 (March/73).

Lam, W. S., 1972, Phys. Letters 40B, 466.

Lander, R. L., 1971, Rochester, p. 71.

Levy, M. and J. Sucher, 1969, Phys. Rev. 186, 1656.

Lovelace, C., 1972, Chicago-Batavia, Vol. 3, p. 73.

MacDowell, S. W. and A. Martin, 1964, Phys. Rev. 135B, 960.

Martin A., 1963, Edinburgh, p. 105.

Martin A., 1966, Nuovo Cimento 42A, 930.

Martin A. D. and T. D. Spearman, 1970, Elementary Particle Theory (North-Holland, Amsterdam).

Michael, C., 1972, Chicago-Batavia, Vol. 3, p. 165.

Miettinen, H. I., 1972, Phys. Letters 38B, 431.

Morrison, D. R. O., 1970, Kiev, Review of Quasi-Two-Body Reactions, Sec. 4 and Fig. 4.2 (issued as a separate report ITP-71-66E by the Institute of Theoretical Physics, Academy of Sciences of the Ukrainian SSR, Kiev, 1971).

Morrison, D. R. O., 1972, Oxford, Vol. 1, p. 253.

Morrison, D. R. O., 1973, CERN/D.Ph.II/Phys. 73-11 (3.4.173).

Mueller, A. H., 1970, Phys. Rev. D2, 2963.

Mueller, A. H., 1972, Chicago-Batavia, Vol. 1, p. 347.

Newton, R. G., 1966, Scattering Theory of Waves and Particles (McGraw-Hill, N.Y.).

Phillips, R. J. N. and G. A. Ringland, 1972, in High Energy Physics, Vol. 5, ed. E. H. S. Burhop (Academic, N.Y.).

Polkinghorne, J. C., 1972, Nuovo Cimento 7A, 555.

Predazzi, E. and G. Veneziano, 1971, Lett. Nuovo Cimento 2, 749.

Quigg, C., 1971, Rochester, p. 40.

Quigg, C. and J. D. Jackson, 1972, National Accelerator Laboratory report NAL-THY-93 (October, 1972).

Roy, S. M., 1972, Phys. Reports (Phys. Letters C) 5, 125.

Sannes, F., et al., 1973, Phys. Rev. Letters 30, 766.

Sivers, D., 1973, Argonne National Laboratory report ANL/HEP 7313 (May, 1973).

Stapp, H. P., 1971, Phys. Rev. D3, 3177.

Stodolsky, L., 1973, Phys. Rev. Letters 31, 139.

Strolin, P., 1973, Vanderbilt, p.

Swift, A. R., 1973, Phys. Rev. D5, 1400.

Tan, C.-I., 1971, Phys. Rev. D4, 2412.

Tiktopoulos, G. and S. B. Treiman, 1971, Phys. Rev. D3, 1037.

Titchmarsh, E. C., 1950, Theory of Functions (corrected 2nd ed.) (Oxford University Press).

Van Hove, L., 1964, Rev. Mod. Phys. 36, 655.

Van Hove, L., 1971, Phys. Reports (Phys. Letters C) 1, 347.

Van Hove, L., 1973, Phys. Letters 43B, 65.

Wang, C. P., 1969, Phys. Rev. 180, 1463.

Wilson, K. G., 1963, Acta Phys. Austriaca, 17, 37.

Wilson, K. G., 1970, Cornell University Report CLNS-131 (November, 1970); also these Proceedings.

Wroblewski, A., 1970, Kiev, p. 42.

Yodh, G. B., Y. Pal, and J. S. Trefil, 1972, Phys. Rev. Letters 28, 1005.

Zachariasen, F., 1971, Phys. Reports (Phys. Letters C) 2, 1.

LEGAL NOTICE

This report was prepared as an account of work sponsored by the United States Government. Neither the United States nor the United States Atomic Energy Commission, nor any of their employees, nor any of their contractors, subcontractors, or their employees, makes any warranty, express or implied, or assumes any legal liability or responsibility for the accuracy, completeness or usefulness of any information, apparatus, product or process disclosed, or represents that its use would not infringe privately owned rights.

TECHNICAL INFORMATION DIVISION
LAWRENCE BERKELEY LABORATORY
UNIVERSITY OF CALIFORNIA
BERKELEY, CALIFORNIA 94720